약학박사학위논문

Disruption of *Ninjurin1* Causes Obsessive-Compulsive Disorder-like Behaviors in Mice

Ninjurin1 결손 마우스에서 강박 장애 유사증상 발현에 관한 연구

2017 년 2 월

서울대학교 대학원

약학과 의약생명과학전공

Le Hoang

ABSTRACT

Disruption of *Ninjurin1* Causes Obsessive-Compulsive Disorder-like Behaviors in Mice

Le Hoang

Division of Pharmaceutical Bioscience

College of Pharmacy

The Graduate School

Seoul National University

Obsessive-compulsive disorder (OCD) is a common psychiatric disorder that affects approximately 2 % of the global population and is characterized by the presence of intrusive and distressing thoughts (obsessions) and/or repetitive behaviors (compulsions). Over the last few decades, molecular neurobiology has uncovered several genes whose deficiency in mice results in behavioral traits associated with human OCD. However, the mechanisms that underlie OCD remain largely unknown. Here I show the relationship

between OCD and Ninjurin 1 (Ninj1), a small cell adhesion molecule that is known to play various roles in nerve regeneration and inflammation. *Ninj1* knockout (KO) mice exhibit compulsive grooming-induced hair loss and self-made lesions as well as increased anxiety-like behaviors that are responsive to fluoxetine, a first-line OCD treatment. Ninj1 is highly expressed in cortico-thalamic circuits, which are critical areas that are implicated in OCD. Histological analysis reveals that Ninj1 is predominantly expressed in cortico-thalamic circuits, and neuron-specific *Ninj1* conditional KO mice manifest aberrant phenotypes similar to the global *Ninj1* KO mice. Intriguingly, *Ninj1* KO brains display reduced numbers of functional synapses and impaired neuronal branching, which results in altered neurotransmission in thalamic circuits. Moreover, the disruption of *Ninj1* leads to abnormalities in glutamate signaling, which reflects the function of Ninj1 as a regulator of N-methyl-D-aspartate (NMDA)-type glutamate receptor stability. Collectively, my results demonstrate that *Ninj1* deficiency in mice causes OCD-like behaviors and that Ninj1 could be a new genetic component of human OCD.

Keywords : **Ninjurin1; obsessive-compulsive disorder; OCD-like behaviors; anxiety-like behaviors; fluoxetine; glutamate signaling**

Student number : **2010-22880**

TABLE OF CONTENTS

LIST OF FIGURES

LIST OF ABBREVIATIONS

Ab	;	antibody
β-gal	;	β-galactosidase
CHX	;	cycloheximide
cKO	;	conditional knockout
CNS	;	central nervous system
Ctrl	;	control
Ctx	;	cortex
DIV	;	day *in vitro*
EM	;	electron microscopy
EPM	;	elevated plus maze
FDA	;	Food and Drug Administration
GFP	;	green fluorescent protein
GluR1	;	α-amino-3-hydroxy-5-methyl-4-isoxazolepropionic acid receptor subunit 1
GluR2	;	α-amino-3-hydroxy-5-methyl-4-isoxazolepropionic acid receptor subunit 2
HA	;	hemagglutinin
HEK293T	;	human embryonic kidney 293T cell
Het	;	hetero
Hip	;	hippocampus
H & E	;	hematoxylin and eosin
KO	;	knockout
MBT	;	marble-burying test
mEPSC	;	miniature excitatory postsynaptic currents
MWM	;	Morris water maze

MSN	;	medium striatal neuron
NFR	;	nuclear fast red
Ninjurin 1	;	Nerve injury-induced protein 1
Ninj1	;	Ninjurin 1
NL1	;	Neuroligin 1
NMDAR	;	N-methyl-D-aspartate receptor
NR1	;	N-methyl-D-aspartate receptor subunit 1
NR2A	;	N-methyl-D-aspartate receptor subunit 2A
NR2B	;	N-methyl-D-aspartate receptor subunit 2B
NST	;	nestlet-shredding test
N2a	;	Neuro2A
OCD	;	obsessive-compulsive disorder
OFT	;	open field test
PSD95	;	postsynaptic density protein 95
RT-qPCR	;	reverse transcription-quantitative polymerase chain reaction
SEP	;	super-ecliptic pHluorin
s.e.m	;	standard error of the mean
siRNA	;	small interfering RNA
Str	;	striatum
Synapto.	;	synaptophysin
TST	;	tail suspension test
Thal	;	thalamus
WT	;	wild type

INTRODUCTION

1. Obsessive-compulsive disorder

Obsessive-compulsive disorder (OCD) is a common psychiatric disorder that affects approximately 2 % of the global population and is characterized by the presence of intrusive and distressing thoughts (obsessions) and/or repetitive behaviors (compulsions) [1,2]. The World Health Organization (WHO) has ranked OCD in the top ten nonfatal global burdens, in terms of diminished quality of life [3,4]. OCD affects men and women in roughly equal numbers and usually starts during childhood [4,5]. People with OCD generally repeat thoughts, doubts, or images about different things such as fear of germ contamination and dirt. They do the same rituals compulsively such as washing hands, locking and unlocking doors, or counting of things [4]. Most OCD patients are aware of the behaviors they are doing, however, they could not control and stop their unwanted thoughts and behaviors [4]. Despite decades of research and tremendous efforts by many scientists, the prevalence of OCD has not decreased [2]. Our understanding of the biological mechanisms that underlie this disease is limited, presumably

owing to etiological complexity and difficulties in examining the living human brain.

Several lines of evidence from human studies indicate that there are genetic components to the pathogenesis of obsessive-compulsive disorder (OCD) [6,7]. Using genetically engineered mice, several genes related to OCD have been revealed. Specifically, the deletion of the *Hoxb8*, *Sapap3*, or *Slitrk5* gene in mice recapitulated several key features of OCD, including (i) repetitive behaviors (excessive grooming to the point of hair loss and self-made lesions), (ii) increased anxiety-like behaviors that were ameliorated by treatment with the selective serotonin reuptake inhibitor fluoxetine, and (iii) altered glutamate signaling in the brain [8-10]. Although many important advances in the understanding of the aetiology of OCD have been made, the molecular basis of this disorder remains poorly understood. Interestingly, a wide variety of cell adhesion molecules have been causally implicated in psychiatric disorders, including OCD, autism, and schizophrenia [11-13]. The cell adhesion molecule Ninj1 has diverse functions in peripheral tissues [14-16]; however, its roles in the central nervous system (CNS) and in OCD have remained uncharacterized.

2. Ninjurin1

Nerve injury-induced protein 1 (Ninjurin1 or Ninj1), a 152-amino-acid cell adhesion molecule, was originally identified based on its strong upregulation after axotomy in neurons and in Schwann cells surrounding the distal sciatic nerve segments in rats in 1996 [14] (**Figure 1A**). In mammals, Ninj1 belongs to Ninjurin family consisting of Ninj1 and Ninj2, which share conserved hydrophobic regions in their transmembrane domains [17]. However, Ninj1 and Ninj2 do not contain comparable adhesion motifs nor do they have similar expression patterns in tissues. In addition, Ninjurins have no considerable homology to any other known proteins [14].

Mouse Ninj1 protein is composed of a N-terminal (amino acid (a.a.) 1-71) and a C-terminal (a.a. 140-152) extracellular domains, two transmembrane domains (a.a. 72-100 and a.a. 118-139), and a cytoplasmic domain (a.a. 101-117, **Figure 1B, left**) [14]. Human Ninj1 is a 152-amino acid protein with both its N- and C-terminus exposed extracellularly (a.a. 1-80 and a.a. 142-152), a short intracellular segment (a.a. 102-119), and two transmembrane domains (a.a. 81-101 and a.a. 121-141, **Figure 1B, right**). It has been known that Ninj1 can interact with each other in a homophilic binding manner through an N-

terminal extracellular 12 residue binding motif located from Pro^{26} to Asn^{37} (PPRWGLRNRPIN) to promote nerve regeneration [18] (**Figure 1A**).

Ninj1 is expressed in many kinds of tissues and cells, predominantly in those of epithelial origin such as liver, kidney, thymus [18]. In addition to a suggested role in promoting nerve regeneration, Ninj1 has been shown to be involved in non-neuronal pathophysiological conditions [19]. Ninj1 is temporally increased in macrophages and mediates the regression of hyaloid blood vessels, a transient existing network of capillaries responsible for the growth and maturation of the lens, via a close interaction between macrophages and vascular endothelial cells during ocular development [20]. Furthermore, Ninj1 is reported to be expressed in myeloid cells and modulated the migration of myeloid cells to central nervous system inflammatory lesions in an autoimmune disease multiple sclerosis and its animal model, experimental autoimmune encephalomyelitis (EAE) [15,16,21]. In addition, Ninj1 contributes to intravascular crawling of myelin-reactive T cells on cerebral blood vessels to mediate neuronal inflammation in multiple sclerosis [22]. Recently, Ninj1 is reportedly elevated under inflammatory conditions and contributed to

inflammation not only by mediating leukocyte migration, but also by modulating Toll-like receptor 4 (TLR4) [23]. Taken together, Ninj1 is an important factor in pathophysiological inflammation and a novel therapeutic target for inflammatory conditions such as multiple sclerosis and sepsis.

In addition to its roles in inflammation, Ninj1 is implicated in the regulation of vascular formation. Yin et al. reported that inhibition of Ninj1 restores erectile function through angiogenic effects in the diabetic mice [24]. Very recently, Ninj1 has been shown to negatively regulates the formation of new blood vessels by reducing the trophic effects of capillary pericytes [25].

Although the protein Ninj1 plays diverse roles in peripheral tissues, its involvement in the central nervous system (CNS) and neuropsychiatric disorders such as OCD remains largely unknown.

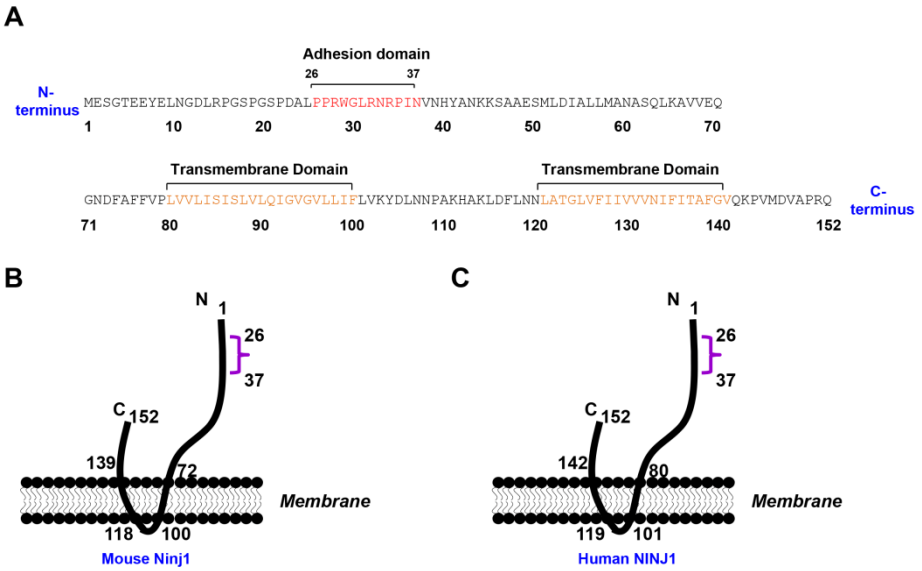

Figure 1. Sequence and structure of Ninj1.

(A) Primary sequence of mouse Ninj1. Ninj1 consists of 152 amino acid (a.a.) with N-terminal and C-terminal ectodomains, two transmembrane domains (orange), and a short cytoplasmic domain. It can mediate the homophilic binding via the 12-residue adhesion domain (red) located at a.a. 26-37 on the N-terminal extracellular domain. **(B)** Structure of mouse Ninj1 and human NINJ1. Adhesion domain (a.a. 26-37) was indicated.

PURPOSE OF THIS STUDY

Obsessive-compulsive disorder (OCD) is a severe anxiety-related disorder that affects approximately 2 % of the population worldwide, regardless of age, gender, or cultural class. WHO has ranked OCD as one of the top ten non-fatal disorders that carry the highest global burden in terms of diminished quality of life. However, the mechanisms that underlie OCD remain to be elucidated due to the heterogeneity of this biological disorder and the involvement of a battery of genes.

Although the cell adhesion molecule Ninj1 plays diverse roles in peripheral tissues, its involvement in the central nervous system (CNS) remains uncharacterized. Moreover, *Ninj1* knockout (KO) mice manifest abnormal behavioral phenotypes, which are likely remininescent to neuropsychiatric disorder OCD. Therefore, in this study I investigated the relationship between Ninj1 and OCD as well as its functions in CNS. I expect that my findings could contribute to understanding the roles of Ninj1 in CNS and OCD.

MATERIALS AND METHODS

1. Animals

The mice were housed on a 12-hour light-dark cycle, with the dark cycle occurring from 19:00 PM to 07:00 AM and had access *ad libitum* to food and water. All animal experiments were approved by the Committees on Animal Research at Seoul National University (approval number SNU-130617-4-3).

1.1 *Ninj1* knockout mice. *Ninj1* knockout (KO) mice were generated as described previously [16]. Briefly, *Ninj1* KO mice were generated by removing exon 1 of the *Ninj1* gene located on the chromosome 13 by homologous recombination. *Ninj1* KO mice were backcrossed with the C57BL/6J strain for at least ten generations. The primer sequences for genotyping are as follows: wild-type (forward), 5′-GAG ATA GAG GGA GCA CGA CG-3′, neo (forward): 5′-ACG CGT CAC CTT AAT ATG CG-3′, and reverse, 5′-CGG GTT GTT GAG GTC ATA CTT G-3′.

1.2 "Knockout first", LacZ-tagged *Ninj1* tm1a mutant mice. Heterozygous *Ninj1 tm1a* mutant mice (*Ninj1*$^{+/tm1a}$) were generated by the Knockout Mouse Project (KOMP; University of California, Davis, USA) using the "knockout-first" strategy [26]. In the *Ninj1 tm1a* allele, a "*SA-LacZ-pA*" trapping cassette was inserted between exons 1 and 2 of the *Ninj1* gene to disrupt the expression of *Ninj1* mRNA. Genotyping primers used are as follows: for *wild-type* allele, forward (*Ninj1-F*, 5′-AAC CAG GGG AAT CAA GGA CAG TAG C-3′) and reverse (*Ninj1-ttR*, 5′-CCC ATC TCT CAT TAT CCC ATG CAG C-3′); for *Ninj1 tm1a* allele, forward (*lox-F*, 5'-GAG ATG GCG CAA CGC AAT TAA TG-3′) and reverse (*Ninj1-R*, 5′-ATC AGC TAT CCA TCC ATG CCT ACG G-3′).

1.3 Generation of *Ninj1* conditional knockout (*Ninj1* c.KO) mice.

Heterozygous *Ninj1 tm1a* mutant mice (*Ninj1*$^{+/tm1a}$) were mated with *Flpo* mice [C57BL/6N-Tg(CAG-Flpo)1Afst/Mmucd; University of California, Davis MMRRC Repository, USA] to obtain heterozygous *Ninj1 tm1c* mice (*Ninj1*$^{+/tm1c}$ or *Ninj1*$^{+/flox}$ mice), which do not have the trapping cassette. In parallel, *Ninj1* KO mice that carry one copy of the

Cre^{Syn} transgene (*Ninj1*$^{-/-}$; *Cre*^{Syn}) were produced by crossing *Ninj1* KO mice with synapsin I-Cre mice [B6.Cg-Tg(Syn1-cre)671Jxm/J; The Jackson Laboratory, USA]. Next, the *Ninj1*$^{+/flox}$ mice were bred with *Ninj1* KO mice bearing *Cre*^{Syn} (*Ninj1*$^{-/-}$; *Cre*^{Syn}), resulting in the production of control (*Ninj1*$^{+/-}$, *Ninj1*$^{+/-}$; *Cre*^{syn}, *Ninj1*$^{-/flox}$) and *Ninj1* c.KO (*Ninj1*$^{-/flox}$; *Cre*^{syn}) mice. Genotyping primers used are as follows: for *Cre*^{syn} transgene, forward (5′-GCG GTC TGG CAG TAA AAA CTA TC-3′) and reverse (5′-GTG AAA CAG CAT TGC TGT CAC TT-3′); for *tm1c* allele, forward (F_{tm1c}, 5′-AAG GCG CAT AAC GAT ACC AC-3′) and reverse (R_{tm1c}, 5′-CCG CCT ACT GCG ACT ATA GAG A-3′).

1.4 Genotyping procedure. Genotyping of mice was performed by polymerase chain reaction (PCR) analysis of genomic DNA isolated from toe tissue using the following procedure. Toe was incubated in lysis buffer of 1 % SDS, 0.1 M NaCl, 100 mM EDTA, 50 mM Tris (pH 8.0), and 1 μg/μL proteinase K at 55 ^{o}C overnight. NaCl (5 M) was then added to remove cell debris, followed by DNA precipitation with cold 2-propanol at –20 ^{o}C. DNA pellets were washed with cold 70 % ethanol. Five hundred nanograms DNA was used as templates for PCR. Products were run on 1.2 % agarose gels, followed by staining with

SYBR® green dye (Life technologies, USA) for visualization.

2. Inclusion criteria of hair loss

A mouse is recorded to have hair loss phenotype if it does not have hair in individual or multiple areas on its body or belly.

3. Behavioral tests

All the analyses presented in this study were performed with adult mice, which were littermates from mated heterozygotes or homozygotes, in a strict gender- and age-matched manner. The behavioral tests were conducted with the mice aged 8–20 weeks old by researchers blinded to the genotype of the mice. The examiners of the behavioral analysis were not blinded to the experimental groups, unless specified otherwise, as *Ninj1* KO mice showed hair loss phenotype. However, the behavioral analyses were confirmed by at least two independent researchers.

3.1 Grooming test. Grooming test was performed from 19:00–21:00 PM [27]. Mice were individually habituated to novel cages [25 cm length (L) x 20 cm width (W) x 20 cm height (H)] for 10 minutes.

Immediately thereafter, the mice were recorded by a video camera (Samsung HMX-F80; Korea). The total time spent grooming the face, head, or body was measured over 1-hour interval and presented as a percentage of the observation period. Abbreviations: L, length; W, width; H, height.

3.2 Marble-burying test. The marble-burying test was conducted as previously described [28]. Mice were individually placed in plastic cages (25 cm x 20 cm x 20 cm) that contained 5-cm-deep fresh bedding material. Twenty marbles (15 mm in diameter) were pre-arranged in 5 x 4 evenly spaced rows on top of this material. After 30 minutes, the number of buried marbles was counted. A marble was considered to be buried if at least two-thirds of its volume was covered by the bedding material.

3.3 Nestlet-shredding test. The nestlet-shredding test was performed as described previously [28]. Prior to the day of the experiment, the materials were dried at 55^{o}C overnight. The tested mouse was given one 5 cm x 5 cm shreddable cotton square (Nestlet; Ancare, USA) in a plastic cage (25 cm x 20 cm x 20 cm) for 30 minutes. The remaining

materials were collected and dried at 55^{o}C overnight. The weight of the nesting material that was shredded was calculated by weighing the dried nestlet before and after the test.

3.4 Open-field test. The open-field test was performed as previously described [9]. Each mouse was placed in the center of an open-field apparatus (40 cm x 40 cm x 40 cm) and then allowed to move freely for 10 minutes. The behavior of the mice was recorded using the video camera. The data were analyzed using EthoVision XT (Noldus, Netherlands) in a blind manner.

3.5 Elevated plus maze test. The elevated plus-maze (EPM) test was conducted as described previously with slight modification [9]. Plus maze apparatus is made of plastic material (closed arms, 25 cm x 5 cm x 15 cm; open arms, 25 cm x 5 cm x 0.5 cm). The arms of the maze were arranged orthogonally 50 cm above the floor. All of the mice were transferred to the behavioral testing room 1 hour before the first trial. To begin a trial, each mouse was placed at the center of the apparatus facing an open arm; then, it was allowed to move freely in the maze for 8 minutes. The EPM test was recorded using the video camera. The

maze was cleaned with a 70 % ethanol solution and dried after each trial to eliminate possible odour cues left by the previous mice. The data were collected and analyzed manually in a blind manner.

3.6 Three-chamber test. The test was performed as described previously with minor modifications [27]. The three-chamber apparatus consists of a transparent glass box with partitions dividing the box into three chambers (20 cm x 45 cm x 25 cm for each). There are two small entrances (5 cm x 5 cm) between each chamber, which can be opened or closed easily with glass doors. The wire cages used to contain the stranger mice are steel cylinder (12 cm in height, 9.0 cm in diameter, and 1 cm bars spaced). Mice were habituated to the testing room for at least 1 hour before starting behavioral tasks. To begin a trial, a tested mouse was introduced into the middle chamber and left to habituate for 5 minutes, while the two entrances to the center chamber were closed; then, an unfamiliar mouse (stranger) was placed into a wire cage in one of the side chambers. Next, the two entrances were opened to allow the tested mouse to freely explore all three chambers for 5 minutes. Time spent in each chamber and time spent exploring the targets were measured using the EthoVison XT.

3.7 Gait analysis. The apparatus has walls made of plastic and is 20 cm in height to prevent mice from escaping and 50 cm in length, with white papers placed along the floor of the entire apparatus. Mouse paws were dipped in red ink (forepaws) and blue ink (hindpaws). Mice were then introduced at the end of the apparatus and allowed to move freely along the corridor of the apparatus. The stride length for a trial was calculated as the longest stride for that trial.

3.8 Morris water maze test. The test was conducted similar to the method described previously [29]. The Morris water maze apparatus is a circular plastic pool (120 cm in diameter) that was filled with water (~23 ^{o}C) containing white and non-toxic tempera paint to make it opaque. A circular steel platform (12 cm in diameter) was submerged 1 cm beneath the surface of the water. For visible platform task, mice were tested for their ability to locate the submerged platform that was marked with a flag. For hidden platform test, mice were trained three trials per day with an inter-trial interval of 1 hour to find the hidden platform in the tank for five consecutive days. At day 6, the probe trial was given for 60 seconds with the platform removed from the pool.

Distance moved, numbers of crossing over the platform area, and percentage of time spent in four quadrants of the pool were analyzed using the EthoVision XT.

3.9 Hot plate test. Mice were placed on a hot plate apparatus (Socrel, DS-37; Italy) at 55 ^{o}C. The escape latency was measured as the time for the mouse to flick/lick its paws. A maximum cutoff time of 60 seconds was used to prevent thermal injury occurring to mice.

4. Plasmids. Ninj1 expression vectors were constructed as previously described [20,30]. Briefly, full-length mouse *Ninj1* (a.a. 1-152, NM_013610) cDNA was produced by reverse transcription (RT)-PCR from NIH-3T3 mouse fibroblasts and inserted into pCS2(+) (Myc tagged) plasmid. *Ninj1* was subsequently subcloned into pCS2(+)-GFP vector (GFP-Ninj1) or pTag2B-Flag (Flag-Ninj1). Plasmid of EGFP-N1 was obtained from Clontech (USA). For neuroligin 1 expression vector, plasmid of HA-tagged Neuroligin 1 (pCAG-HA-NL1) was purchased from Addgene (plasmid #15260, generated by Dr. Peter Scheiffele's lab). Plasmid of SEP-tagged NR2A (pCI-SEP-NR2A) was from Addgene (plasmid #23997, generated by Dr. Roberto Malinow's lab).

5. RNA interference. For *Ninj1* knockdown by small interfering RNA (siRNA), siNinj1 against mouse *Ninj1* (NM_013610) was synthesized and characterized as previously described [31]. Negative control siRNAs (siCtrl) was from Bioneer Inc. (Daejeon, Korea). Sequences of the siRNAs are as follows: siCtrl: 5'-CCT ACG CCA CCA AUU UCG UdTdT-3', siNinj1: 5'-ACC GGC CCA UCA AUG UAA ACC AUU A-3'. The cells were transfected for 72 hours with 50 pmol for 60 mm dish or 10 pmol for each well of 24-well plate of the siRNAs using Lipofectamine 2000 (ThermoFisher Scientific, USA) following the manufacturer's instructions.

6. Primary culture of cortical neurons and neuronal tranfection.

Mouse embryos at embryonic days 16.5–18.5 were isolated and incubated with trypsin-EDTA and DNAse for 20 minutes. After neutralization with fetal bovine serum (FBS), cortices were dissociated slowly with pipette 10 ml (15 times) and further with pipette 5 ml (10 times). Dissociated cells were filtered through cell strainer (70 μm; BD Bioscience, USA). After centrifuged and counted, cells were

resuspended in Neurobasal media supplemented with B27, glutamine, 100 units/mL penicillin, and 100 μg/mL streptomycin (all were from Gibco, Invitrogen, USA) and seeded onto 60 mm dishes or 24-well plates coated with 0.05 mg/mL poly-D-lysine (P6407; Sigma, USA). Neurons were maintained in an incubator with a humidified atmosphere of 95 % O_2 and 5 % CO_2 at 37 ^{o}C. Half of media were changed after 3 days *in vitro* (DIV 3) with fresh media supplemented with arabinofuranosyl cytidine (Ara-C; Sigma, USA) at final concentration of 1 μg/mL. From DIV 4, half of media were changed with fresh media every 3 days. For neuronal transfection, cortical neurons were transfected with indicated vectors on DIV 4 or DIV 7 using Lipofectamine 2000 reagent according to the manufacturer's protocols.

7. Preparation of synaptosomes and synaptosomal fractions.

The brains of 8-week-old mice were isolated, cut into small pieces with scissors, and homogenized in ice-cold HEPES-sucrose buffer (320 mM sucrose and 4 mM HEPES; pH 7.4) that was supplemented with a protease inhibitor cocktail (Calbiochem, USA). Homogenates (Hom.) were centrifuged at low-speed (1000×*g* for 5 minutes) to obtain the P1

pellet (nuclear pellet and debris). The supernatant (S1, synaptosome suspension) was subsequently centrifuged at high speed (10,000×g for 15 minutes) to get pellet P2 (crude synaptosomal fraction) and supernatant (S2, light membrane and cytosolic fraction). Next, the P2 pelleted fraction was resuspended in the ice-cold HEPES-sucrose buffer and re-centrifuged at 10,000×g for 15 minutes to obtain pellet P2' (washed synaptosomal fraction). The P2' pelleted fraction was further lysed by hypo-osmotic shock in nine volumes of ice-cold distilled water that contained the protease inhibitor cocktail, pipetted 3 times and rapidly supplemented with ice-cold 1 M HEPES stock solution, which was adjusted to a final concentration of 4 mM HEPES, to obtain S3 (lysed synaptosomal fraction). S3 was then centrifuged at 21,000×g for 20 minutes to yield pellet LP1 (synaptosomal membrane fraction) and supernatant S3' (crude synaptic vesicle fraction). Then, 10 μg of total protein from each fraction was subjected to Western blot analysis.

8. Cell culture, transfection, and inhibitor treatment. Human Embryonic Kidney 293T (HEK293T) cells were cultured in Dulbecco's Modified Eagle's Medium (DMEM) supplemented with 10 % (v/v) FBS, 100 units/mL penicillin, and 100 μg/mL streptomycin

at 37 ^{o}C in an incubator with a humidified atmosphere of 5 % CO_2 and 95 % O_2. Cells were transfected with indicated plasmids using polyethylenimine reagent (PEI; Sigma, USA). Cells were incubated for 8 hours with cycloheximide (CHX, 500 μM; Sigma, USA), in the presence or absence of lysosomal inhibitors (50 mM NH_4Cl and 100 μM chloroquine; Sigma, USA) or a proteasome inhibitor (10 μM MG132; Calbiochem, USA). After treatment, cells were lysed and subjected to Western blot analysis.

9. Antibodies. The anti-Ninj1 rabbit polyclonal antibody was generated and characterized as previously described [30]. Antibodies used for the Western blots and/or immunostainings are β-actin (Sigma; A2066, 1:5000), α-tubulin (Biogenex; MU-121UC, 1:5000), GAPDH (Santa Cruz; SC-365062, 1:1000), NMDAR 1 (Cell Signaling Technology; 5704S, 1:2000), NMDAR 2A (Millipore; 05-901R, 1:2000), NMDAR 2B (ThermoFisher Scientific; MA1-2014, 1:2000), GluR1 (Abcam; ab31232, 1:2000), GluR2 (Millipore; MAB397, 1:2000), NeuN (Millipore; MAB377, 1:500), PSD95 (Neuromab; 73-028, 1:2000), synaptophysin (Millipore; MAB5258-20UG, 1:2000), synapsin (BD Biosciences; 611392, 1:2000), FosB (Santa Cruz; SC-48,

1:200), c-Fos (Santa Cruz; SC-52, 1:1000), GFP (Abcam; Ab6556, 1:200), Flag (Sigma; F1804, 1:500), and β-galactosidase (Millipore; AB1211-5MG, 1:200).

10. Western blot analysis. Specimens were homogenized in a lysis buffer containing 20 mM Tris-HCl (pH 7.5), 150 mM NaCl, 1 mM Na_2EDTA, 1 mM EGTA, 1 % Triton, 2.5 mM sodium pyrophosphate, 1 mM beta-glycerophosphate, 1 mM Na_3VO_4, and 1 μg/mL leupeptin plus the protease inhibitor cocktail. Protein concentrations were measured by the BCA protein assay kit (Pierce, USA). Total proteins were separated by SDS-PAGE. Proteins with low molecular weight such as Ninj1 were separated on 12.5 % tricine gels.

11. Histochemical analysis of reporter gene expression. Cryosections (16 μm) were equilibrated in 0.1 M phosphate-buffered saline (PBS) at pH 7.4 for 15 minutes at room temperature. Samples were incubated with X-gal solution containing 2 mg/mL 5-bromo-4-chloro-3-indolyl-β-D-galactopyranoside (ThermoFisher Scientific, USA), 0.5 % Nonidet P-40 (NP-40), 5 mM potassium ferrocyanide, and 5 mM potassium ferricyanide in PBS at 37 ^{o}C overnight. Reaction was

stopped by rinsing three times (5 minutes each) with PBS. Samples were counterstained with nucleus fast red (NFR) solution (Sigma, USA), dehydrated in a series of graded ethanol, cleared in xylene, and mounted with Crystal Mount (Biomeda, USA). Samples were examined under a microscope (Leica DM5000B; Leica Microsystems, Inc., Germany). Multiple images covering whole-brain sections were merged by photoshop to obtain panoramic images of brain stained with X-gal.

12. Immunohistochemical analysis. Mice were perfused with PBS (pH 7.4) and 4 % paraformaldehyde (PFA) in PBS. Brains were isolated, fixed in 4 % PFA/PBS overnight, dehydrated in series of gradient sucrose (10, 20, and 30 %) in PBS. After embedded in optimal cutting temperature (OCT) embedding compound (Tissue-Tek, Japan), brains were coronally sectioned into 16 μm slices by free-floating method using a microtome (HM525; Thermo Scientific, USA). Brain slices were washed three times (5 minutes each) with PBS (pH 7.4), blocked with blocking buffer containing 0.3 % Triton X-100 and 5 % (v/v) donkey serum (Sigma, USA). Primary antibodies were diluted in blocking buffer and incubated at 4 ^{o}C overnight. On the following day, samples were washed three times (10 minutes each) with PBS (pH 7.4),

and treated with Alexa 488- or 546-conjugated donkey secondary antibodies (Molecular Probe, Invitrogen, USA) for 1 hour at room temperature. Samples were counterstained with Hoechst 33442 (Molecular Probe, Invitrogen, USA) and mounted on silane-coated glass slides (Muto-Glass, Tokyo, Japan) with Gel Mount (Biomeda, USA). Samples were visualized under a confocal microscope (LSM 700; Carl Zeiss, Germany).

13. Immunocytochemical analysis. Samples were fixed in 4 % PFA/PBS or cold methanol for 10 minutes. After permeabilization with 0.2 % Triton X-100/PBS (pH 7.4) for 10 minutes on ice, non-specific proteins were blocked with the blocking buffer. Primary antibodies and fluorochrome-conjugated secondary antibodies were treated following the above procedure for immunohistochemical analysis.

14. Golgi staining. Golgi staining was performed by using standard Golgi-Cox impregnation technique with the FD Rapid GolgiStain Kit (Neurodigitech, USA). Brains of 8-week-old WT and *Ninj1* KO mice were transcardially perfused with heparinized PBS (pH 7.4) and post-fixed with 4 % PFA. Brains were impregnated in Golgi-Cox solution of

the kit for 18 days at room temperature (~25 ^{o}C) in the dark. Serial coronal sections at 150 μm thickness of mouse brains were obtained by using the microtome (HM525) and stained with the kit following strictly the manufacturer's protocol. Neurons were visualized under a microscopy (Leica DM5000B) at ×10- and ×40-magnifications.

15. Transmission electron microscopy. Eight-week-old WT and *Ninj1* KO mice were deeply anesthetized, intracardially perfused with heparinized PBS (pH 7.4), and fixed with a freshly prepared fixative solution containing 2.5 % glutaraldehyde and 2 % PFA in PBS (pH 7.4). Brains were isolated, gradually frozen in dry ice-cold isopentane (Junsei, Korea), and sectioned with the microtome at 100-μm thickness. The sections of brain were post-fixed in the modified Karnovsky's fixative solution of 2.5 % glutaraldehyde and 2 % PFA in 0.05 M sodium cacodylate buffer (pH 7.2) for 2 hours at 4 ^{o}C, osmicated with 1 % osmium tetroxide in 0.05 M sodium cacodylate buffer (pH 7.2) for 2 hours at 4 ^{o}C, dehydrated in graded ethanol series (30, 50, 70, 80, 90, and three times 100 %; for 10 minutes each) at room temperature, embedded in a mixture of propylene oxide and Spurr's resin for 2 hours, and polymerized for 24 hours at 70 ^{o}C. Ultrathin sections containing

striatum (70 nm) were cut with RMC ultramicrotome (MT-X; Tucson, Arizona, USA), mounted on formvar-coated nickel grids, stained with 2 % uranyl acetate and Reynold's lead citrate, and examined under an electron microscope (JEOL JEM-1010; Tokyo, Japan) equipped with a GaJ05 CCD camera (Gatan Inc., USA) at an electron beam of 80 kV. Samples were randomly photomicrographed at a ×60,000 magnification and used for quantification.

16. Neurochemical analysis. Samples were collected from the cerebrums of WT and *Ninj1* KO mice. All specimens were homogenized in 0.1 M perchloric acid in glacial acid (Sigma, USA) containing 100 ng/mL 3,4-dihydroxybenzylamine (DHBA; Sigma, USA) as an internal standard. Homogenates were centrifuged for 10 minutes at 10,000*g*. After microfiltration, supernatants were analyzed for levels of glutamate, norepinephrine, dopamine, serotonin, and 5-hydroxyindoleacetic acid (5-HIAA, the main metabolite of serotonin) with corresponding standards purchased from Sigma(USA), using high-performance liquid chromatography-electrochemical detection (HPLC-ECD) system (Gilson, USA) at the NICEM (SNU, Korea).

17. Cell surface biotinylation assay. Biotinylation was carried out following the previously described protocol [32]. Briefly, cells were washed twice with ice-cold PBS, incubated at 4 ^{o}C with 0.5 mg/mL Sulfo-NHS-LC-biotin (Pierce, USA) for 45 minutes, washed twice with PBS, and neutralized with 1X tris-buffered saline (pH 7.6). Cell lysates were prepared in a cell lysis buffer containing NP-40. After precipitated with streptavidin-conjugated beads (GE Healthcare, USA), biotinylated proteins were eluted by boiling with loading sample buffer and subjected to Western blot analysis.

18. Whole-cell patch-clamp recordings for brain slices. Nine-to 11-week-old male WT and *Ninj1* KO littermates were anesthetized by intraperitonial injection of avertin (2, 2, 2-tribromoethanol) and sacrificed. The isolated brains were immersed in ice-cold artificial cerebrospinal fluid (ACSF; in mM: 125 NaCl, 2.5 KCl, 1.25 NaH_2PO_4, 25 $NaHCO_3$, 25 dextrose, 2 $CaCl_2$, 2 $MgCl_2$, 3 Na-pyruvate, and 1 ascorbic acid; maintained at pH 7.4 by gassing with 95 % O_2 and 5 % CO_2) and sliced into 250μm-thick coronal sections using a Vibratome (VT-1200S; Leica, Germany). The slices were transferred to an incubation chamber filled with NMDG recovery

solution (in mM: 92 N-methyl-D-glucamine (NMDG), 92 HCl, 30 $NaHCO_3$, 2.5 KCl, 0.5 $CaCl_2$, 10 $MgSO_4$, 1.2 NaH_2PO4, 20 HEPES, 5 Na-ascorbate, 3 Na-pyruvate, 2 thiourea, and 25 dextrose, maintained at pH 7.4 by gassing with 95 % O_2 and 5 % CO_2) for 15 minutes at 36 ^oC. The slices were then maintained in oxygenated ACSF at room temperature for at least 1 hour prior to use. Ventral lateral (VL) thalamic neurons were recorded in oxygenated ACSF at 28–30 ^oC and visualized under an upright microscope (BX-51WI; Olympus, Japan). Whole-cell patch clamp recordings were performed using glass pipettes (3–4 MΩ) filled with an internal solution (in mM: 130 K-gluconate, 2 NaCl, 4 $MgCl_2$, 20 HEPES, 4 Na_2ATP, 0.4 Na_3GTP, and 0.5 EGTA, pH 7.25, 290–295 mOsm). VL thalamic neurons were ruptured at –67mV holding, and all recording processes were performed at that voltage to negate inhibitory post-synaptic current (IPSC) influence. Miniature excitatory post-synaptic current (mEPSC) was recorded for at least 2 minutes at voltage clamp gap-free mode. The cells were treated with 1 μM tetrodotoxin (TTX) and 10 μM bicuculine by bath application during whole-cell recordings. Access resistance was routinely monitored throughout the recordings, and data were excluded if the access resistance varied by more than 25 % of the initial state or the

holding current was not stable. All data were acquired with a patch clamp amplifier (Multiclamp 700B; Molecular Devices, USA), digitized at 1kHz with an A-D converter (Digidata 1550; Molecular Devices, USA), and 2 minutes of each recording was analyzed using Clampfit (Molecular Devices, USA).

19. Drug treatment. Mice were given fluoxetine with a dose of 18 mg/kg (LKT Laboratories, USA) via drinking tap water for three weeks [9]. Memantine hydrochloride (Sigma, USA) was dissolved in PBS and intraperitoneally injected daily at dose of 10 mg/kg for three weeks.

20. Statistical analysis. Statistical analyses were carried out using GraphPad Prism version 6.0. Differences between two groups were analyzed by using the two-tailed Student's *t* and Fisher's exact tests and considered to be statistically significant if the *P* value was < 0.05: $*P < 0.05$; $**P < 0.01$; $***P < 0.001$; $^{\#}P < 0.0001$.

RESULTS

1. *Ninj1* KO mice show hair loss and self-injuries

To investigate the biological functions of Ninj1 in the CNS, we generated *Ninj1* KO mice [16]. Some of them had dome-shaped heads and died within 2 months after birth (**Figure 2A**). In addition, approximately 2 % *Ninj1* KO mice exhibit increased levels of motor hyperactivity compared with wild-type (WT) littermates, including repetitive circling (**Figure 2B**) and hyperlocomotion (**Figure 2C**), starting at 3 weeks of age. However, most of the homozygous *Ninj1* KO mice were healthy and similar to their wild-type (WT) littermates (**Figure 3**), and they were therefore used in further experiments.

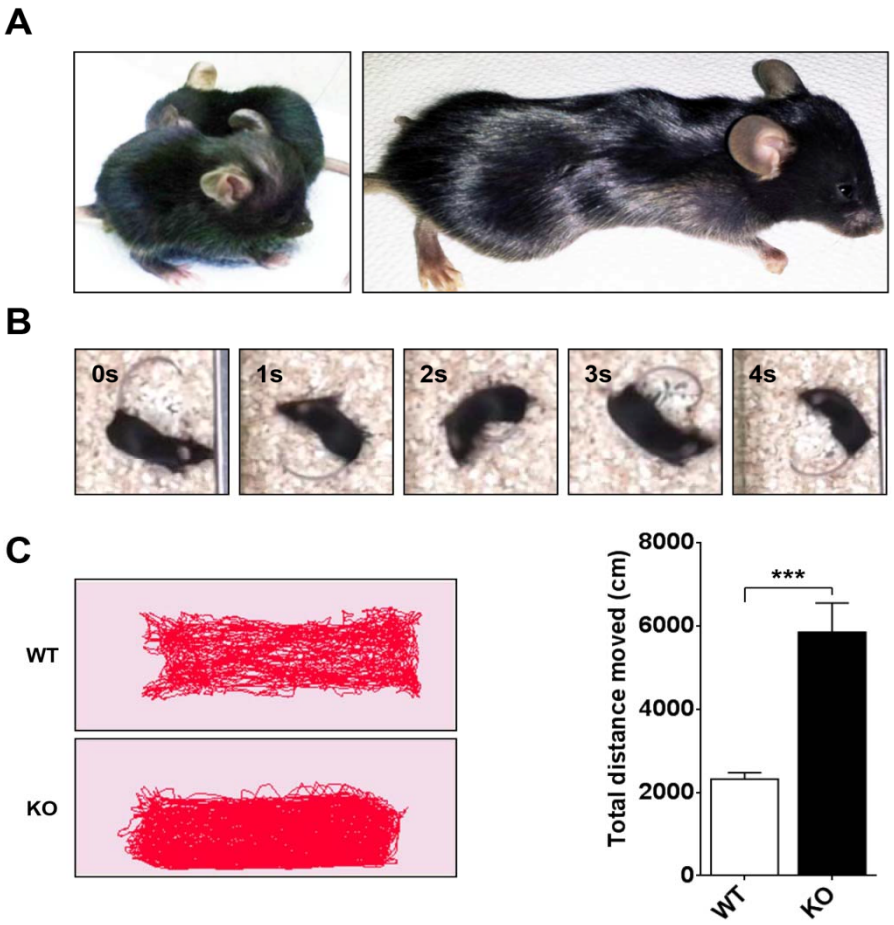

Figure 2. Characterization of the abnormal phenotypes of the *Ninj1* KO mice.

(A), Some *Ninj1* KO mice had dome-shaped heads and small bodies

and died within two months. (**B, C)**, Some *Ninj1* KO mice displayed circling behavior and hyperactivity in their cages. (**B)**, A series of images showing that the *Ninj1* KO mice ran repetitively in many circles. (**C**) Representative images of the trajectories (left) and a quantification of distance moved (cm) (right) of WT and the *Ninj1* KO mice during a 10-minute exploration of the cage (n = 6 mice per genotype). The error bars indicate the standard error of the mean (s.e.m.).

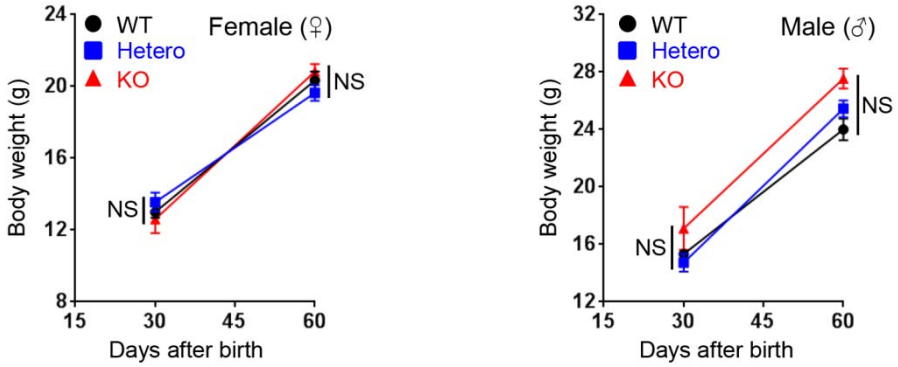

Figure 3. Characterization of the body weight of the *Ninj1* KO mice.

At the indicated times, no significant differences in body weight were observed between the genotypes for either males or females. Numbers of mice: P30, male, WT (n = 9); Hetero (n = 11); KO (n = 9); and female, WT (n = 7); Hetero (n = 9); KO (n = 8); P60, male, WT (n = 10); Hetero (n = 11); KO (n = 9) and female, WT (n = 12); Hetero (n = 11); KO (n = 12). The error bars indicate s.e.m.

Surprisingly, at three months of age, the *Ninj1* KO mice began to develop hair loss (approximately 70 % penetrance; **Figure 4A**) and had hair trapped in their teeth (**Figure 4B**), suggesting that the *Ninj1* KO mice exhibited excessive grooming behaviors. Moreover, approximately 10 % of the *Ninj1* KO mice developed lesions on their face, ear, eye, scruff, back, inguinal and axillary areas, in both male and female mice at 6–9 months of age, regardless of the presence of cage mates, thereby excluding the possibility that lesions were resulted by allo-grooming or fighting (**Figure 5A**). To check whether peripheral defects would be a reason for the lesions, I performed a sensory test but failed to see any difference between *Ninj1* KO and WT mice (**Figure 5B**). Thus, this phenotype is suggestive of excessive self-injurious behavior, which was reported in OCD-like mice with deficiencies in the *Hoxb8*, *Sapap3*, or *Slitrk5* gene [8-10].

Hair loss was also observed in WT mice that were caged with the *Ninj1* KO mice (**Figure 6A**). Specifically, when placing mice of each genotype together, the WT mice developed hair loss and then regrew the hair after they were separated from their *Ninj1* KO counterparts (**Figure 6B**). These observations indicate that *Ninj1* KO mice compulsively allo-groomed their cage mates, resulting in the hair

loss phenotype, which is very similar to the obsessive-compulsive spectrum disorder trichotillomania [33,34]. Collectively, these findings suggest that *Ninj1* KO mice are reminiscent of mouse models of neuropsychiatric disorders such as OCD.

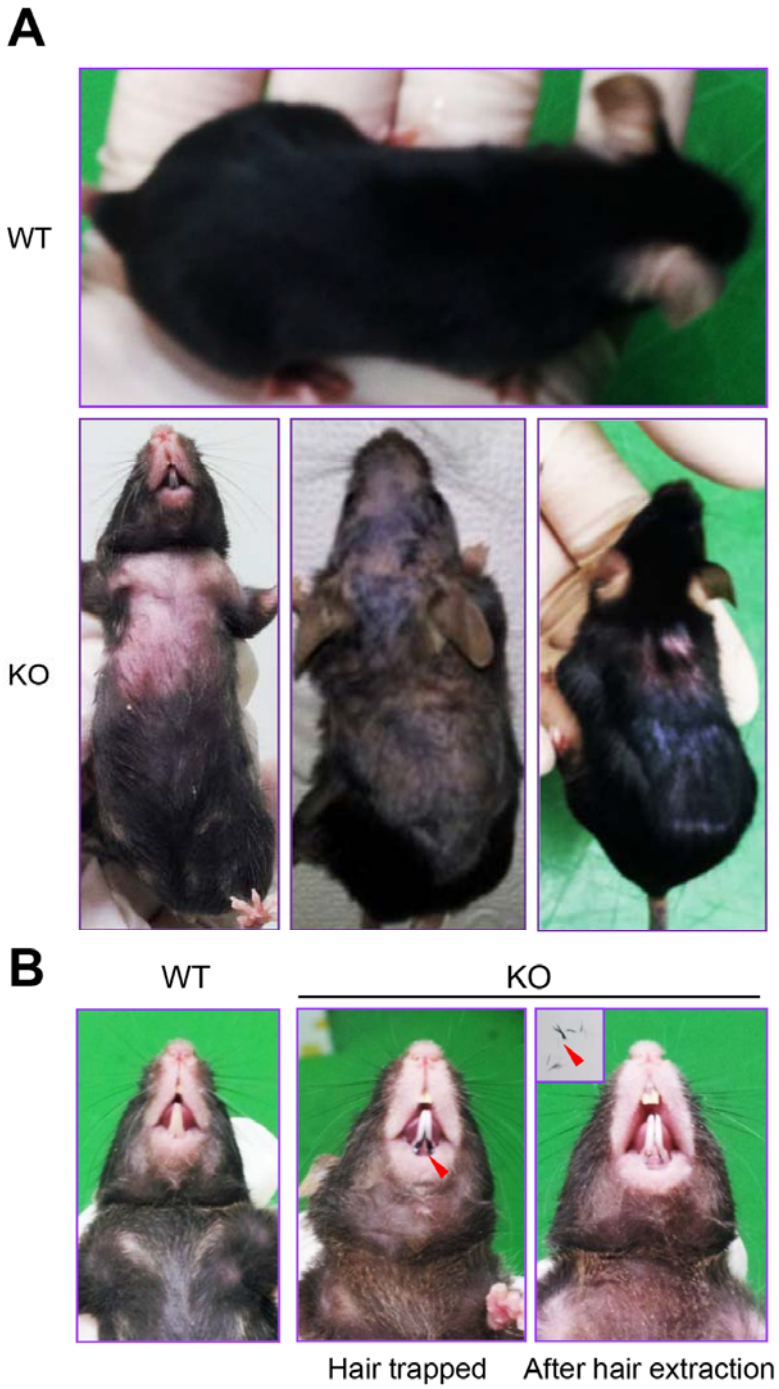

Figure 4. *Ninj1* KO mice show hair loss phenotype.

(**A**), Representative images of WT and *Ninj1* KO mice at four months of age. Hair loss in *Ninj1* KO mice, but not WT littermates. (**B**), Accumulation of hair in the teeth of the *Ninj1* KO but not the WT mice. Representative images of trapped hair in the teeth of *Ninj1* KO mice (middle, red arrowhead) and extracted from the teeth (*right*, red arrowhead). No trapped hair was observed in the teeth of the WT mice (*left*).

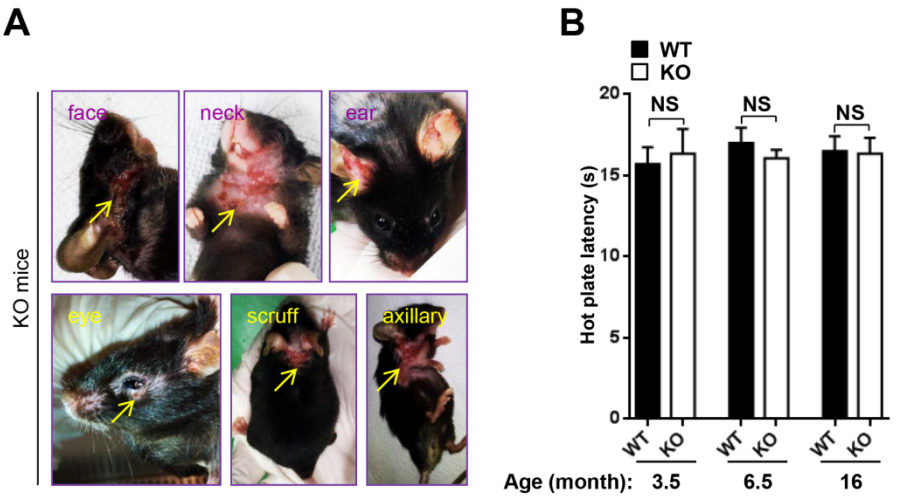

Figure 5. *Ninj1* KO mice showed self-injuries.

(**A**), Representative images showing injuries (yellow arrows) in various areas of *Ninj1* KO mice. (**B**), Hot plate test was performed at 55 ^{o}C (*n* = 10 to 13 mice per genotype). *Ninj1* KO mice showed normal nociception, similar to that in WT littermates.

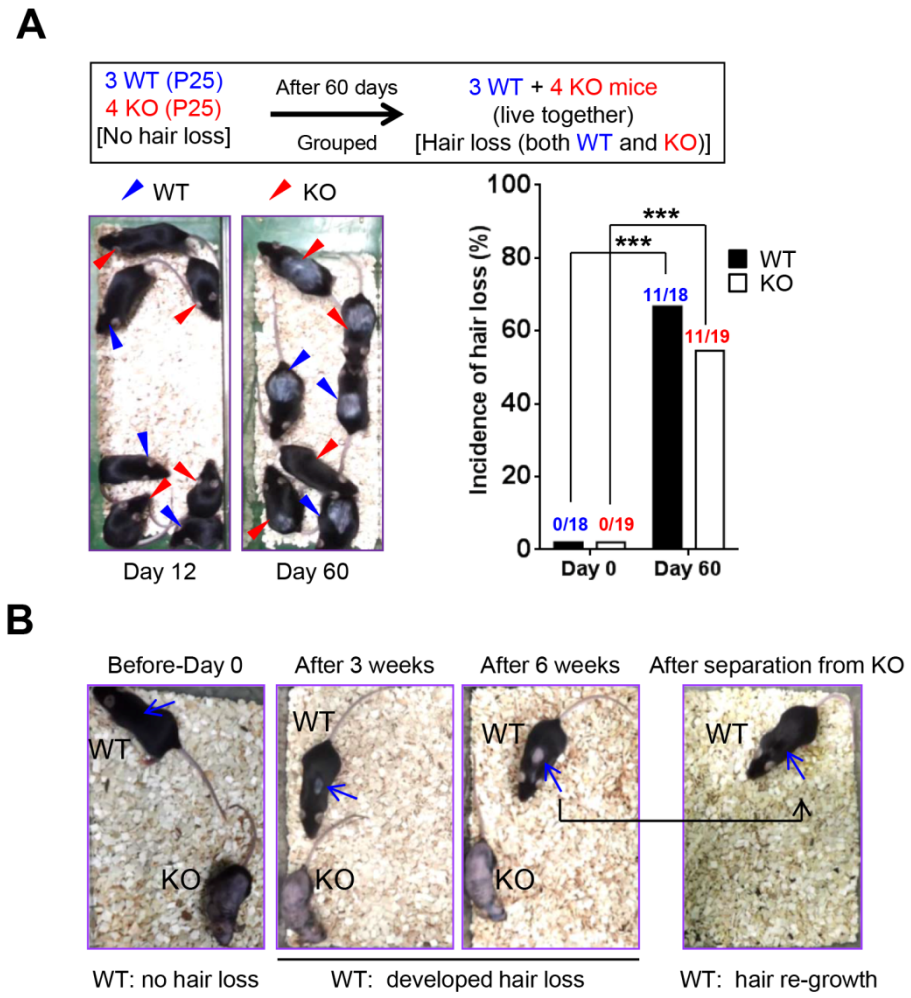

Figure 6. *Ninj1* KO mice allo-groom their cage mates.

(A), Hair loss phenotype in both WT (blue arrowheads) and *Ninj1* KO (red arrowheads) mice due to the allo-grooming behavior of the *Ninj1* KO mice. Mice were placed in the same cage (3 to 4 mice per genotype) at the time of weaning [approximately 25 days after birth (P25)]. (**B**), *Ninj1* KO mice excessively allo-groomed their cage mates,

which caused hair loss on their backs (indicated by a blue arrow). After they were separated from the *Ninj1* KO mice, the WT mice re-grew their lost hair, illustrating the excessive allo-grooming behaviors of the *Ninj1* KO mice.

2. *Ninj1* KO mice display increased repetitive and anxiety -like behaviors but normal social interaction and cognitive function

Ninj1 KO mice and their WT littermates were subjected to a number of behavioral assays for neuropsychiatric disorders including tests for repetitive and anxiety-like behaviors as well as social interaction, motor, and cognitive tests.

Repetitive behaviors are a heterogeneous group of behaviors present in many neuropsychiatric disorders and may manifest as motor stereotypies, such as washing hands, locking and unlocking doors, pulling hair, or self-injurious behaviors [3,35], which can be modeled in rodents via certain behavioral assays, including grooming and marble-burying tests [9,27,28]. The abnormal phenotypes of *Ninj1* KO mice suggested that they displayed excessive grooming behavior. Accordingly, subsequent measurements revealed increased duration of self-grooming in *Ninj1* KO mice (**Figure 7A**). In addition to over-grooming, the *Ninj1* KO mice demonstrated compulsive-like behaviors in marble-burying (**Figure 7B**) and nestlet-shredding tests (**Figure 7C**) as they showed a marked increase in the number of marbles buried and percentage of shredded materials compared with WT littermates.

Anxiety is a typical feature of neuropsychiatric disorders such as ASD and OCD [36,37], and therefore, anxiety-like behaviors of *Ninj1* KO mice and WT littermates were examined using two paradigms. In the open field test, *Ninj1* KO mice spent less time in the center zone of the open field (**Figure 8, A and B**), whereas total activities were not different between the two genotypes (**Figure 8C**). Furthermore, *Ninj1* KO mice explored the risk areas (open arms) less and the safe areas (closed arms) more than WT littermates (**Figure 9**) in the elevated plus maze test. Together, these results indicate that *Ninj1* KO mice were more anxious than their WT counterparts.

Because *Ninj1* KO mice display several symptoms of ASD, we next determined whether *Ninj1* KO mice have deficits in social interaction, which are the most recognizable manifestation of autistic behaviors in humans [27,29]. In three-chamber test, which measured time a mouse spent in the compartment containing the social partner (**Figure 10A**) or in close interaction (**Figure 10B**), *Ninj1* KO mice exhibited normal social interaction behavior as they displayed a preferential interaction with the social partner rather than with the empty cage, similar to WT littermates (**Figure 10**).

Taking into account the contribution of motor deficits to

behavioral impairment, we further tested motor functions by footprint test. The motor activity of *Ninj1* KO mice was indistinguishable from their WT littermates in both male and female mice (**Figure 11**).

To examine whether the abnormal behavioral phenotypes in *Ninj1* KO mice are associated with a gain or a loss of cognitive ability, we tested spatial learning and memory in *Ninj1* KO mice using the Morris water maze (MWM) test (**Figure 12**). *Ninj1* KO mice learned to locate and mount a visible platform as well as WT littermates (**Figure 12A**). When the platform was hidden, both *Ninj1* KO and WT mice showed similar learning curves in the training phase of the MWM test (**Figure 12B**). During the probe trial, *Ninj1* KO and WT mice performed comparably as they both displayed a similar number of platform passes and a significant preference for the target versus the opposite quadrant (**Figure 12, C-E**). These results imply that *Ninj1* KO mice show normal cognitive ability.

Collectively, these data indicate that the repetitive and anxiety-like behaviors of *Ninj1* KO mice appear to be related with neuropsychiatric disorders such as OCD.

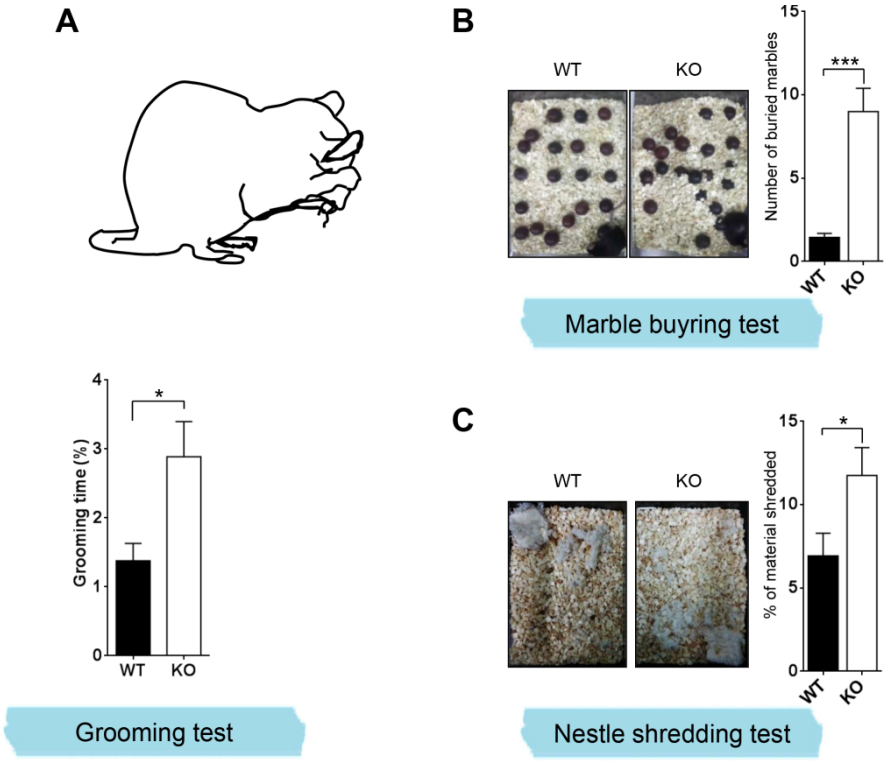

Figure 7. *Ninj1* KO mice show repetitive behaviors in marble-burying (MBT) and nestlet-shredding tests (NST).

(**A**), Increased self-grooming in *Ninj1* KO mice (*n* = 8 mice per

genotype). (**B**), Representative images of MBT from WT and *Ninj1* KO mice (*left*) and a histogram (*right*) showing quantification of numbers of buried marbles over the course of 30 minutes (n = 9 mice per genotype). (**C**), Representative images of NST from WT and *Ninj1* KO mice (*left*) and a quantification graph (*right*) presents the percentage (%) of material shredded after 30 minutes for each genotype [n = 16 (WT) and 15 (KO)]. The *Ninj1* KO mice groomed more time (**A**), buried more marbles (**B**), and shredded more material (**C**) compared with their WT littermates. All of the data are presented as the mean ± s.e.m.; $*P < 0.05$; $***P < 0.001$; two-tailed Student's t-test. The error bars indicate s.e.m.

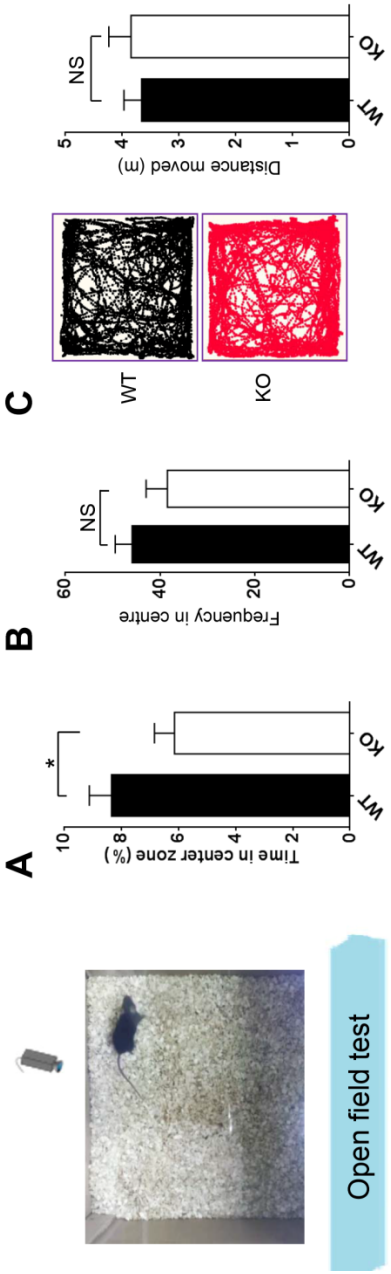

Figure 8. *Ninj1* KO mice show anxiety-like behaviors in open field test (OFT).

WT and *Ninj1* KO mice were evaluated using the open field test (OFT). (**A, B**) The graphs show the time in centre zone (**A**) and the frequency (number of centre zone visits; **B**) with which the *Ninj1* KO mice and their WT littermates explored the centre zone of the open field arena; *n* = 16 mice per genotype. (**C**), Examples of the trajectories (*left*) and distance moved (m) (*right*) of WT and *Ninj1* KO mice during a 10-minute exploration of the open field. All of the data are presented as the mean ± s.e.m.; $*P < 0.05$; NS, not significant; two-tailed Student's *t*-test.

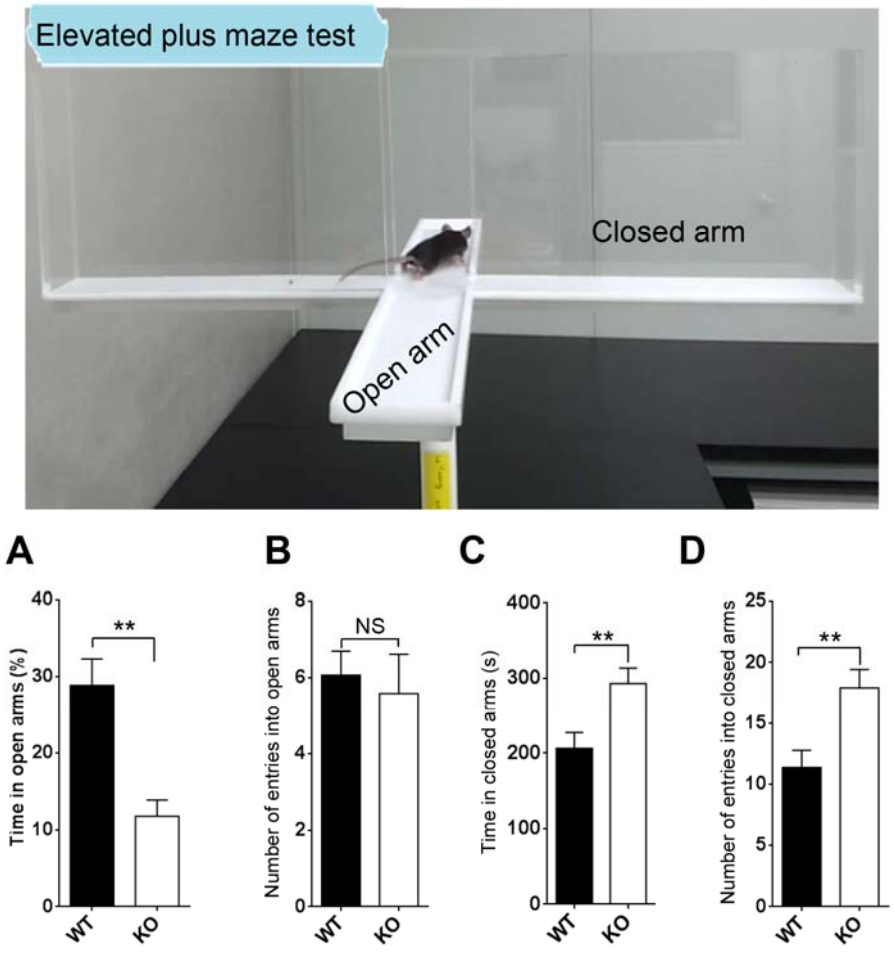

Figure 9. ***Ninj1*** **KO mice show anxiety-like behaviors in elevated plus maze (EPM) test.**

Quantification graphs that show the time spent in the open arms (**A**),

the number of entries into the open arms (**B**), the time spent in the closed arms (**C**), and the number of entries into the closed arms (**D**) in the EPM test; n = 14 (WT) and 11 (KO). Note that the *Ninj1* KO mice spent less time in the open arms and more time in the closed arms than their WT littermates. All of the data are presented as the mean ± s.e.m.; $^{**}P < 0.01$; NS, not significant; two-tailed Student's *t*-test.

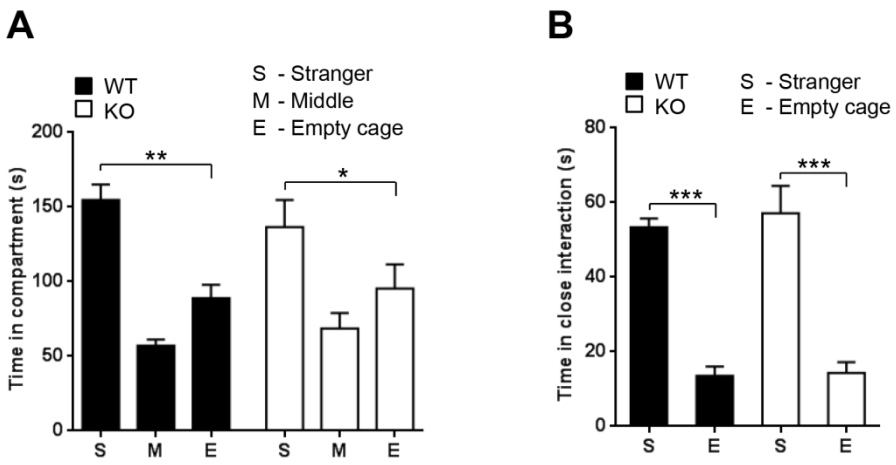

Figure 10. *Ninj1* KO mice display normal social interaction.

Three chamber tests. *Ninj1* KO mice displayed normal social interactions as they spent more time exploring the compartment containing the social partner **(A)** and time in close interaction with the social partner **(B)**, similar to WT mice did (n = 7 mice per genotype). *$P < 0.05$, **$P < 0.01$, ***$P < 0.001$; two-tailed Student's t-test. Error bars indicate s.e.m.

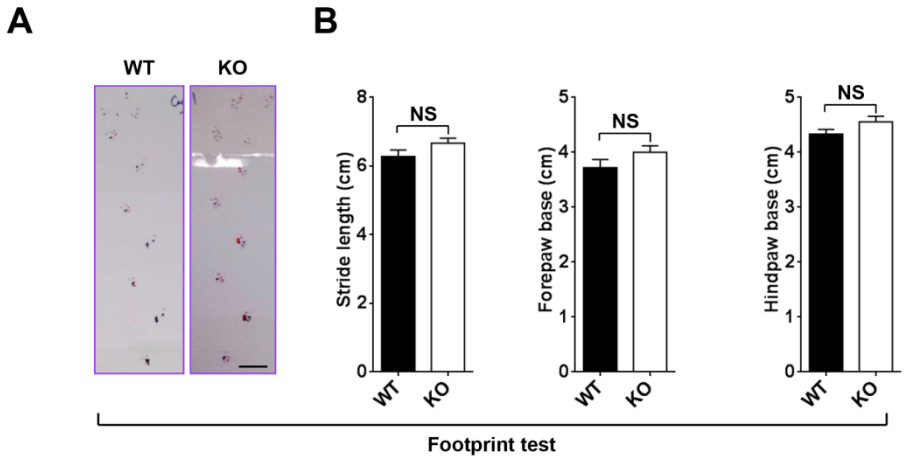

Figure 11. *Ninj1* KO mice showed normal motor performance in foot print test (FPT).

In this test, mouse paws were dipped in ink (forepaw: red, hindpaw: blue) and mice were allowed to walk along a corridor (40 cm in length). Representative footprint images of WT and *Ninj1* KO mice in FPT **(A)** and measurements of stride lengths (*left*) and base widths of forepaws (*middle*) and hind paws (*right*) were quantified (n = 9 mice per genotype) **(B)**. *Ninj1* KO mice had normal motor function compared with WT littermates in FPT. Scale bar: 2 cm. NS, not significant; two-tailed Student's *t*-test. Error bars indicate s.e.m.

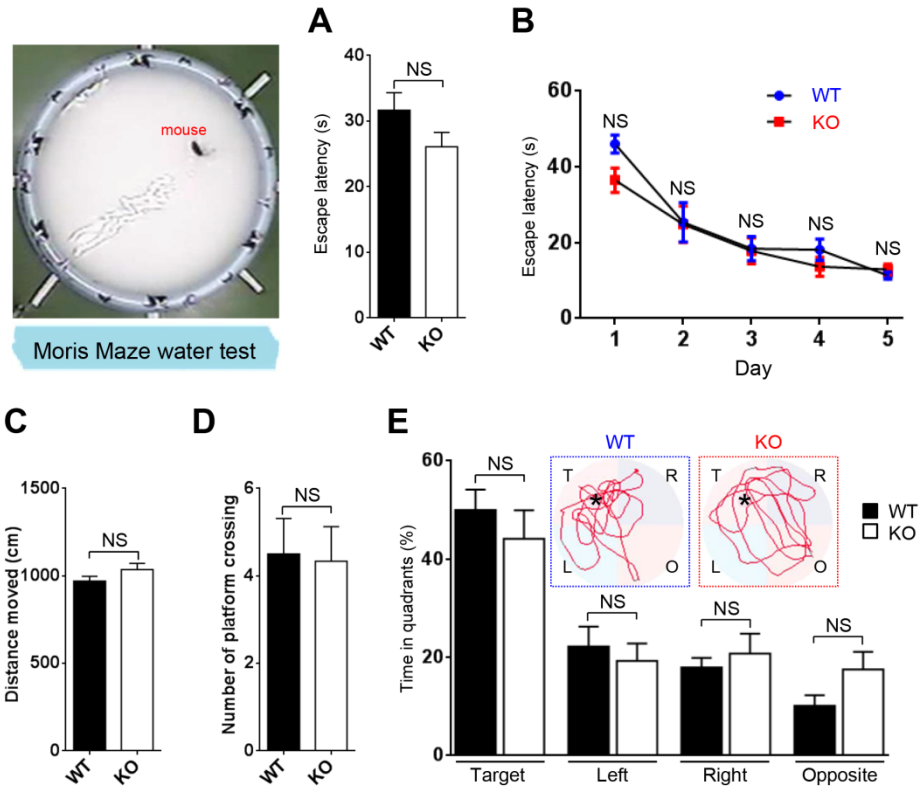

Figure 12. *Ninj1* KO mice show normal spatial learning and memory in Morris water maze test (MWM).

(A), Visible platform test. *Ninj1* KO mice recognized the visible platform as well as WT littermates as indicated by escape latency (s). **(B),** Hidden platform test. The curves show latency to reach the hidden platform each day during spatial training in the MWM of WT (blue circles) and *Ninj1* KO (red squares) mice. *Ninj1* KO mice showed similar capacities to find the hidden platform when compared with WT littermates. **(C-E),** Probe trial test on day 6. *Ninj1* KO mice swam similar distances **(C)** and had similar frequencies of crossing the former hidden platform site **(D)** relative to WT littermates. **(E)** Representative trajectory images (*top*) and graph (*bottom*) showing that WT and *Ninj1* KO mice exhibited comparable memory, as indicated by abilities to find the former hidden platform area (n = 9 to 12 mice per genotype). NS, not significant; two-tailed Student's t-test. Error bars indicate s.e.m. Abbreviations: T, target; O, opposite; R, right; and L, left. Black asterisks indicate the hidden platform sites.

3. Alleviation of behavioral abnormalities of *Ninj1* KO mice by fluoxetine treatment

I subsequently tested whether I could pharmacologically rescue the abnormal behaviors of *Ninj1* KO mice by treating *Ninj1* KO mice with fluoxetine, which is a FDA-approved SSRI drug for patients with depression or OCD and reportedly alleviates repetitive behaviors in mice [8,9,38]. Chronic oral administration of fluoxetine prevented the progression of hair loss (**Figure 13**) and reduced the duration of self-grooming (**Figure 14A**) and anxiety-like behavior (**Figure 14B**) of *Ninj1* KO mice without affecting their total activity (**Figure 14C**) in the open field test. Collectively, these results indicate that the aberrant behaviors in *Ninj1* KO mice could be ameliorated by fluoxetine.

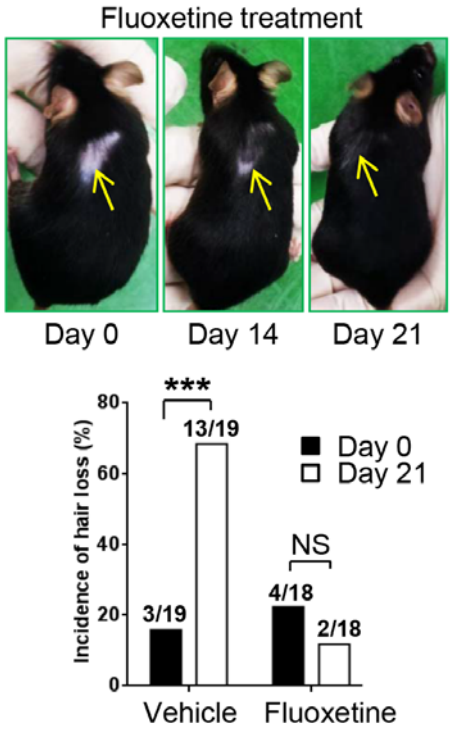

Figure 13. Fluoxetine treatment prevented the progression of hair loss in *Ninj1* KO mice.

WT and *Ninj1* KO mice were given vehicle (tap water) or fluoxetine (in drinking water) over the course of 3 weeks. Representative images (*upper* panel) and a quantification (*lower* panel) demonstrate that fluoxetine treatment prevented the progression of hair loss (arrows) in *Ninj1* KO mice. $^{***}P < 0.001$; NS, not significant; Fisher's exact test. The number of mice used is included in the bar graph.

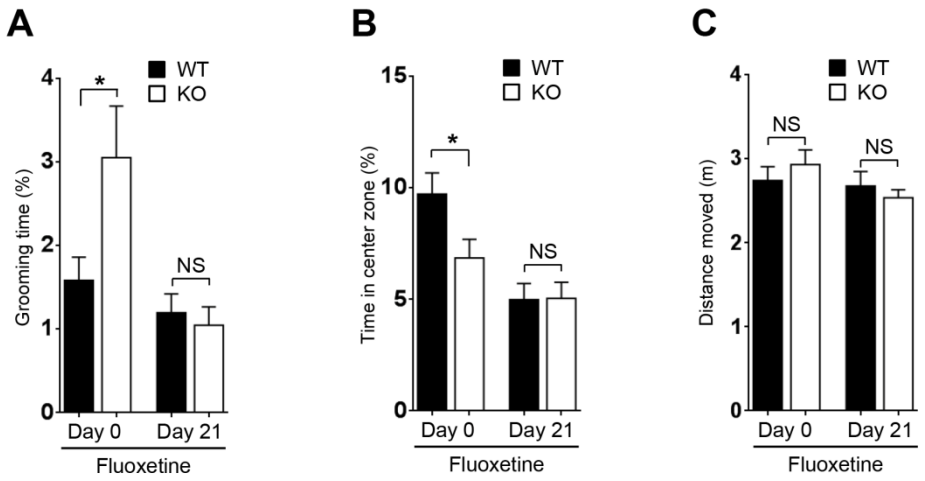

Figure 14. Serotonin re-uptake inhibitor fluoxetine alleviates compulsive grooming and anxiety-like behaviors of *Ninj1* KO mice

WT and *Ninj1* KO mice were given vehicle (tap water) or fluoxetine (in drinking water) over the course of 3 weeks. Three weeks of fluoxetine treatment alleviated the excessive grooming (**A**) and anxiety-like behavior (**B**) of the *Ninj1* KO mice without affecting the distance moved (m) (**C**) in the OFT [$n = 9$ (WT) and 7 (KO)]. All of the data are presented as the mean ± s.e.m.; $^{*}P < 0.05$; NS, not significant; two-tailed Student's *t*-test.

4. Temporo-spatial expression of Ninj1 in the central nervous system (CNS)

To gain an insight into the mechanisms that underlie the abnormal behaviors of the *Ninj1* KO mice, I investigated the temporo-spatial expression of Ninj1 in the CNS. I first observed that Ninj1 gradually increased during the first two weeks of postnatal brain development (**Figure 15**); this expression pattern is similar to those of synaptic molecules such as neuroligin 1 (NL1), the NMDA receptor subunit 2A (NR2A), and synaptophysin, which suggests the involvement of Ninj1 in brain development.

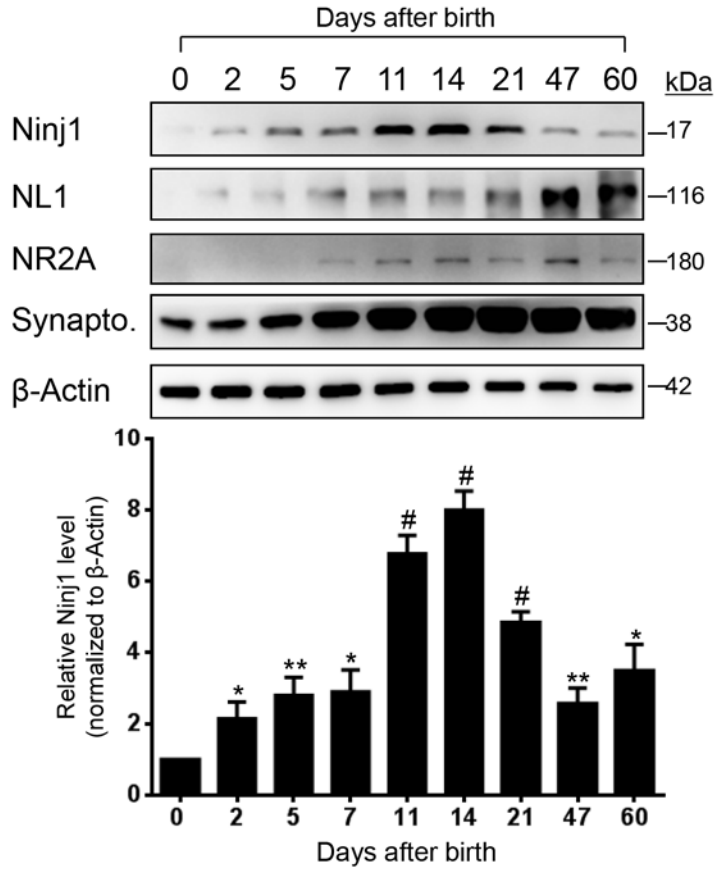

Figure 15. Temporal kinetics of Ninj1 expression during brain development.

Representative Western blot (WB) of whole-brain lysates (*upper* panel) and the corresponding quantification of Ninj1 expression (*lower* panel; n = 3 mice per time point) during mouse brain development. Abbreviation: Synapto., synaptophysin. NL1, NR2A, and synaptophysin were included as markers of brain development.

Asterisks and hashtags above the data points indicate significance relative to day 0. $*P < 0.05$, $**P < 0.01$, $^{\#}P < 0.0001$; NS, not significant; two-tailed Student's *t*-test. Error bars indicate s.e.m.

To identify the cell types that express Ninj1, I isolated brain tissue from mice that carried a "knockout-first" allele (*tm1a*) of *Ninj1* using *lacZ* as a reporter gene [26] (see **Materials and Methods**) and revealed that β-galactosidase, which indicates the expression of Ninj1, was mainly found in the thalamus, cortex, pituitary gland, and medulla oblongata (**Figure 16**). Moreover, double-labeling experiments explicitly demonstrated the predominantly neuronal expression of Ninj1 (**Figures 17 and 18**).

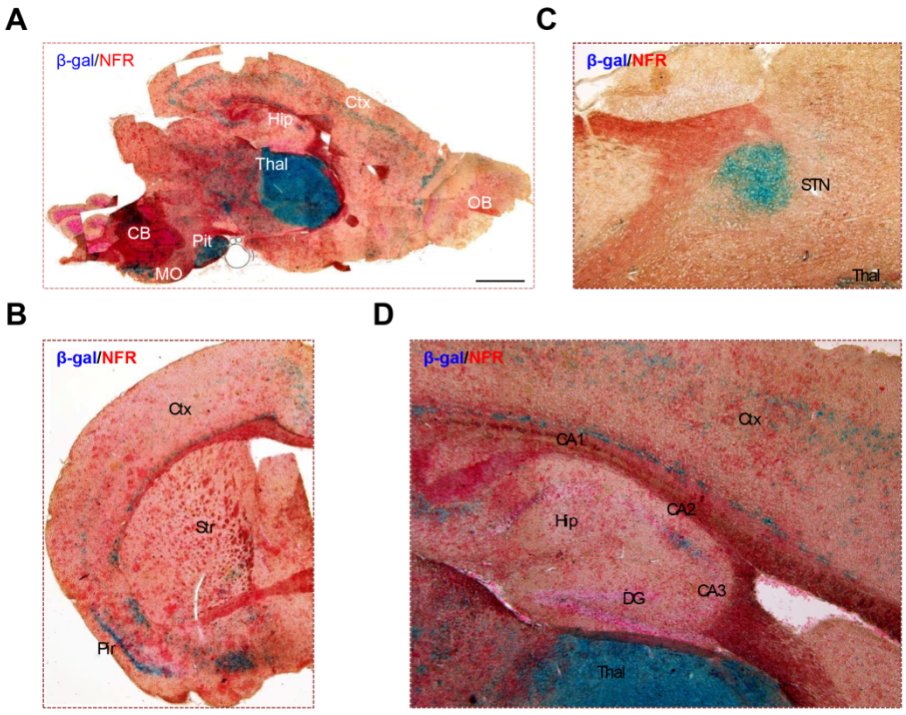

Figure 16. Spatial expression pattern of Ninj1 in mouse brain tissue. β-galactosidase (β-gal; arrowheads) staining of mouse brain tissue from *Ninj1* mutant mice (*Ninj1*$^{+/tm1a}$). Nuclear fast red (NFR) was used for counterstaining. **(A),** A sagittal section of mouse brain taken at low magnification that shows strong β-gal signals in Thal, Ctx, MO, and Pit. **(B),** A high magnification image of a sagittal section of mouse brain that also shows strong β-gal signals in the STN area. **(C),** β-gal is highly expressed in the Pir and dorsal Str in a coronal section of forebrain tissue. **(D),** In the mouse hippocampus, Ninj1 is most abundant in the CA2 region. Abbreviations: Thal, thalamus; Hip,

hippocampus; Ctx, cortex; OB, olfactory bulb; CB, cerebellum; MO, medulla oblongata; Pit, pituitary gland; STN, subthalamus nuclei; Str, striatum; Pir, piriform cortex; CA, cornus ammonis. Scale bar, 200 μm.

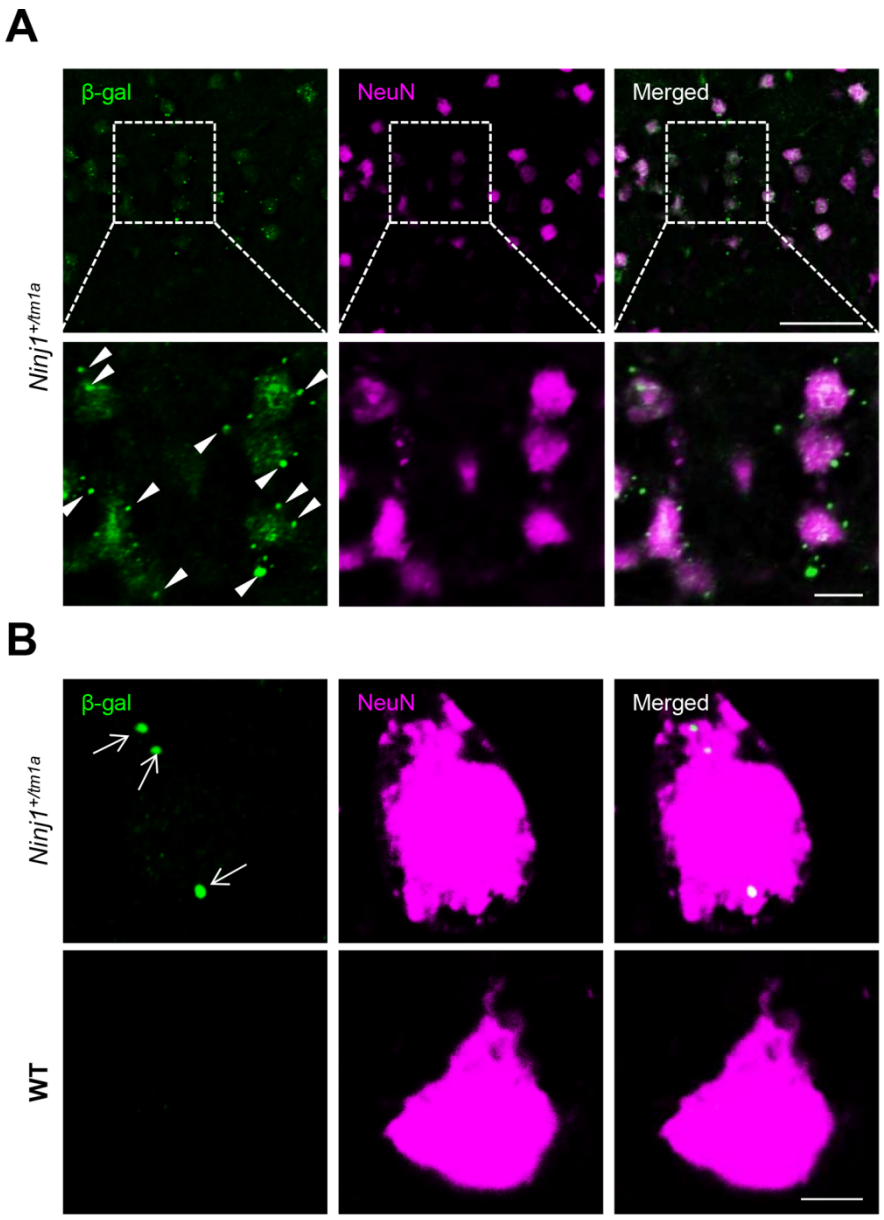

Figure 17. Ninj1 is prominantly expressed in CNS neurons. Immunostaining of a frontal cortex section with antibodies against β-galactosidase (green, arrowheads) and NeuN (magenta) indicating the

localization of Ninj1 in neurons. **(A),** Low magnification. **(B),** High magnification. β-galactosidase expression had a spot-like pattern (arrowheads) and specificity was indicated by the absence of signals in WT samples. Scale bars, 50 μm (**A**, upper); 10 μm (**A**, lower); 5 μm (**B**).

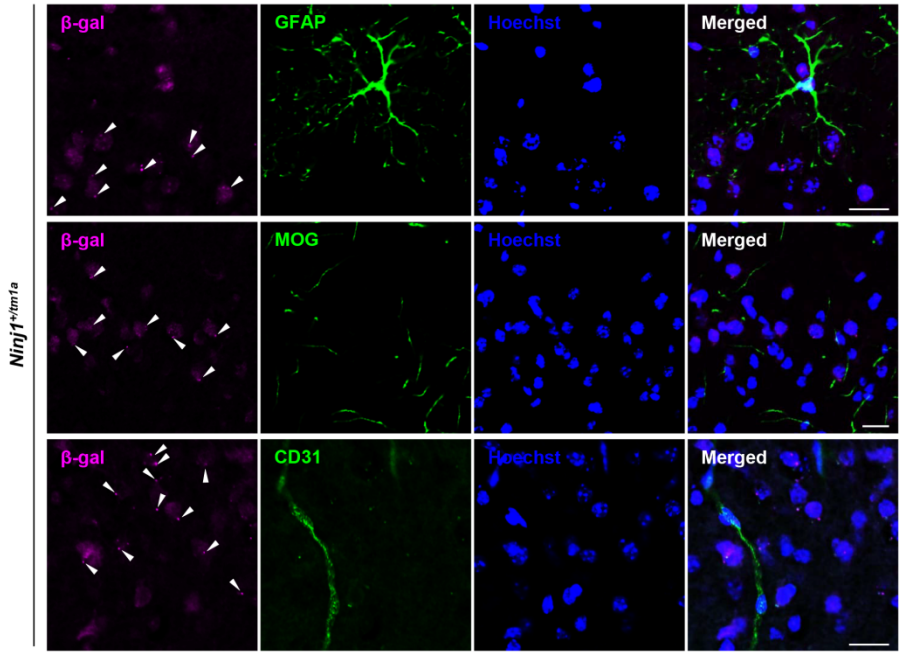

Figure 18. Ninj1 is not expressed in either brain glial or endothelial cells.

Double immunostaining of frontal cortex tissues from heterozygous *Ninj1* mutant mice (*Ninj1*$^{+/tm1a}$) with antibodies against β-galactosidase (anti-β-gal, magenta, arrowheads) and the brain cell-type specific markers GFAP (anti-GFAP, green, top) for astrocytes, MOG (anti-MOG, green, middle) for oligodendrocytes, and CD31 for endothelial cells (anti-CD31, green, bottom). Scale bars, 20 μm.

In addition, I confirmed the expression of Ninj1 in cultured cortical neurons (**Figure 19A**), which showed a sharp increase in Ninj1 levels during neuronal differentiation (**Figure 19B**).

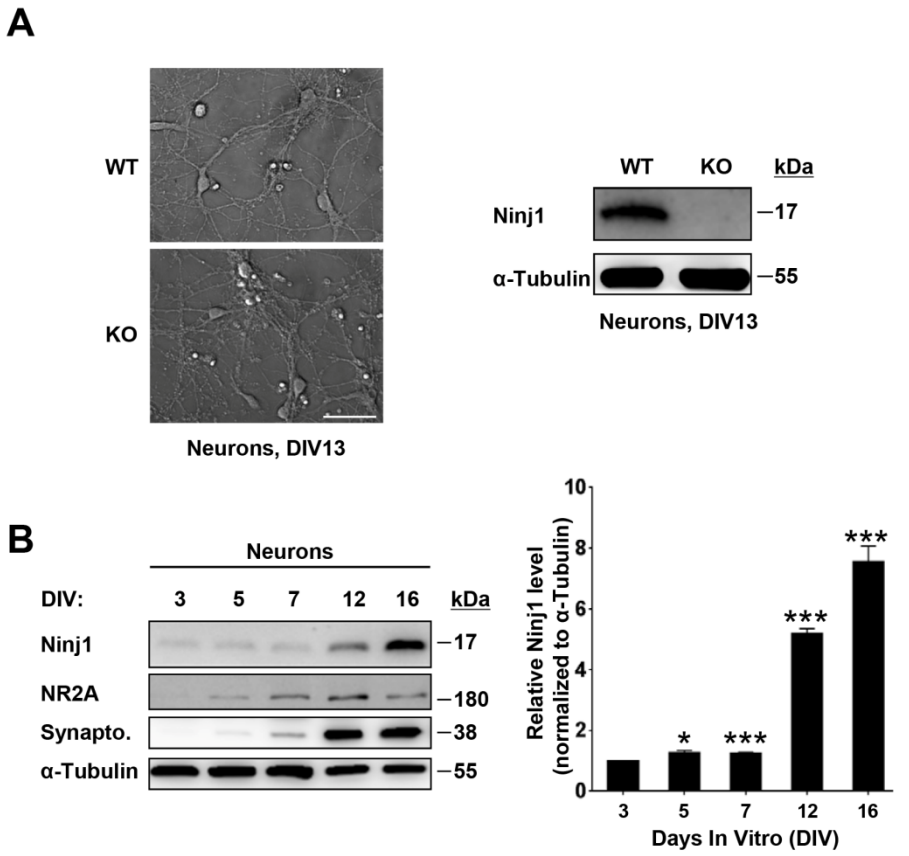

Figure 19. Ninj1 is expressed in cortical neurons, and is upregulated during the neuronal differentiation process.

(A), Representative differential interference contrast (DIC) images of primarily cultured cortical neurons from WT and *Ninj1* knockout (KO) after 13 days in vitro (DIV 13; *left*) and Western blot analysis of Ninj1 protein in cortical neuron lysates on DIV 13 (*right*). No Ninj1 signal was observed in *Ninj1* KO cortical neuron lysates, indicating specificity of the Ninj1 antibody. α-Tubulin was used as a loading control. Scale

bar, 50 μm. **(B),** Western blot analysis of Ninj1 protein levels in cortical neurons at indicated times. A representative Western blot data of primary cultures (*left*) from 3 independent experiments and quantification graph (*right*) are shown. Bands that corresponded to Ninj1 were quantified and normalized to α-Tubulin expression. Note that Ninj1 is upregulated during neuronal differentiation, along with the synaptic proteins NR2A (a post-synaptic molecule) and synaptophysin (a pre-synaptic molecule). α-Tubulin was used as a loading control. n = 3 samples at each time point. Abbreviations: DIV, days *in vitro*; NR2A, N-methyl-D-aspartate (NMDA) receptor subunit 2A; Synapto., synaptophysin. Asterisks above the data points in (**B**, *right*) indicate significance relative to DIV 3. The error bars indicate the s.e.m.; $^{*}P < 0.05$, $^{***}P < 0.001$; two-tailed Student's *t*-test.

5. Synaptic localization of Ninj1 in neurons

I next examined the localization of Ninj1 in neurons using biochemical fractionation of the mouse brain tissue. Ninj1 was highly enriched in synaptosomes, especially in the synaptic plasma membranes, as were with other synaptic proteins such as NR2A and PSD95 (**Figure 20**). Additionally, immunostaining of cultured cortical neurons transfected with either GFP-Ninj1 or Flag-Ninj1 revealed punctate expression of Ninj1 (**Figure 21A**), which overlapped with NL1 expression in dendritic spines (**Figure 21B**). Taken together, these results unambiguously indicate the synaptic localization of Ninj1 in CNS neurons.

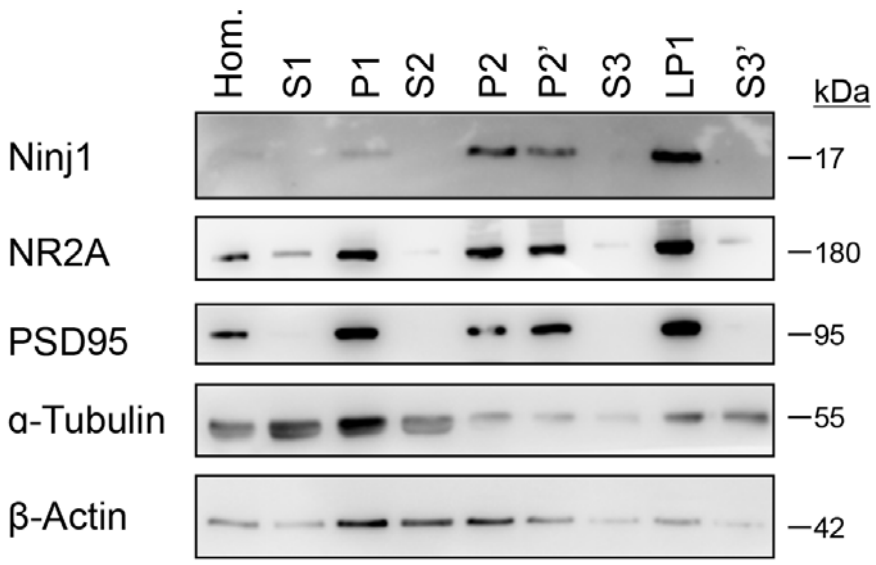

Figure 20. Subcellular localization of Ninj1.

Immunoblotting was performed after subcellular fractionation of mouse brain tissue (*n* = 3 biologically independent repeats). Ninj1 was more abundant in synaptic fractions (P2, P2′, and LP1) than in other subcellular fractions. Hom., homogenate; S1, synaptosome suspension; P1, nuclear pellet and debris; S2, light membrane and cytosolic fraction; P2, crude synaptosomal fraction; P2′, washed synaptosomal fraction; S3, lysed synaptosomal fraction; LP1, synaptosomal membrane fraction; S3′, crude synaptic vesicle fraction. NR2A and PSD95 are post-synaptic proteins. β-Actin/α-Tubulin were used as loading controls.

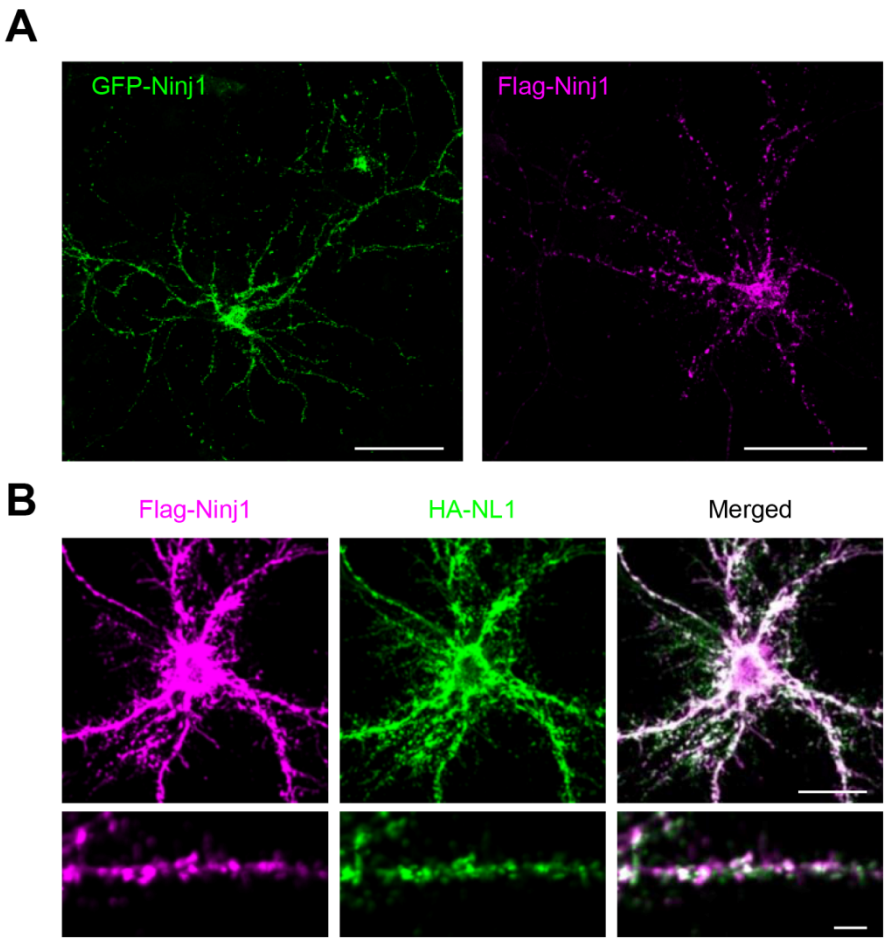

Figure 21. Ninj1 is localized at CNS synapses.

(A), Primary cortical neurons were transfected with either GFP-Ninj1 or Flag-Ninj1 on DIV 7. The neurons were fixed on DIV 11 and were immunostained with GFP (anti-GFP, green, left) or Flag (anti-Flag, magenta, right) antibodies. Ninj1 was expressed in puncta-like structures in both the GFP-Ninj1- and Flag-Ninj1-transfected neurons.

(B), Colocalization of Ninj1 with a synaptic adhesion molecule NL1. Cortical neurons that were co-transfected with expression constructs for Flag-Ninj1 and HA-NL1 were double labeled with anti-Flag (magenta) and anti-HA (green) antibodies. Scale bars, 50 μm (**A**); 20 μm (**B**, *upper* panels); 5 μm (**B**, *lower* panels).

6. Neuron-specific conditional *Ninj1* KO mice recapitulate the aberrant phenotypes of *Ninj1* KO mice

To clarify whether deficiencies of neuron-derived Ninj1 lead to the abnormal behaviors observed in the *Ninj1* KO mice, I generated *Ninj1* conditional KO mice (*Ninj1* c.KO), which had *Ninj1* specifically deleted in CNS neurons, by crossing *Ninj1* floxed mice (see **Materials and Methods** and [26]) with synapsin-I-Cre mice, which express Cre recombinase specifically in CNS neurons [39] (**Figure 22**). As shown in **Figure 23**, Ninj1 protein level was dramatically reduced in *Ninj1* c.KO brains compared with that of control mice, indicating that Cre-mediated recombination was successful and that neurons were the major source of Ninj1 in the mouse brains. *Ninj1* c.KO mice showed accumulation of hair trapped in their teeth and the hair loss phenotype (**Figure 24, A and B**). Moreover, the *Ninj1* c.KO mice spent less time exploring the open arms during the elevated plus maze test than their control littermates (**Figure 24C**), which indicates that the *Ninj1* c.KO mice also displayed anxiety-like behavior. Therefore, the abnormal phenotypes of *Ninj1* KO mice is likely attributable to the depletion of *Ninj1* in the CNS neurons.

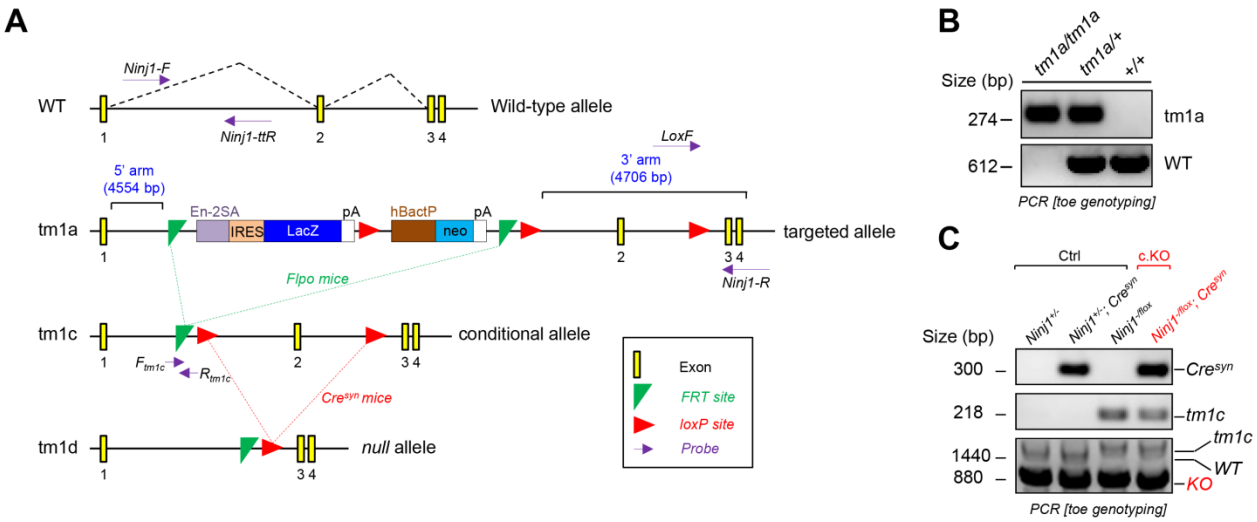
A
Ninj1-F
WT
Wild-type allele
1
Ninj1-ttR
2
3 4
LoxF
5' arm
(4554 bp)
3' arm
(4706 bp)
En-2SA
IRES
LacZ
pA
hBactP
neo
pA
tm1a
targeted allele
Flpo mice
Ninj1-R
tm1c
conditional allele
Cre^syn mice
tm1d
null allele
Exon
FRT site
loxP site
Probe
B
tm1a/tm1a
tm1a/+
+/+
Size (bp)
274
612
tm1a
WT
PCR [toe genotyping]
C
Ctrl
c.KO
Ninj1+/-
Ninj1+/-; Cresyn
Ninj1flox
Ninj1flox; Cresyn
Size (bp)
300
218
1440
880
Cresyn
tm1c
tm1c
WT
KO
PCR [toe genotyping]

Figure 22. Generation and genotyping of the neuron-specific *Ninj1* conditional KO mice (*Ninj1* c.KO).

(A), Schematic diagram showing the strategy for the generation of the *Ninj1* c.KO mice. In the WT allele, the yellow boxes with numbers represent exons, and the black dotted lines denote splice events. In the $Ninj1^{tm1a}$ mutant allele, a trapping cassette that included the *LacZ* and *neo* genes was inserted into the first intron of the *Ninj1* gene and was flanked by *FRT* sites (green triangles). *LoxP* sites (red triangles) flanked the critical exon 2 of the *Ninj1* gene, as indicated. The presence of an *Engrailed (En2) Splice Acceptor (SA)* disrupts *Ninj1* gene function, which leads to lacZ fusion and localized gene expression. The relative positions of the PCR primers used for genotyping are presented. In the presence of Flp recombinase, the *FRT* sequences (green triangles) flank the trapping cassette are deleted, converting the potentially conditional $Ninj1^{tm1a}$ allele to a readily conditional $Ninj1^{tm1c}$ allele and restoring Ninj1 protein expression. Thus, mice that carry the $Ninj1^{tm1c}$ allele ($Ninj1^{flox}$ mice) can be considered as equivalent to WT mice. Subsequent breeding of the $Ninj1^{flox}$ mice with neuron-specific Cre^{syn} mice led to the removal of the floxed exon 2 of the $Ninj1^{tm1c}$ allele, resulting in a *Ninj1* conditional KO allele ($Ninj1^{tm1d}$) in neurons.

The locations of the PCR primers used for genotyping are indicated by lavender arrows (F_{tm1c} and R_{tm1c}). **(B)**, Genotyping of the *Ninj1*^{tm1a} mice. Representative agarose gels show the PCR product for each allele. The WT allele (+) produced one 612-base-pair (bp) band using primer pair 1 (*Ninj1-F* and *Ninj1-ttR*), whereas the "knockout-first" allele (*Ninj1*^{tm1a}) produced a single 274-bp band using primer pair 2 (*LoxF* and *Ninj1-R*). Heterozygous (hetero) mutant mice produced two bands of 612 and 274 bp. **(C)**, Genotyping of the *Ninj1* c.KO mice, see also Methods. Agarose gels show the PCR products. The *Cre*^{syn} transgene produced one band of 300 bp, while the *Ninj1*^{tm1c} allele produced one band of 218 bp. *Ninj1* KO allele produced one band of 880 bp.

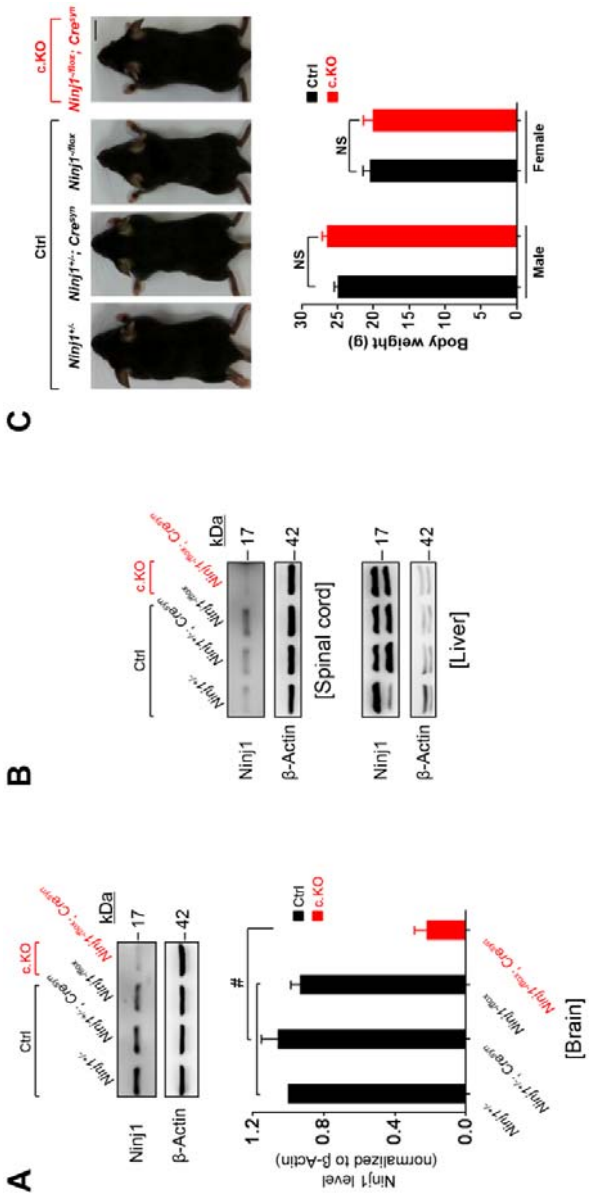

Figure 23. Analysis of Ninj1 protein expression in *Ninj1* c.KO and initial characterization of *Ninj1* c.KO.

(**A**), Brain homogenates were prepared from five-week-old control

(*Ninj1*$^{+/-}$, *Ninj1*$^{+/-}$; *Cre*^{syn}, *Ninj1*$^{-/flox}$) and *Ninj1* c.KO (*Ninj1*$^{-/flox}$; *Cre*^{syn}) mice. Representative blots (top) and densitometric quantification (bottom) (n = 4 mice per genotype) that show Ninj1 protein levels in mouse brains of the indicated genotypes. β-Actin was used as a loading control. The Ninj1 protein levels were dramatically reduced in the *Ninj1* c.KO brains compared with those of the control mice. **(B)**, Immunoblot analysis of Ninj1 in spinal cords (top) and livers (bottom) of control and *Ninj1* c.KO mice. Ninj1 protein levels were significantly reduced in the spinal cords but not in the livers of *Ninj1* the c.KO mice relative to those in control mice, indicating by Cre^{syn}-mediated *Ninj1* deletion specifically in CNS neurons. β-Actin was used as a loading control. **(C),** *Ninj1* c.KO mice are indistinguishable from control littermates in gross morphology. Representative images of *Ninj1* c.KO mice and control littermates at postnatal day 30 (*upper* panel) and a graph presenting body weights from both genders at postnatal day 65 (*lower* panel). Numbers of mice: male, Ctrl (n = 10); *Ninj1* c.KO (n = 5); and female, Ctrl (n = 7); *Ninj1* c.KO (n = 4). $^{\#}P < 0.0001$; NS, not significant; two-tailed Student's t-test. Error bars indicate the s.e.m.

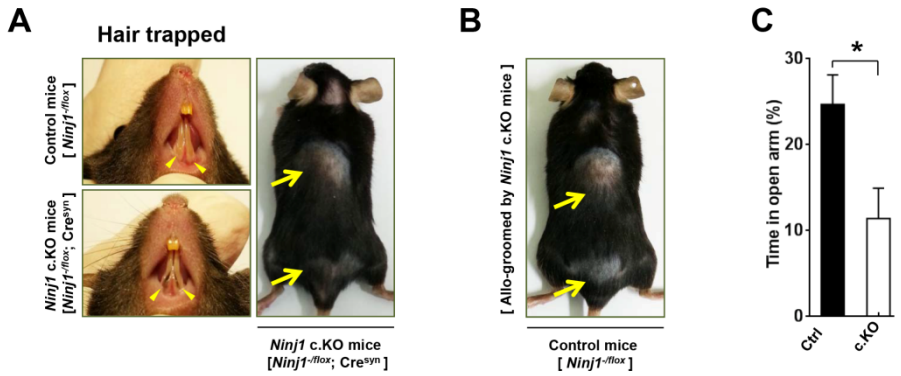

Figure 24. Neuron-specific *Ninj1* c.KO mice recapitulates key features of OCD-like behaviors.

(A, B), *Ninj1* c.KO mice allo-groomed their cage mates, leading to the trapping of hair in their teeth (arrowheads) and a hairless phenotype (arrows). **(C)**, *Ninj1* c.KO mice spent less time in the open arms than the controls in the EPM test [n = 13 (Ctrl) and 7 (c.KO)]. The error bars in (**C**) indicate the s.e.m. $^{\#}P < 0.0001$; NS, not significant; two-tailed Student's *t*-test.

7. Disruption of *Ninj1* impairs neural circuits

Although OCD reportedly reflects neural circuit dysfunction, the underlying mechanisms remain poorly characterized [8,9,38,40-43]. Thus, to pinpoint the mechanisms of the OCD-like behaviors of the *Ninj1* KO mice, I performed anatomical, histological, and electrophysiological analyses of *Ninj1* KO brains. Compared to WT littermates, the brain of the *Ninj1* KO mice were less heavy (**Figure 25**), but did not exhibit differences in overall architecture (**Figure 26**). Therefore, neuronal morphology was examined in the *Ninj1* KO mice using Golgi staining to visualize cortico-striatal circuits, which were highly activated in the *Ninj1* KO mice (**Figure 27**) and have previously been implicated in the pathogenesis of OCD [8,9]. The dendritic complexity of the striatal medium spiny and cortical neurons of the *Ninj1* KO mice was markedly decreased compared with that in the WT mice (**Figure 28**). These observations were supported by further assays that demonstrate that Ninj1 was important for dendritic branching in cultured cortical neurons (**Figures 29 and 30**).

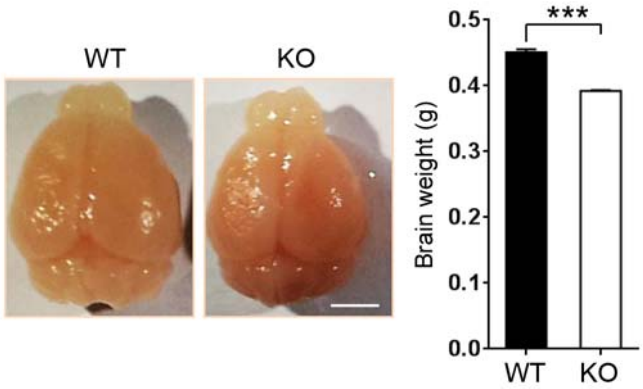

Figure 25. *Ninj1* KO mice show reduced brain volume.

Representative images (*left*) and quantification histogram of brain weights (n = 3 mice per genotype; *right*). Scale bar, 2 mm. $^{***}P < 0.001$; two-tailed Student's t-test. Error bars indicate the s.e.m.

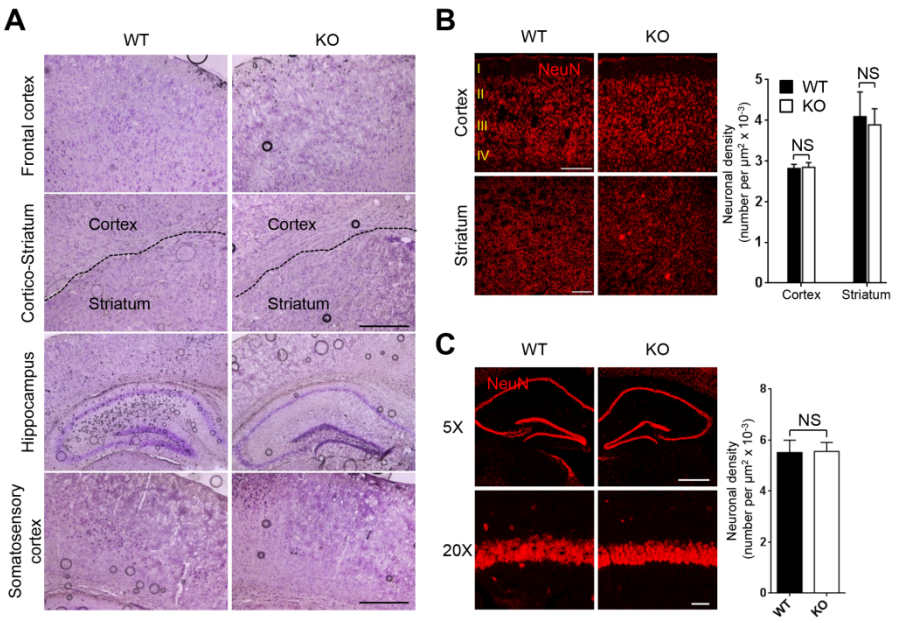

Figure 26. Gross anatomical normalities in the brains of *Ninj1* KO mice.

(A), Nissl staining of coronal sections of the brains of WT and *Ninj1* KO mice. The dotted lines represent the borders between the cortex and striatum. *Ninj1* KO mice have normal gross brain morphology compared with WT littermates. **(B)**, Immunofluorescence confocal images of the cortex (layer I-IV) (*upper*) and striatum (*lower*) from WT and *Ninj1* KO brains stained with a NeuN antibody (red; *left*) and quantification of neuronal density within each area (n = 3 mice per genotype; right). **(C)**, Immunofluorescence images of hippocampal tissue of WT and *Ninj1* KO mice that was stained with a NeuN

antibody (left) and the quantification of neuronal cell numbers in these areas (n = 3 mice per genotype; *right*). The neuronal density in the *Ninj1* KO mice did not differ from that in their WT littermates. Scale bars, 50 μm (**A**); 200 μm (**B**); 500 μm (**C**, *upper*); 50 μm (**C**, *lower*). NS, not significant; two-tailed Student's *t*-test. The error bars indicate the s.e.m.

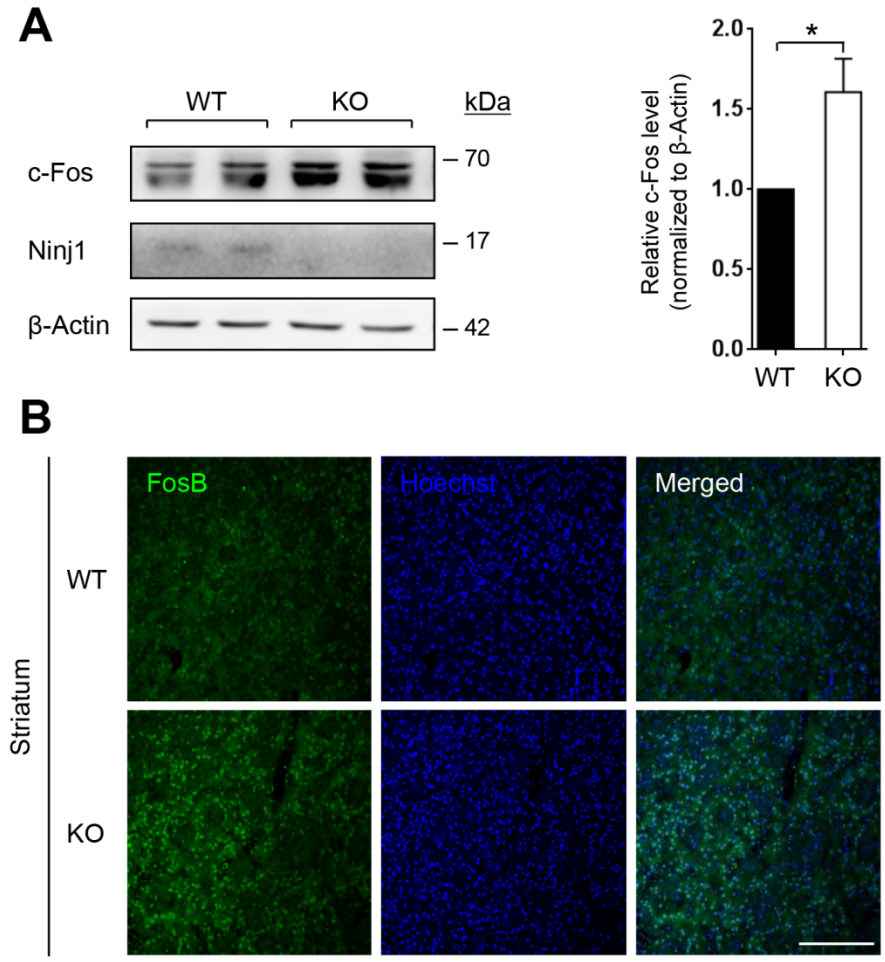

Figure 27. Hyperactivity of cortico-striatal circuit in *Ninj1* KO mice.

(A), A representative Western blot (*left*) and the corresponding quantification of c-Fos (a marker of neuronal activation) protein levels (n = 4 mice per genotype; *right*) are shown. **(B)**, Confocal images show the upregulation of FosB (another marker of neuronal activation) in the

striatum of the *Ninj1* KO mice compared with the expression in the WT littermates (n = 2 mice per genotype). Hoechst 33342 was used to counterstain nuclei. Scale bars, 200 μm (**B)**. $^{*}P < 0.05$; two-tailed Student's *t*-test. The error bars indicate the s.e.m.

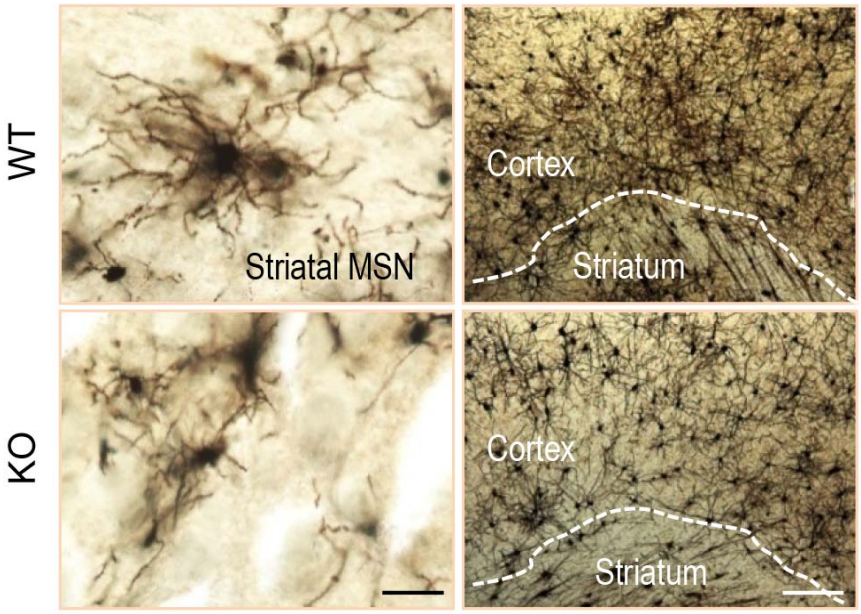

Figure 28. *Ninj1* KO brain displays a decrease in dendritic complexity.

Representative images of Golgi staining of striatal medium spiny neurons (MSNs) (*left*) and cortico-striatal areas (*right*) showing the reduced dendritic complexity of the neurons of the *Ninj1* KO mice compared to that of the neurons of the WT littermates. Scale bars, 25 μm (*left*); 200 μm (*right*).

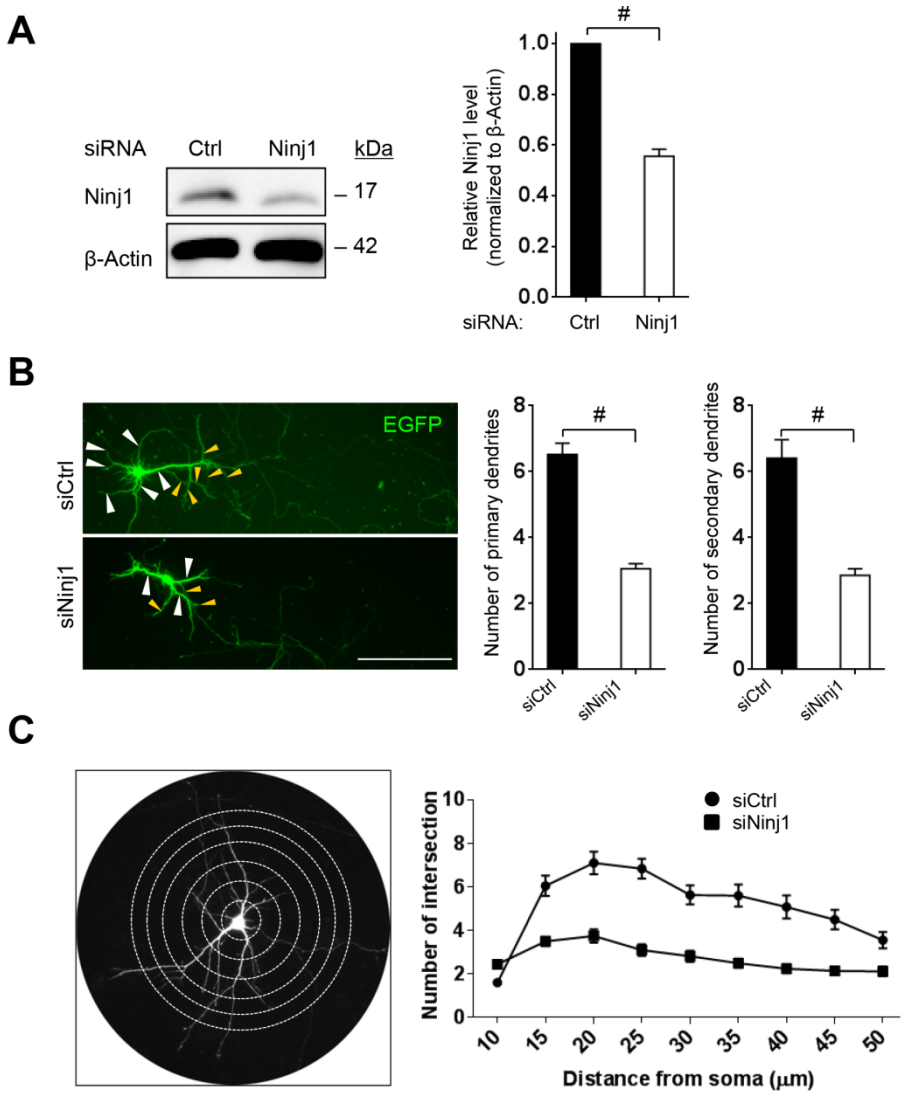

Figure 29. Knockdown of *Ninj1* results in decreased dendritic branching in cortical neurons.

Primary cortical neurons were co-transfected with EGFP-N1 (for the visualization of neuronal morphology) and siCtrl or siNinj1 on DIV 4,

fixed with 4 % paraformaldehyde (PFA), and immunostained with GFP antibody on DIV 8. **(A),** Efficiency of *Ninj1* knockdown in cortical neurons. A representative Western blot (*left*) and the corresponding quantification of Ninj1 protein levels (normalized to β-Actin; *right*) are shown. In the siNinj1-transfected neurons, Ninj1 protein levels were decreased to approximately 50 % of control levels. The presented data are representative of at least three independent primary cultures. **(B),** Knockdown of *Ninj1* leads to reduced dendritic branching, as indicated by the number of primary dendrites that originated from the soma (white arrowheads) and the number of secondary dendrites that originated from the primary dendrites (yellow arrowheads) [n = 42 (siCtrl) and 56 (siNinj1) neurons]. Scale bar, 200 μm. (**C**), Representative Sholl analysis of a neuron performed by counting the number of dendrite intersections (*left*). Graph shows quantification of Sholl analysis of primary cortical neurons transfected with the indicated siRNAs (*right*). $^{\#}P < 0.0001$; two-tailed Student's *t*-test. The error bars indicate the s.e.m.

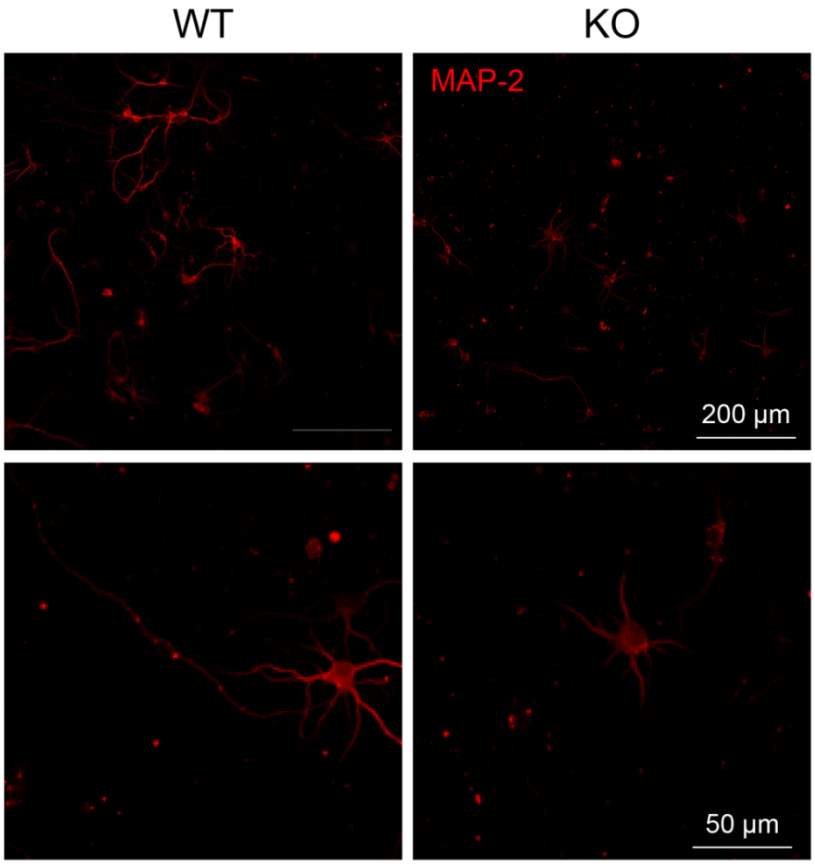

Figure 30. Deficiency of *Ninj1* reduces dendritic branching in cortical neuron.

Ninj1 KO and WT primary cortical neurons were stained with MAP2 antibody (red), a specific marker of dendrites at DIV 7. *Ninj1* KO neurons showed a decrease of dendritic branching.

Moreover, *Ninj1* ablation led to a substantial reduction in synapse number (**Figure 31**), which was in part due to reduced dendritic branching. In addition, Ninj1 promoted pre-synapse formation *in vitro* (**Figure 32**), suggesting that it is required not only for neuronal branching but also for synapse formation.

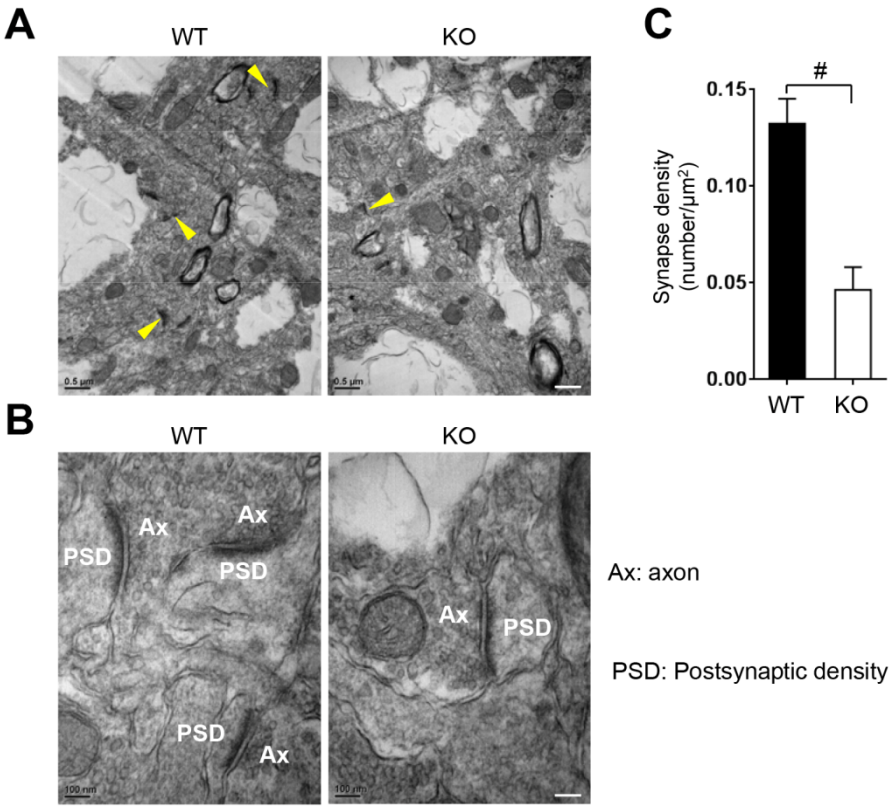

Figure 31. *Ninj1* KO brain shows reduced number of synapses. Electron micrographs of brain sections of WT and *Ninj1* KO mice in low magnification (**A,** *upper*) and in high one (**B,** *lower*) and quantification of synapse number [n = 20 (WT) and 17 (KO) images from 2 mice per genotype; **C**]. Arrowheads indicate synapses. Scale bar, 500 nm (**A**); 100 nm (**B**). $^{\#}P < 0.0001$; two-tailed Student's t test. Error bars in (**C**) denote the s.e.m.

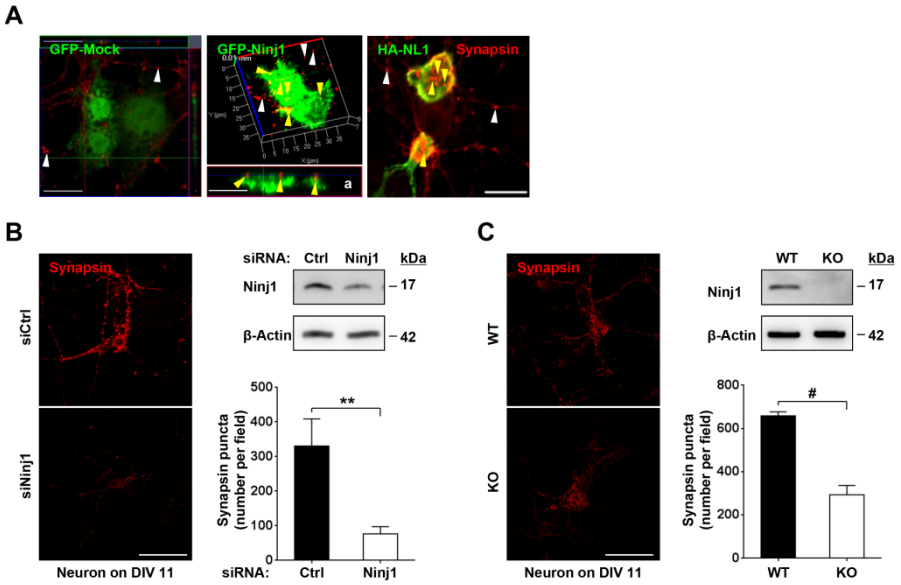

Figure 32. Ninj1 promotes pre-synapse formation in cortical neurons.

(A), Artificial synapse formation assay. Primary cortical neurons on DIV 9 were co-cultured with HEK293T cells transfected with GFP-mock or GFP-Ninj1, and fixed on DIV 11. Cells were then immunostained with synapsin (red) and GFP (green) antibodies. A cross section through a transfected HEK293T cell with synapsin punctas on top of cell surface expressing GFP-Ninj1. Ninj1 induced synapsin clustered on the cell surface, suggesting that it mediates pre-synapse formation. Yellow arrowheads: puncta on top of HEK293T cells, white arrowheads: regular interneuronal synapses surrounding HEK293T

cells. Data are representative of three independent cortical neuron cultures, 5-10 cells were analyzed at each culture. HA-NL1 was used as a positive control. Scale bar, 50 μm. **(B)**, Knockdown of *Ninj1* reduces the number of pre-synapses in cortical neurons. Cultured cortical neurons were transfected with siCtrl or siNinj1 on DIV 9, fixed with 4 % PFA, and immunostained with a synapsin antibody (red) on DIV 11. Representative confocal images (*left*) and the corresponding quantification (n = 11-12 images per group; *right*) are shown. **(C)**, Ninj1 deficiency leads to decreased numbers of pre-synapses. Cultured cortical neurons from WT and *Ninj1* KO mice were fixed with 4 % PFA, and were immunostained with a synapsin antibody (red) on DIV 11. Representative confocal images (*left*) and the corresponding quantification (n = 12 images per group; *right*) are shown. Scale bars, 50 μm (**A**); 100 μm (**B** and **C**). $^{**}P < 0.01$, $^{\#}P < 0.0001$; two-tailed Student's *t*-test. The error bars indicate the s.e.m.

8. *Ninj1* deletion leads to reduced level of glutamate neurotransmitter in the mouse brain

A body of evidence suggests that neurotransmitters, such as glutamate, dopamine, and serotonin are dysregulated in neuropsychiatric disorders, and this dysregulation may contribute to the pathophysiology of these disorders [44-46]. Thus, to address whether neurochemical changes are associated with the behavioral abnormalities of *Ninj1* KO mice, I examined the levels of the main neurotransmitters in the mouse brain tissue using high performance liquid chromatography-electrochemical detection (HPLC-ECD). Interestingly, I found a reduction in the level of glutamate, which is the principal excitatory neurotransmitter in the brain (**Figure 33A**), but failed to observe any changes in the levels of norepinephrine, dopamine, and serotonin and its main metabolite, 5-hydroxyindoleacetic acid (5-HIAA) in *Ninj1* KO mice as compared to those of WT littermates (**Figure 33B**). Together, these results suggest the glutamate reduction in the brain could contribute to the abnormal behavioral phenotypes of *Ninj1* KO mice.

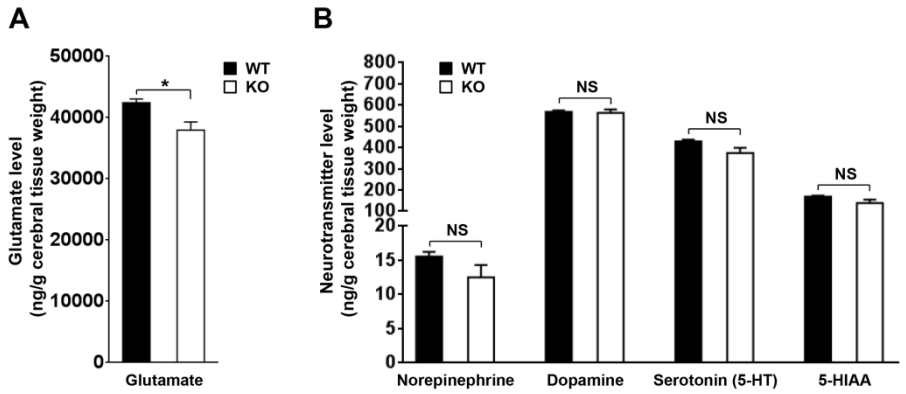

Figure 33. Profile of major neurotransmitters in *Ninj1* KO mice. Indicated neurotransmitter levels in cerebral cortex of *Ninj1* KO mice and WT littermates were measured using high performance liquid chromatography-electrochemical detection (HPLC-ECD). Levels of glutamate (**A**) and norepinephrine, dopamine, serotonin, and the major metabolite of serotonin 5-hydroxyindoleacetic acid (5-HIAA) are shown [n = 4 (WT) and 3 (KO)] (**B**). *Ninj1* KO mice showed reduced glutamate concentrations, but other neurotransmitter levels were normal compared with WT littermates. *$P < 0.05$; NS, not significant; two-tailed Student's t-test. Error bars indicate the s.e.m.

9. *Ninj1* KO mice display altered synaptic transmission in thalamic neurons

Alteration of synaptic transmission has been reportedly associated with neuropsychiatric disorders [2,8,9,27]. Thus, to pinpoint the mechanisms of the aberrant behaviors of *Ninj1* KO mice, in collaboration with Dr. Daesoo Kim (Department of Biological Sciences, Korea Advanced Institute of Science and Technology (KAIST), Korea), we performed an electrophysiological analysis in the ventral lateral thalamic nucleus, in accordance with the high expression of Ninj1 in the thalamus (**Figure 16**). In whole-cell voltage-clamp recordings from acute brain slices, the frequency of miniature excitatory post-synaptic currents (mEPSCs) in slices from *Ninj1* KO mice was significantly decreased (by approximately 50 %) compared to that in slices from WT littermates (**Figure 34A**), indicating a reduced number of functional synapses and/or reduced glutamate-mediated neurotransmission with postsynaptic receptors. Additionally, *Ninj1* deletion led to increased amplitude of the mEPSCs (**Figure 34B**), suggesting a greater number of glutamate receptors per synapse in *Ninj1* KO neurons compared with that in WT neurons. These data corroborate previous studies of abnormal neurotransmission in mouse cortico-striato-thalamo-cortical

circuits, which are well-known primary sites of synaptic dysfunction in neuropsychiatric disorders such as ASD and OCD [27,29,40,47]. Taken together, these results indicate that altered neural circuits are central to the abnormal phenotypes of the *Ninj1* KO mice.

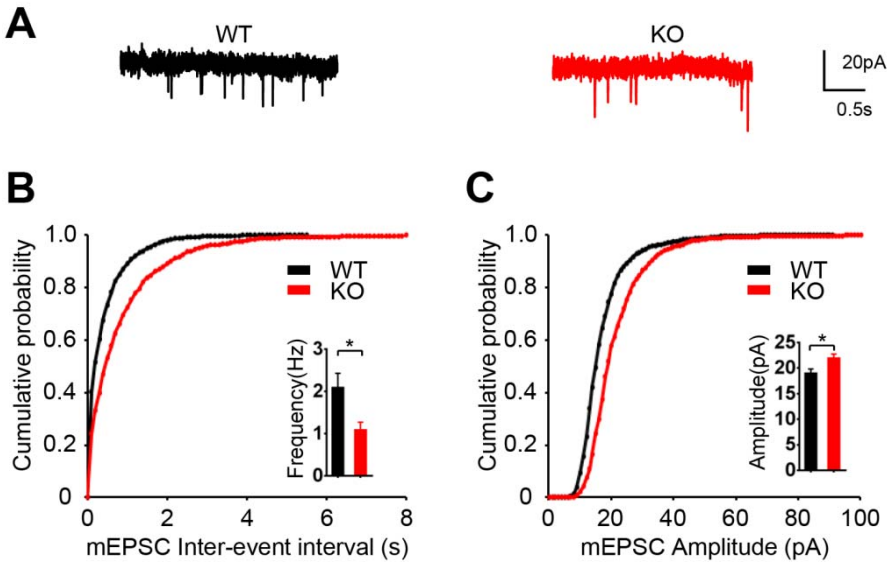

Figure 34. Disruption of *Ninj1* leads to altered glutamatergic synaptic transmission in thalamic neurons.

Whole-cell patch-clamp electrophysiology of ventral lateral thalamic neurons shows the alterations of mEPSCs in *Ninj1* KO mice. (**A**), Representative mEPSC recordings are shown. Scale bars, 20 pA and 500 ms. (**B, C**), Cumulative plots and average values (insets) of mEPSC frequency (**B**) and amplitude (**C**); *n* (cells) = 7 (WT) and 8 (KO) from 3 mice per genotype. *$P < 0.05$; two-tailed Student's t test. Error bars show the s.e.m.

10. Ninj1 modulates glutamate signaling

Synaptic transmission in neural circuits that control mouse behaviors could be modulated by ionotropic glutamate receptors. Accordingly, increasing evidence has implicated the dysregulation of glutamate signaling in the pathology of neuropsychiatric disorders such as OCD [47-50]. Here, I found that *Ninj1* deficiency resulted in the upregulation of N-methyl-D-aspartate (NMDA) receptors (NR1, NR2A, and NR2B subunits) and α-amino-3-hydroxy-5-methyl-4-isoxazolepropionic acid (AMPA) receptors (GluR1 and GluR2 subunits) in synaptosomes of mouse brain tissue (**Figure 35**). These data suggest that Ninj1 could be involved in the regulation of synaptic transmission through ionotropic glutamate receptors. In addition, level of NR2A subunit was also increased in total brain lysates of *Ninj1* KO mice compared with that of WT littermates (**Figure 36A**). Furthermore, knockdown of *Ninj1* upregulated the NR1 and NR2A subunits of NMDARs in cultured neurons (**Figure 36B**), suggesting that Ninj1 is a regulator of N-methyl-D-aspartate (NMDA)-type glutamate receptor.

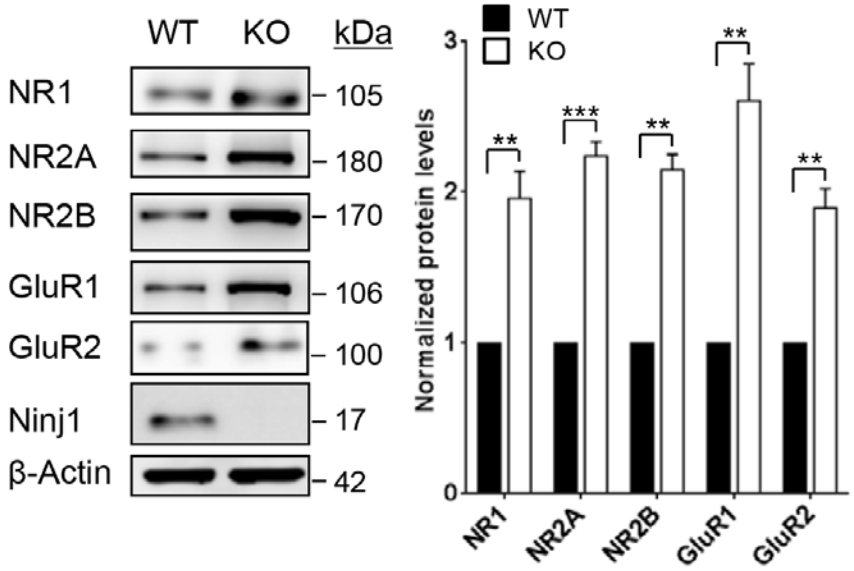

Figure 35. Ninj1 modulates glutamate signaling at synapses.

A representative WB (*left*) and the corresponding quantification (n = 3 mice per genotype; *right*) show that *Ninj1* deletion leads to the upregulation of NMDAR (including NR1, NR2A, and NR2B subunits) and AMPAR (including GluR1 and GluR2 subunits) protein levels in synaptosomes of mouse brain cerebrums. β-Actin was used as a loading control. $^{**}P < 0.01$, $^{***}P < 0.001$; two-tailed Student's t test. Error bars indicate the s.e.m.

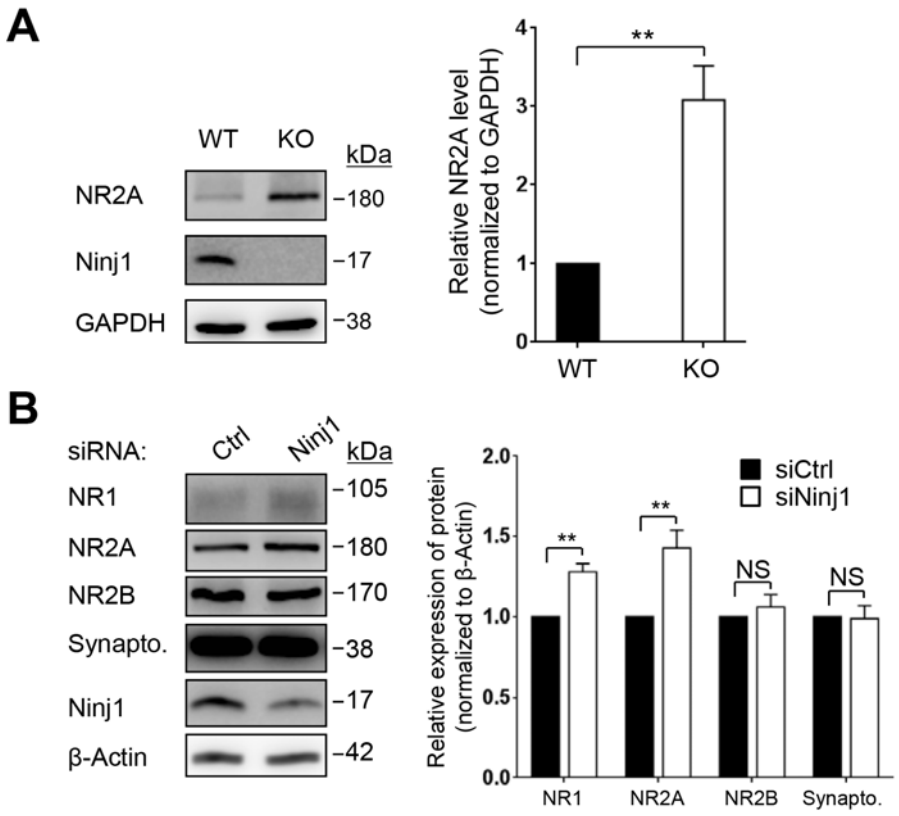

Figure 36. Ninj1 regulates NMDAR protein levels in CNS neurons. **(A)**, *Ninj1* deletion leads to the upregulation of NMDAR protein levels in total lysates of mouse cerebrums. A representative Western blot (*left*) and the corresponding quantification (n = 4 mice per genotype; *right*) are shown. GAPDH was used as a loading control. **(B)**, Knockdown of *Ninj1* in neurons disrupted NMDAR protein levels. On DIV 4, cortical neurons were transfected with control (Ctrl) or *Ninj1* siRNAs for three days. A representative Western blot (*left*) and the corresponding

quantification (n = 3 per condition; *right*) are shown. β-Actin was used as a loading control. **P < 0.01; NS, not significant;; two-tailed Student's t test. Error bars indicate the s.e.m.

Thus, to investigate the molecular mechanisms by which Ninj1 regulates NMDARs, I initially co-transfected HEK293T cells with the NR2A subunit and Flag-mock or Flag-Ninj1 plasmids and monitored receptor expression. I observed a notable decrease in NR2A level in the presence of Ninj1 (**Figure 37**), which suggests that Ninj1 affects NR2A stability. In subsequent analyses of NR2A receptor turnover using cycloheximide pulse-chase experiments, Ninj1 facilitated NR2A degradation (**Figure 38**).

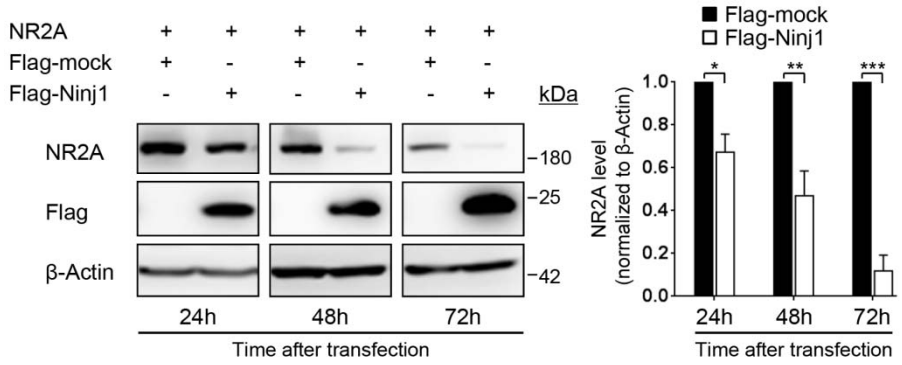

Figure 37. Ninj1 downregulates NR2A protein level *in vitro*.

A representative WB (*left*) and the corresponding quantification (n = 3 per time point; *right*) that show NR2A protein levels during co-transfection of NR2A and Flag-mock or Flag-Ninj1 plasmids into HEK293T cells. β-Actin was used as a loading control. *P < 0.05, **P < 0.01, ***P < 0.001; two-tailed Student's t test. Error bars indicate the s.e.m.

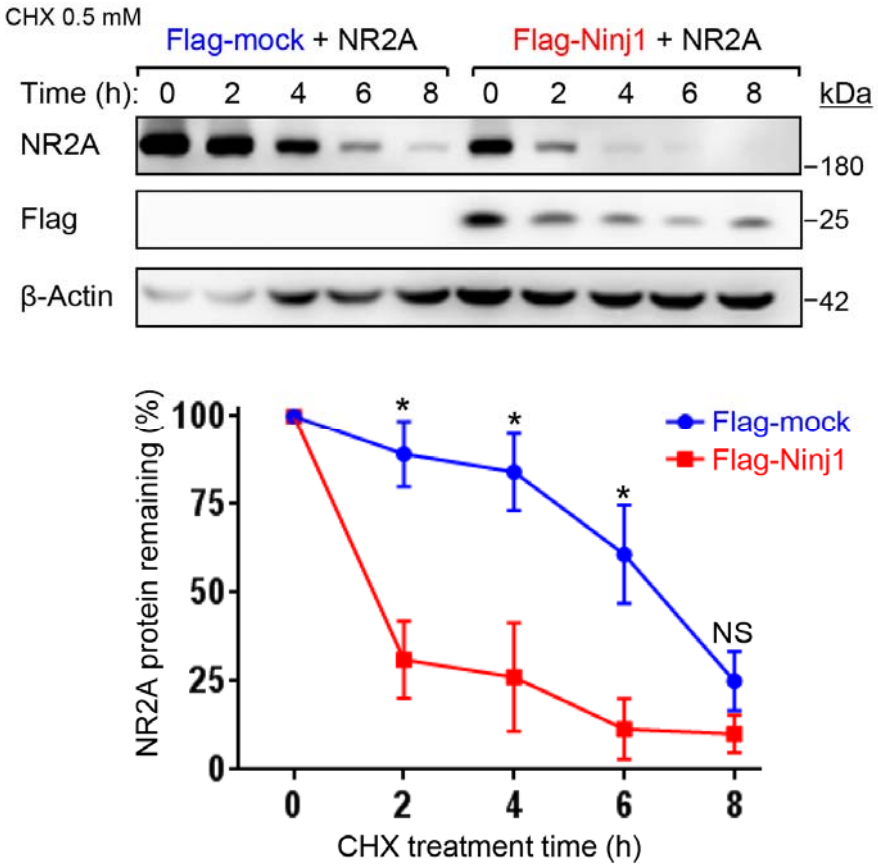

Figure 38. Ninj1 affects NR2A stability.

Pulse-chase cycloheximide (CHX) assays in HEK293T cells that were co-transfected with NR2A and Flag-mock or Flag-Ninj1 plasmids. A representative WB (*upper*) and corresponding quantification (*lower*; *n* = 3 biologically independent repeats) that show NR2A protein levels during treatment. β-Actin was used as a loading control. **P* < 0.05; NS, not significant; two-tailed Student's *t* test. Error bars indicate the s.e.m.

I next examined the membrane distribution of NR2A using cell surface biotinylation assays, and we noted that overexpression of Ninj1 decreased the cell surface presentation of NR2A (**Figure 39A**). To confirm that Ninj1 regulates the cell membrane level of NR2A, I utilized a construct of NR2A in which a super-ecliptic pHluorin was used to tag its extracellular N-terminus (SEP-NR2A); this tag produces green fluorescence upon localization at the pH-neutral cell membrane surface [51]. I consistently found that Ninj1 inhibited plasma membrane recruitment of SEP-NR2A in HEK293T cells (**Figure 39B**). Together, these results demonstrate the importance of Ninj1 for the stability and membrane recruitment of NMDARs.

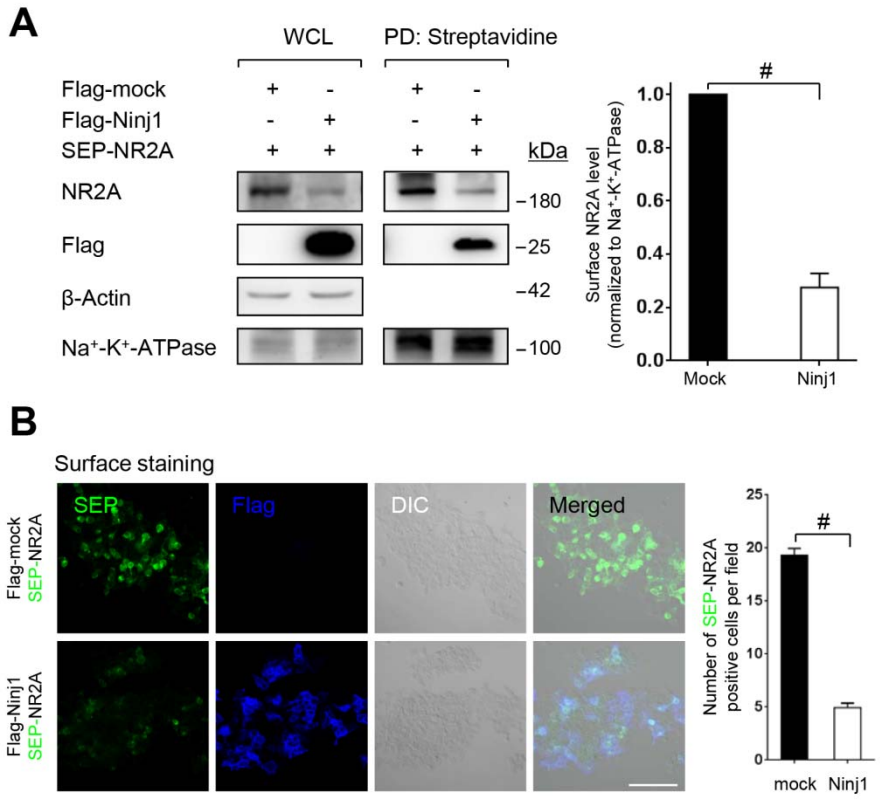

Figure 39. Ninj1 inhibits membrane recruitment of NR2A.

(A), HEK293T cells were co-transfected with NR2A and Flag-mock or Flag-Ninj1 plasmids for 24 hours. The cell surface proteins were then labelled with biotinylation reagent (NHS-Biotin) for 1 hour at 4^{o}C. After the cells were lysed, the resulting proteins were pulled down with streptavidin-conjugated beads and then immunoblotted. A representative Western blot (*left*) and the corresponding quantification (n = 3 biologically independent repeats; *right*) that showed decreased

NR2A protein levels at the cell membrane surface. Na^+-K^+-ATPase was used as a plasma membrane marker. **(B)**, HEK293T cells were co-transfected with SEP-NR2A and Flag-mock or Flag-Ninj1 plasmids. Cells were then fixed and immunostained without detergents using an anti-Flag antibody (blue). Representative confocal images (*left*) and corresponding quantification (*right*; n = 15 images per group from at least 3 biologically independent repeats), which show that the green signal (SEP) was decreased in the presence of Ninj1. Scale bar, 100 μm. $^{\#}P < 0.0001$; two-tailed Student's *t*-test. Error bars indicate s.e.m.

Finally, to translate these findings into therapeutic applications, I next evaluated the therapeutic potential of memantine, an NMDAR antagonist that has been approved for the treatment of Alzheimer's disease [52]. Intraperitoneal injections of this drug into injured *Ninj1* KO mice dramatically reduced clinical symptoms, including the extent of the injury (**Figure 40A**) and grooming times (**Figure 40B**). These observations closely agree with the results of several ongoing clinical trials of memantine for OCD and provide additional evidence for the "glutamate hypothesis" of OCD pathogenesis [53,54]. Collectively, the present findings suggest that abnormal glutamate signaling contributes to the OCD-like behaviors of the *Ninj1*-deficient mice.

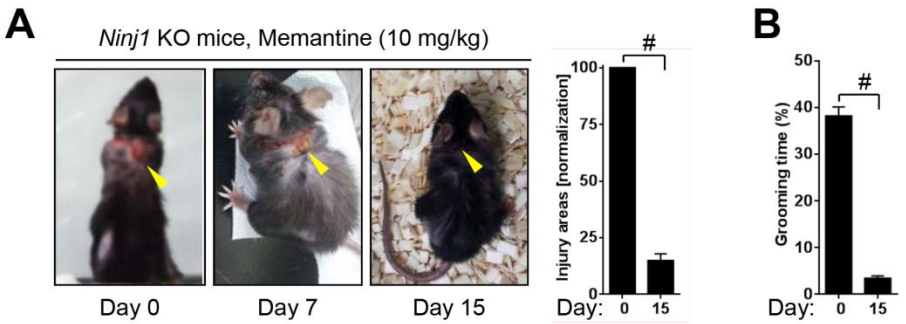

Figure 40. Blocking of NMDA receptors alleviates abnormal behaviors of *Ninj1* KO mice.

Daily administration of 10 mg/kg memantine ameliorated the OCD-like behaviors of injured *Ninj1* KO mice, including a reduction in the extent of injury (arrowheads; A) and in grooming time (n = 3 mice; B). *#P < 0.0001*; two-tailed Student's t test. Error bars in all of the panels indicate the s.e.m.

DISCUSSION

In the present study, I demonstrate for the first time that deletion of *Ninj1* in mice leads to abnormal behaviors. Specifically, I showed that *Ninj1* KO mice compulsively groomed their cage mates, leading to the hair loss phenotype. In addition, compared with WT mice, *Ninj1* KO mice were more anxious in the open field and elevated plus maze tests. These abnormal phenotypes could be rescued by chronic treatment with fluoxetine, a selective serotonin reuptake inhibitor (SSRI) reportedly used to ameliorate compulsive behaviors in mice and also a first-line drug for depression and OCD patients. I further demonstrated that Ninj1 was predominantly expressed in neurons of the cortico-thalamic circuits and mice with neuron-specific ablation of *Ninj1* exhibited grooming-induced hair loss and anxiety-like behavior. Finally, I provided evidence of defects in brains of *Ninj1* KO mice in histological, electrophysiological, and biochemical analyses.

Modeling psychiatric disorders such as OCD, ASD, and schizophrenia is highly challenging. Although there have been numerous studies on psychiatric disorders in humans, their underlying mechanisms have not been clarified because it is typically unacceptable to intervene with human genes. Additionally, psychiatric disorders are

heterogeneous with the potential involvement of a battery of genes; hence, genetic mouse models are needed. Mouse models are paving the way toward insights into neuropsychiatric disorders at multiple levels, from molecular, physiological to behavioral levels [55]. With the availability of genetic manipulation, mouse models facilitate identification of new candidate genes related to these diseases. Using a set of behavioral assays, I found that *Ninj1* KO mice manifested behavioral abnormalities, including repetitive and anxiety-like behaviors. *Ninj1* KO mice compulsively groomed, leading to hair removal and lesions similar to the reported mice with ASD- or OCD-like behaviors, such as *Shank3*-, *Sapap3*-, or *Slitrk5*-deficient mice [8,9,27]. Importantly, *Ninj1* KO mice also groomed their cage mates, suggesting that excessive grooming behavior is unlikely attributable to peripheral nervous system or skin abnormalities. Furthermore, individuals with a specific psychiatric disorder commonly experiences additional psychiatric disorder simultaneously or at some time during their lifetime [56-59]. Thus, it might be argued that the abnormal behaviors existing in *Ninj1* KO mice might be a shared feature of several psychiatric disorders, such as OCD and autistic-like behaviors. Nevertheless, my results indicate that *Ninj1* KO mice exhibited normal

social interactions and cognitive function, thereby excluding the ASD-like behaviors.

OCD is characterized by obsessions and compulsions; most patients experience both symptoms throughout the course of their illness, while some only show one or the other . Obsessions are repetitive, intrusive, unwanted thoughts that are often about cleanliness, religion, safety, or violence and are associated with anxiety. Compulsions are repetitive behaviors, typically associated with specific obsessions to neutralize the anxiety [36]. Affected individuals are unable to control either the thoughts or the behaviors, leading to substantial morbidity [2,3]. OCD is incompletely understood; however, neuroimaging studies have implicated the cortico-striato-thalamo-cortical (CSTC) circuits in the pathophysiology of OCD [2,41,60]. In addition, genetic and treatment studies have further demonstrated the involvement of glutamatergic dysfunction within the CSTC circuits as the underpinning etiology of OCD and the OC-spectrum disorders [47,48,61]. Here, my data indicate that Ninj1 is predominantly expressed in cortico-thalamic circuits and involved in regulating synaptic transmission in the brain. In addition, in the same line with the "glutamate hypothesis" of OCD pathogenesis [46,62], I found that

Ninj1 deletion led to glutamatergic alterations in the CNS. Notably, *Ninj1* KO mice were responsive to fluoxetine, which is an effective treatment for OCD patients and reportedly alleviates OCD-like behaviors in mice. Collectively, the biochemical, electrophysiological, and pharmacological studies further support a possibility of presence of OCD-like behaviors in *Ninj1* KO mice.

A critical feature of my findings is that Ninj1 is predominantly expressed in CNS neurons; hence, the behavioral abnormalities of *Ninj1* KO mice might be caused by altered neural circuits. Consistently, conditional KO mice lacking *Ninj1* specifically in CNS neurons recapitulated the abnormal phenotypes of global *Ninj1* KO mice, confirming that the loss of neuron-derived Ninj1 is primarily responsible for these defects. In addition, Ninj1 appears to be localized at synapses, which are the sites mediating signal transmission between neurons. Changes in synaptic function have been described in a wide range of neuropsychiatric disorders, such as ASD, OCD, depression, and schizophrenia [47,63-67]. Thus, I speculate that altered synaptic transmission in the brain of *Ninj1* KO mice could be a plausible link to the etiology of the behavioral aberrations. Supporting this hypothesis, I observed a reduction in the frequency and an increase in the amplitude

of mEPSCs in the thalamic neurons of *Ninj1* KO mice. These results are notable because synaptic dysfunctions within the cortico-striato-thalamo-cortical (CSTC) circuits are widely accepted in ASD and OCD [2,27,47]. Therefore, an important question that needs to be addressed is how *Ninj1* deficiency causes synaptic dysfunctions. I noticed that *Ninj1* deletion led to glutamatergic abnormalities in the CNS. The brains of *Ninj1* KO mice showed increased levels of glutamate receptors in synaptosomal fractions, in strong agreement with an increase in the mEPSC amplitudes of neurons. On the other hand, the level of glutamate neurotransmitter was found to be downregulated in the brains of *Ninj1* KO mice, which coupled with a reduction in synapse number substantiated the decrease in the mEPSC frequency of neurons. Further investigation would be required to determine the exact mechanisms by which Ninj1 modulates the glutamatergic abnormalities. Identifying partners of Ninj1 in the brain could pave the way to fulfill this task.

Interestingly, I found postsynaptic adhesion molecule localized at glutamatergic synapses neuroligin 1 (NL1), a postsynaptic adhesion molecule localized at glutamatergic synapses, but not NL2, as a potential binding partner by series of immunoprecipitation (IP) assays

(**Figure 41**) and immunocytochemical analysis in HEK293T cells, Neuro2A (a mouse neural crest-derived cell line), and cultured neurons co-overexpressing Ninj1 and NL1 (**Figure 42, A-C**). Specifically, in dendrites of mature neurons, Ninj1 was co-localized precisely with NL1 at spines (**Figure 42D**). These data suggest that Ninj1 could interact with NL1, thereby moderating CNS synapses including the synapse formation and activity. It is noteworthy to notice that mice deficient for *Nlgn1*, which encodes for NL1, exhibited increased repetitive behaviors, including grooming behavior [68]. Thus, the coupling of NL1 and Ninj1 might be the key for normal brain function and disruption of this interaction could lead to abnormal behaviors as seen in *Nlgn1* or *Ninj1* KO mice.

My findings reveal that chronic administration of fluoxetine alleviated the behavioral deficits of *Ninj1* KO mice. There are several possibilities for explaining the mechanisms underlying the alleviating effects of fluoxetine. First, fluoxetine inhibits 5-hydroxytryptamine (HT) receptors in pre-synaptic neurons to increase the availability of 5-HT (known as serotonin) at post-synaptic receptors [69]. However, the levels of serotonin neurotransmitter and its main metabolite 5-HIAA in *Ninj1* KO mice were comparable with those of WT littermates. Since

the functions of 5-HT receptors in the brains of *Ninj1* KO mice have not yet been examined, there is a possible involvement of neurotransmission mediated by these receptors in affecting the abnormal behaviors of *Ninj1* KO mice. Second, the therapeutic efficacy of fluoxetine could be associated with other processes in addition to its effects on serotonin receptors. In several recent studies, it has been reported that fluoxetine exhibits direct inhibitory effects on the NMDA receptors [70-72]. Similarly, I found that disruption of *Ninj1* led to the increased synaptic expression of the ionotropic glutamate receptors and amplitude of the mEPSCs. Therefore, I speculate that fluoxetine might block the glutamate receptors to mitigate the compulsive grooming and anxiety-like behaviors in *Ninj1* KO mice. Taken together, serotoninergic and glutamatergic neurotransmission, either independently of each other or coordinately, could mediate the behaviors of *Ninj1* KO mice. The latter postulation in particular merits further investigation.

To find any mutations of *NINJ1* in human OCD patients, I have thoroughly examined the published articles (via PubMed, https://www.ncbi.nlm.nih.gov/pubmed/) as well as public data sources such as dbSNP (The Single Nucleotide Polymorphism database,

https://www.ncbi.nlm.nih.gov/projects/SNP/), GeneCards (GeneCards®: The Human Gene Database, http://www.genecards.org/), and OMIM (Online Mendelian Inheritance in Man, https://www.ncbi.nlm.nih.gov/omim) and have not found any genetic mutations in *NINJ1* in human OCD or anxiety patients. However, in a genome-wide association study (GWAS) of OCD conducted by the International OCD Foundation Genetic Collaborative (IOCDF-GC) [73], we found that some single nucleotide polymorphisms (SNP) of other genes such as rs9641218, rs1876359, and rs11869351 statistically significantly affect *NINJ1* mRNA level and status of *NINJ1* methylation in brain tissue of human OCD patients by eQTL (expression quantitative trait loci) and mQTL (methylation quantitative trait loci) analyses. Thus, the roles of Ninj1 in human neuropsychiatric disorders such as OCD or anxiety disorders would benefit from further investigation.

Several questions need to be addressed in the future. First, in addition to the contribution of Ninj1 in glutamatergic synaptic transmission that I have found in this study, it would be interesting to further explore other roles of Ninj1 in the thalamic circuit. Using combinatorial tools of optogenetic techniques [74] and *Ninj1*

conditional KO mice, which lack *Ninj1* specifically in this brain area through the utilization of Cre mice bearing thalamic-specific promoters such as *potassium voltage-gated channel subfamily C member 2* (*Kcnc2, or Kv3.2)* and *somatostatin (som)* [75,76], would be helpful in elucidating the functions of Ninj1 in thalamus and OCD. Next, although this study provided profound evidence of the defects of neural circuits in *Ninj1* KO mice, a potential involvement of oxidative stress, which has been reportedly to play roles in animal behaviors and neuropsychiatric diseases including OCD [77-79], shoud be determined. It would be valuable to test effects of antioxidants such as N-acetyl cysteine (NAC) on the abnormal behaviors of *Ninj1*-deficient mice. In clinical studies, NAC has been demonstrated to improve the clinical symptoms of OCD patients [80,81]. Furthermore, the therapeutic effect of NMDA receptor antagonists such as memantine on the hair loss phenotype of *Ninj1* KO mice remains uncharacterized and would merit further investigation.

In conclusion, my findings provide evidence that Ninj1 is a molecular link between impaired neural circuits, altered glutamate signaling, and OCD-like behaviors in mice (**Figure 43**). Therefore, I propose that *Ninj1* is a strong candidate for mutation scanning in OCD

patients and that *Ninj1*-deficient mice are an appropriate model for future studies of OCD, which opens opportunities for the development of novel therapeutic strategies for OCD.

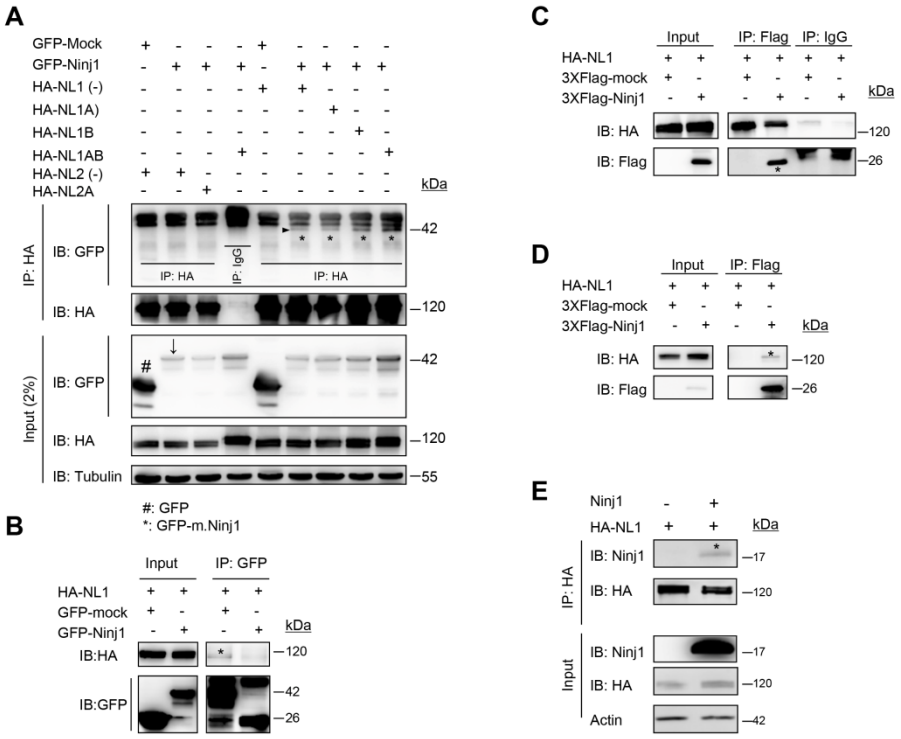

Figure 41. Ninj1 interacts with Neuroligin 1, but not Neuroligin 2 *in vitro*.

(**A**), Immunoprecipitation assays (IP) were performed in HEK293T cells co-overexpressing with GFP mock or GFP-mouse Ninj1 and various HA-tagged isoforms of Neuroligin 1 [NL1 (-); NL1A; NL1B; NL1AB] and Neuroligin 2 [NL2 (-); NL2A] as indicated. Total protein lysates were immunoprecipitated with mouse anti-HA antibody and subsequently immunoblotted with GFP and HA antibodies. Normal mouse IgG was used as a non-specific control. Hashtag (#) indicates

GFP, while arrow (↓) shows GFP-Ninj1. Arrowhead (►) denotes the site of immunoprecipitated protein (GFP-Ninj1). Note that Ninj1 binds to all NL1 isoforms, but not NL2 isoforms. (**B**), Inversed IP strategy was conducted. IP assays were performed in HEK293T cells co-transfected with HA-NL1 (-) and GFP mock or GFP-Ninj1 by using GFP antibody. The subsequent Western blots were probed using the indicated antibodies. Note that HA-NL1 (-) was co-immunoprecipitated with GFP-Ninj1, but not with GFP mock. (**C, D**) The interaction between Ninj1 and NL1 was further confirmed in 3XFlag tagged form of Ninj1 by using IP with Flag antibody (**C**) and inverse IP with HA antibody (**D**). In both cases, NL1 were found to be co-immunoprecipitated with Ninj1 (**C**) and vice versa (**D**). (**E**), To exclude to possibility that tags (GFP- and 3XFlag-) could influence the binding of Ninj1 and NL1, we generated a non-tagged form of Ninj1 [pcDNA3.1-Myc/His-mouse Ninj1] with a stop codon inserted after Ninj1 coding sequence and before Myc/His sequences] and applied IP assays with HA antibody. These assays clearly confirmed the interaction between Ninj1 and NL1. Molecular weight (kDa) is shown on the right of each blot. Asterisks (*) represent the immunoprecipitated proteins. α-Tubulin and β-actin were probed as

loading controls. Similar results were replicated in at least two independent experiments for all data shown in this figure.

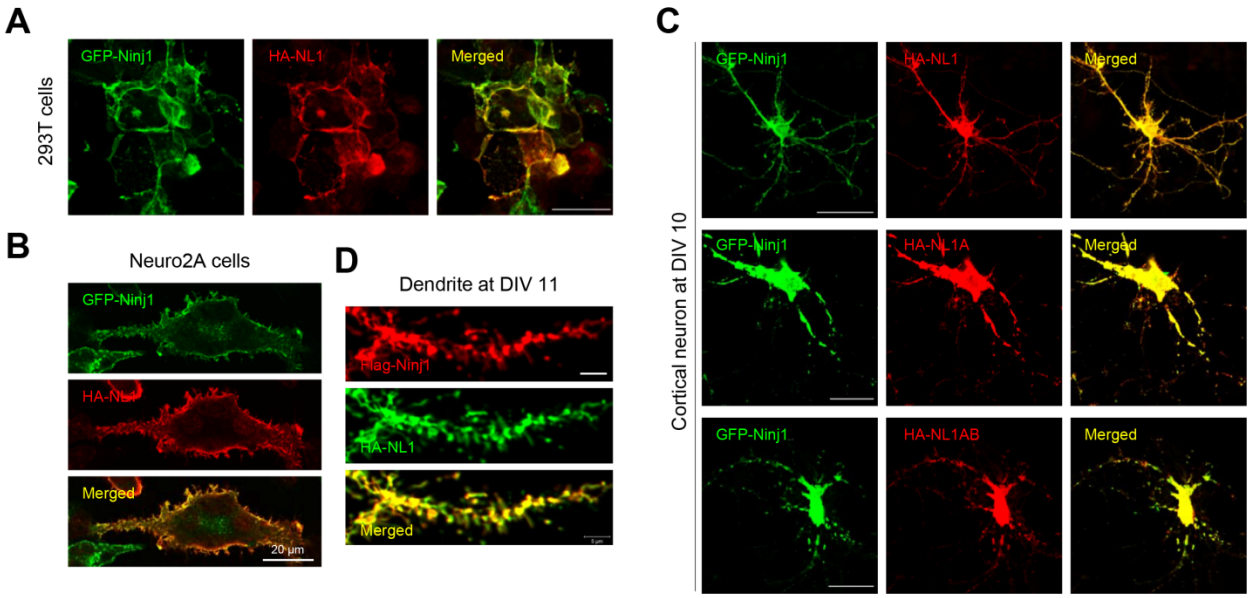
A
293T cells
GFP-Ninj1
HA-NL1
Merged
B
Neuro2A cells
GFP-Ninj1
HA-NL1
Merged
20 μm
D
Dendrite at DIV 11
Flag-Ninj1
HA-NL1
Merged
C
Cortical neuron at DIV 10
GFP-Ninj1
HA-NL1
Merged
GFP-Ninj1
HA-NL1A
Merged
GFP-Ninj1
HA-NL1AB
Merged

Figure 42. Ninj1 interacts with Neuroligin 1 *in vivo*.

(**A, B**) Confocal images showing the colocalization of Ninj1 (green) and NL1 immunostained in red in co-transfected HEK293T cells (**A**) and mouse Neuro 2A cells (**B**). (**C**), Colocalization of Ninj1 and NL1 isoforms in neurons. Cortical neurons (DIV 4) were co-transfected with GFP-Ninj1 and indicated NL1 isoforms including NL1 (-), NL1A, and NL1AB. Samples were fixed and double immunostained on DIV 10 with HA (red) and GFP (green) antibodies. Confocal images showed complete colocalization of Ninj1 and indicated NL1 isoforms in neurons. (**D**), Ninj1 is expressed in dendritic spines with similar pattern to NL1. Primary cortical neurons were co-transfected with Flag-Ninj1 and HA-NL1 on DIV 4 and fixed on DIV 11. Samples were then double immunostained with Flag (red) and HA (green) antibodies. Scale bars: 50 μm (**A, C**); 10 μm (**B**); 5 μm (**D**). Colocalization appears yellow.

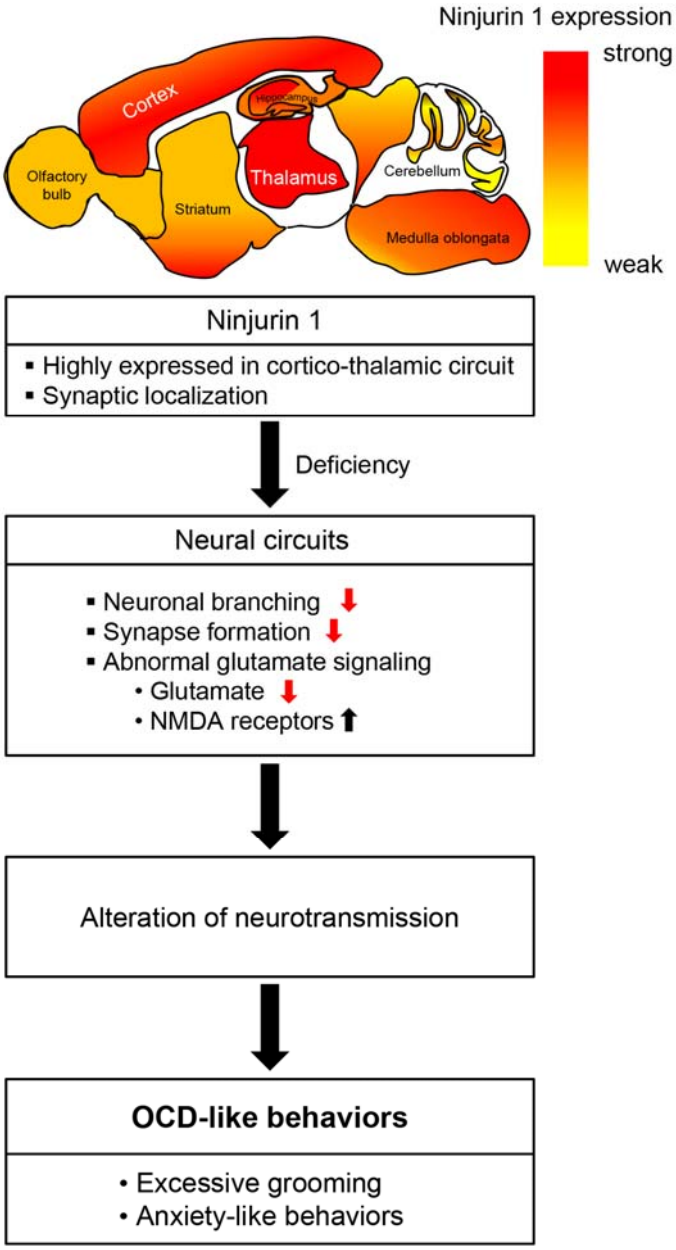
Ninjurin 1 expression
strong
weak
Cortex
Hippocampus
Olfactory bulb
Striatum
Thalamus
Cerebellum
Medulla oblongata
Ninjurin 1
▪ Highly expressed in cortico-thalamic circuit
▪ Synaptic localization
Deficiency
Neural circuits
▪ Neuronal branching ⬇
▪ Synapse formation ⬇
▪ Abnormal glutamate signaling
• Glutamate ⬇
• NMDA receptors ⬆
Alteration of neurotransmission
OCD-like behaviors
• Excessive grooming
• Anxiety-like behaviors

Figure 43. Proposed model for the mechanisms that underlie the OCD-like behaviors of the *Ninj1*-deficient mice.

Ninj1 is highly expressed in cortico-thalamic circuits (red colour in a cartoon of a sagittal section of the mouse brain), especially in neurons, and is required for the maintenance of neural circuits. Thus, the disruption of *Ninj1* results in reduced neuronal branching, decreased numbers of functional synapses, and abnormalities in glutamate signaling. The resulting altered neurotransmission then leads to the OCD-like phenotypes of the *Ninj1*-deficient mice.

In addition to the contribution of Ninj1 to neuronal branching and synapse formation, my preliminary data demonstrated that Ninj1 could involve in neurogenesis, a process by which neurons are generated from the neural stem cells and progenitor cells (**Figure 44, A and B**). In the mouse brain, Ninj1 is highly expressed in neuroblast cells (PSA-NCAM (+)) of subventricular zone (SVZ) of lateral ventricle (LV) (data not shown) and rostral migratory stream (RMS) (**Figure 44C**). It would be of great interest to test the functions of Ninj1 in neurogenesis as this process is important for maintaining neuronal population in brain and for repairing circuits after injuries such as stroke, traumatic brain injury, and neurodegeneration diseases [82-85].

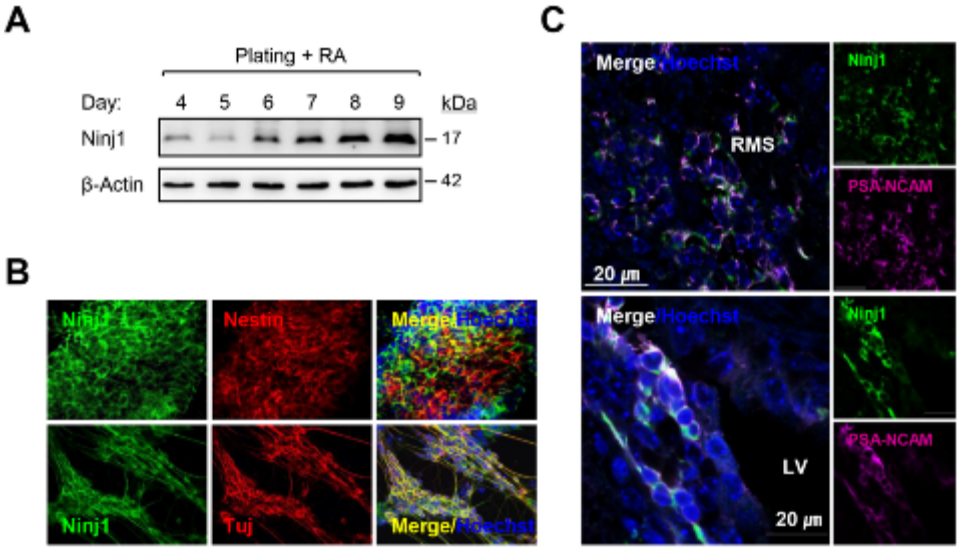

Figure 44. The possible involvement of Ninj1 during neurogenesis. (**A**) P19 embryonic stem cell was induced to differentiation by retinoic acid (RA). The levels of Ninj1 during the was examined by Western blott. (**B**) Retinoic acid (RA)-induced P19 cells at day 5 (upper) and day 6 (lower) were double stained with antibodies against Ninj1 (green) and Nestin or Tuj1 (red), respectively. (**C**) Ninj1 (green) is expressed in neuroblasts of RMS and LV as seen by their coexpression of the marker PSA-NCAM (magenta).

REFERENCES

1. Ruscio AM, Stein DJ, Chiu WT, Kessler RC (2010) The epidemiology of obsessive-compulsive disorder in the National Comorbidity Survey Replication. Mol Psychiatry 15 (1):53-63

2. Pauls DL, Abramovitch A, Rauch SL, Geller DA (2014) Obsessive-compulsive disorder: an integrative genetic and neurobiological perspective. Nat Rev Neurosci 15 (6):410-424

3. Subramaniam M, Soh P, Vaingankar JA, Picco L, Chong SA (2013) Quality of life in obsessive-compulsive disorder: impact of the disorder and of treatment. CNS Drugs 27 (5):367-383

4. Veale D, Roberts A (2014) Obsessive-compulsive disorder. BMJ 348:g2183

5. Zohar AH (1999) The epidemiology of obsessive-compulsive disorder in children and adolescents. Child Adolesc Psychiatr Clin N Am 8 (3):445-460

6. Miguel EC, Leckman JF, Rauch S, do Rosario-Campos MC, Hounie AG, Mercadante MT, Chacon P, Pauls DL (2005) Obsessive-compulsive disorder phenotypes: implications for genetic studies. Molecular psychiatry 10 (3):258-275

7. Pauls DL (2010) The genetics of obsessive-compulsive disorder: a review. Dialogues in clinical neuroscience 12 (2):149-163

8. Welch JM, Lu J, Rodriguiz RM, Trotta NC, Peca J, Ding JD, Feliciano C, Chen M, Adams JP, Luo J, Dudek SM, Weinberg RJ, Calakos N, Wetsel WC, Feng G (2007) Cortico-striatal synaptic defects and OCD-like behaviours in Sapap3-mutant mice. Nature 448 (7156):894-900

9. Shmelkov SV, Hormigo A, Jing D, Proenca CC, Bath KG, Milde T, Shmelkov E, Kushner JS, Baljevic M, Dincheva I, Murphy AJ, Valenzuela DM, Gale NW, Yancopoulos GD, Ninan I, Lee FS, Rafii S (2010) Slitrk5 deficiency impairs corticostriatal circuitry and leads to obsessive-compulsive-like behaviors in mice. Nat Med 16 (5):598-602

10. Chen SK, Tvrdik P, Peden E, Cho S, Wu S, Spangrude G, Capecchi MR (2010) Hematopoietic origin of pathological grooming in Hoxb8 mutant mice. Cell 141 (5):775-785

11. Barbeau D, Liang JJ, Robitalille Y, Quirion R, Srivastava LK (1995) Decreased expression of the embryonic form of the neural cell adhesion molecule in schizophrenic brains. Proc Natl Acad Sci U S A 92 (7):2785-2789

12. Dalva MB, McClelland AC, Kayser MS (2007) Cell adhesion molecules: signalling functions at the synapse. Nat Rev Neurosci 8 (3):206-220

13. Moya PR, Dodman NH, Timpano KR, Rubenstein LM, Rana Z, Fried RL, Reichardt LF, Heiman GA, Tischfield JA, King RA, Galdzicka M, Ginns EI, Wendland JR (2013) Rare missense neuronal cadherin gene (CDH2) variants in specific obsessive-compulsive

disorder and Tourette disorder phenotypes. Eur J Hum Genet 21 (8):850-854

14. Araki T, Milbrandt J (1996) Ninjurin, a novel adhesion molecule, is induced by nerve injury and promotes axonal growth. Neuron 17 (2):353-361

15. Ifergan I, Kebir H, Terouz S, Alvarez JI, Lecuyer MA, Gendron S, Bourbonniere L, Dunay IR, Bouthillier A, Moumdjian R, Fontana A, Haqqani A, Klopstein A, Prinz M, Lopez-Vales R, Birchler T, Prat A (2011) Role of Ninjurin-1 in the migration of myeloid cells to central nervous system inflammatory lesions. Ann Neurol 70 (5):751-763

16. Ahn BJ, Le H, Shin MW, Bae SJ, Lee EJ, Wee HJ, Cha JH, Lee HJ, Lee HS, Kim JH, Kim CY, Seo JH, Lo EH, Jeon S, Lee MN, Oh GT, Yin GN, Ryu JK, Suh JK, Kim KW (2014) Ninjurin1 deficiency attenuates susceptibility of experimental autoimmune encephalomyelitis in mice. J Biol Chem 289 (6):3328-3338

17. Araki T, Milbrandt J (2000) Ninjurin2, a novel homophilic adhesion molecule, is expressed in mature sensory and enteric neurons and promotes neurite outgrowth. J Neurosci 20 (1):187-195

18. Araki T, Zimonjic DB, Popescu NC, Milbrandt J (1997) Mechanism of homophilic binding mediated by ninjurin, a novel widely expressed adhesion molecule. J Biol Chem 272 (34):21373-21380

19. Lee HJ, Ahn BJ, Shin MW, Choi JH, Kim KW (2010) Ninjurin1: a potential adhesion molecule and its role in inflammation and tissue

remodeling. Mol Cells 29 (3):223-227

20. Lee HJ, Ahn BJ, Shin MW, Jeong JW, Kim JH, Kim KW (2009) Ninjurin1 mediates macrophage-induced programmed cell death during early ocular development. Cell Death Differ 16 (10):1395-1407

21. Ahn BJ, Lee HJ, Shin MW, Choi JH, Jeong JW, Kim KW (2009) Ninjurin1 is expressed in myeloid cells and mediates endothelium adhesion in the brains of EAE rats. Biochem Biophys Res Commun 387 (2):321-325

22. Odoardi F, Sie C, Streyl K, Ulaganathan VK, Schlager C, Lodygin D, Heckelsmiller K, Nietfeld W, Ellwart J, Klinkert WE, Lottaz C, Nosov M, Brinkmann V, Spang R, Lehrach H, Vingron M, Wekerle H, Flugel-Koch C, Flugel A (2012) T cells become licensed in the lung to enter the central nervous system. Nature 488 (7413):675-679

23. Jennewein C, Sowa R, Faber AC, Dildey M, von Knethen A, Meybohm P, Scheller B, Drose S, Zacharowski K (2015) Contribution of Ninjurin1 to Toll-like receptor 4 signaling and systemic inflammation. Am J Respir Cell Mol Biol 53 (5):656-663

24. Yin GN, Choi MJ, Kim WJ, Kwon MH, Song KM, Park JM, Das ND, Kwon KD, Batbold D, Oh GT, Koh GY, Kim KW, Ryu JK, Suh JK (2014) Inhibition of Ninjurin 1 restores erectile function through dual angiogenic and neurotrophic effects in the diabetic mouse. Proc Natl Acad Sci U S A 111 (26):E2731-2740

25. Matsuki M, Kabara M, Saito Y, Shimamura K, Minoshima A,

Nishimura M, Aonuma T, Takehara N, Hasebe N, Kawabe J (2015) Ninjurin1 is a novel factor to regulate angiogenesis through the function of pericytes. Circ J 79 (6):1363-1371

26. Skarnes WC, Rosen B, West AP, Koutsourakis M, Bushell W, Iyer V, Mujica AO, Thomas M, Harrow J, Cox T, Jackson D, Severin J, Biggs P, Fu J, Nefedov M, de Jong PJ, Stewart AF, Bradley A (2011) A conditional knockout resource for the genome-wide study of mouse gene function. Nature 474 (7351):337-342

27. Peca J, Feliciano C, Ting JT, Wang W, Wells MF, Venkatraman TN, Lascola CD, Fu Z, Feng G (2011) Shank3 mutant mice display autistic-like behaviours and striatal dysfunction. Nature 472 (7344):437-442

28. Angoa-Perez M, Kane MJ, Briggs DI, Francescutti DM, Kuhn DM (2013) Marble burying and nestlet shredding as tests of repetitive, compulsive-like behaviors in mice. J Vis Exp (82):50978

29. Won H, Lee HR, Gee HY, Mah W, Kim JI, Lee J, Ha S, Chung C, Jung ES, Cho YS, Park SG, Lee JS, Lee K, Kim D, Bae YC, Kaang BK, Lee MG, Kim E (2012) Autistic-like social behaviour in Shank2-mutant mice improved by restoring NMDA receptor function. Nature 486 (7402):261-265

30. Ahn BJ, Le H, Shin MW, Bae SJ, Lee EJ, Wee HJ, Cha JH, Park JH, Lee HS, Lee HJ, Jung H, Park ZY, Park SH, Han BW, Seo JH, Lo EH, Kim KW (2012) The N-terminal ectodomain of Ninjurin1 liberated by MMP9 has chemotactic activity. Biochem Biophys Res Commun 428 (4):438-444

31. Ahn BJ, Le H, Shin MW, Bae SJ, Lee EJ, Lee SY, Yang JH, Wee HJ, Cha JH, Seo JH, Lee HS, Lee HJ, Arai K, Lo EH, Jeon S, Oh GT, Kim WJ, Ryu JK, Suh JK, Kim KW (2014) Ninjurin1 enhances the basal motility and transendothelial migration of immune cells by inducing protrusive membrane dynamics. The Journal of biological chemistry 289 (32):21926-21936

32. Wang X, Zhao Y, Zhang X, Badie H, Zhou Y, Mu Y, Loo LS, Cai L, Thompson RC, Yang B, Chen Y, Johnson PF, Wu C, Bu G, Mobley WC, Zhang D, Gage FH, Ranscht B, Zhang YW, Lipton SA, Hong W, Xu H (2013) Loss of sorting nexin 27 contributes to excitatory synaptic dysfunction by modulating glutamate receptor recycling in Down's syndrome. Nature medicine 19 (4):473-480

33. Greer JM, Capecchi MR (2002) Hoxb8 is required for normal grooming behavior in mice. Neuron 33 (1):23-34

34. Garner JP, Weisker SM, Dufour B, Mench JA (2004) Barbering (fur and whisker trimming) by laboratory mice as a model of human trichotillomania and obsessive-compulsive spectrum disorders. Comp Med 54 (2):216-224

35. Carcani-Rathwell I, Rabe-Hasketh S, Santosh PJ (2006) Repetitive and stereotyped behaviours in pervasive developmental disorders. J Child Psychol Psychiatry 47 (6):573-581

36. Leckman JF, Denys D, Simpson HB, Mataix-Cols D, Hollander E, Saxena S, Miguel EC, Rauch SL, Goodman WK, Phillips KA, Stein DJ (2010) Obsessive-compulsive disorder: a review of the diagnostic

criteria and possible subtypes and dimensional specifiers for DSM-V. Depress Anxiety 27 (6):507-527

37. Reaven J (2011) The treatment of anxiety symptoms in youth with high-functioning autism spectrum disorders: developmental considerations for parents. Brain Res 1380:255-263

38. Ahmari SE, Spellman T, Douglass NL, Kheirbek MA, Simpson HB, Deisseroth K, Gordon JA, Hen R (2013) Repeated cortico-striatal stimulation generates persistent OCD-like behavior. Science 340 (6137):1234-1239

39. Zhu Y, Romero MI, Ghosh P, Ye Z, Charnay P, Rushing EJ, Marth JD, Parada LF (2001) Ablation of NF1 function in neurons induces abnormal development of cerebral cortex and reactive gliosis in the brain. Genes Dev 15 (7):859-876

40. Ting JT, Feng G (2011) Neurobiology of obsessive-compulsive disorder: insights into neural circuitry dysfunction through mouse genetics. Curr Opin Neurobiol 21 (6):842-848

41. Milad MR, Rauch SL (2012) Obsessive-compulsive disorder: beyond segregated cortico-striatal pathways. Trends Cogn Sci 16 (1):43-51

42. Burguiere E, Monteiro P, Feng G, Graybiel AM (2013) Optogenetic stimulation of lateral orbitofronto-striatal pathway suppresses compulsive behaviors. Science 340 (6137):1243-1246

43. Wu K, Hanna GL, Easter P, Kennedy JL, Rosenberg DR, Arnold PD

(2013) Glutamate system genes and brain volume alterations in pediatric obsessive-compulsive disorder: a preliminary study. Psychiatry Res 211 (3):214-220

44. Sarter M, Bruno JP, Parikh V (2007) Abnormal neurotransmitter release underlying behavioral and cognitive disorders: toward concepts of dynamic and function-specific dysregulation. Neuropsychopharmacology 32 (7):1452-1461

45. Goddard AW, Shekhar A, Whiteman AF, McDougle CJ (2008) Serotoninergic mechanisms in the treatment of obsessive-compulsive disorder. Drug Discov Today 13 (7-8):325-332

46. Wu K, Hanna GL, Rosenberg DR, Arnold PD (2012) The role of glutamate signaling in the pathogenesis and treatment of obsessive-compulsive disorder. Pharmacol Biochem Behav 100 (4):726-735

47. Ting JT, Feng G (2008) Glutamatergic Synaptic Dysfunction and Obsessive-Compulsive Disorder. Curr Chem Genomics 2:62-75

48. Pittenger C, Bloch MH, Williams K (2011) Glutamate abnormalities in obsessive compulsive disorder: neurobiology, pathophysiology, and treatment. Pharmacol Ther 132 (3):314-332

49. Lin CH, Lane HY, Tsai GE (2012) Glutamate signaling in the pathophysiology and therapy of schizophrenia. Pharmacol Biochem Behav 100 (4):665-677

50. Lee EJ, Choi SY, Kim E (2015) NMDA receptor dysfunction in autism spectrum disorders. Curr Opin Pharmacol 20:8-13

51. Kopec CD, Li B, Wei W, Boehm J, Malinow R (2006) Glutamate receptor exocytosis and spine enlargement during chemically induced long-term potentiation. J Neurosci 26 (7):2000-2009

52. Witt A, Macdonald N, Kirkpatrick P (2004) Memantine hydrochloride. Nat Rev Drug Discov 3 (2):109-110

53. Ghaleiha A, Entezari N, Modabbernia A, Najand B, Askari N, Tabrizi M, Ashrafi M, Hajiaghaee R, Akhondzadeh S (2013) Memantine add-on in moderate to severe obsessive-compulsive disorder: randomized double-blind placebo-controlled study. Journal of psychiatric research 47 (2):175-180

54. Haghighi M, Jahangard L, Mohammad-Beigi H, Bajoghli H, Hafezian H, Rahimi A, Afshar H, Holsboer-Trachsler E, Brand S (2013) In a double-blind, randomized and placebo-controlled trial, adjuvant memantine improved symptoms in inpatients suffering from refractory obsessive-compulsive disorders (OCD). Psychopharmacology 228 (4):633-640

55. Fernando AB, Robbins TW (2011) Animal models of neuropsychiatric disorders. Annu Rev Clin Psychol 7:39-61

56. Overbeek T, Schruers K, Vermetten E, Griez E (2002) Comorbidity of obsessive-compulsive disorder and depression: prevalence, symptom severity, and treatment effect. J Clin Psychiatry 63 (12):1106-1112

57. Anholt GE, Cath DC, van Oppen P, Eikelenboom M, Smit JH, van Megen H, van Balkom AJ (2010) Autism and ADHD symptoms in

patients with OCD: are they associated with specific OC symptom dimensions or OC symptom severity? J Autism Dev Disord 40 (5):580-589

58. Murphy DL, Timpano KR, Wheaton MG, Greenberg BD, Miguel EC (2010) Obsessive-compulsive disorder and its related disorders: a reappraisal of obsessive-compulsive spectrum concepts. Dialogues Clin Neurosci 12 (2):131-148

59. Pallanti S, Grassi G, Sarrecchia ED, Cantisani A, Pellegrini M (2011) Obsessive-compulsive disorder comorbidity: clinical assessment and therapeutic implications. Front Psychiatry 2:70

60. Velikova S, Locatelli M, Insacco C, Smeraldi E, Comi G, Leocani L (2010) Dysfunctional brain circuitry in obsessive-compulsive disorder: source and coherence analysis of EEG rhythms. Neuroimage 49 (1):977-983

61. Chakrabarty K, Bhattacharyya S, Christopher R, Khanna S (2005) Glutamatergic dysfunction in OCD. Neuropsychopharmacology 30 (9):1735-1740

62. Kariuki-Nyuthe C, Gomez-Mancilla B, Stein DJ (2014) Obsessive compulsive disorder and the glutamatergic system. Curr Opin Psychiatry 27 (1):32-37

63. van Spronsen M, Hoogenraad CC (2010) Synapse pathology in psychiatric and neurologic disease. Curr Neurol Neurosci Rep 10 (3):207-214

64. Spooren W, Lindemann L, Ghosh A, Santarelli L (2012) Synapse dysfunction in autism: a molecular medicine approach to drug discovery in neurodevelopmental disorders. Trends Pharmacol Sci 33 (12):669-684

65. Duman RS, Aghajanian GK (2012) Synaptic dysfunction in depression: potential therapeutic targets. Science 338 (6103):68-72

66. Crabtree GW, Gogos JA (2014) Synaptic plasticity, neural circuits, and the emerging role of altered short-term information processing in schizophrenia. Front Synaptic Neurosci 6:28

67. Bourgeron T (2015) From the genetic architecture to synaptic plasticity in autism spectrum disorder. Nat Rev Neurosci 16 (9):551-563

68. Blundell J, Blaiss CA, Etherton MR, Espinosa F, Tabuchi K, Walz C, Bolliger MF, Sudhof TC, Powell CM (2010) Neuroligin-1 deletion results in impaired spatial memory and increased repetitive behavior. J Neurosci 30 (6):2115-2129

69. Wong DT, Perry KW, Bymaster FP (2005) Case history: the discovery of fluoxetine hydrochloride (Prozac). Nat Rev Drug Discov 4 (9):764-774

70. Li YF, Zhang YZ, Liu YQ, Wang HL, Cao JB, Guan TT, Luo ZP (2006) Inhibition of N-methyl-D-aspartate receptor function appears to be one of the common actions for antidepressants. J Psychopharmacol 20 (5):629-635

71. Szasz BK, Mike A, Karoly R, Gerevich Z, Illes P, Vizi ES, Kiss JP (2007) Direct inhibitory effect of fluoxetine on N-methyl-D-aspartate receptors in the central nervous system. Biol Psychiatry 62 (11):1303-1309

72. Kiss JP, Szasz BK, Fodor L, Mike A, Lenkey N, Kurko D, Nagy J, Vizi ES (2012) GluN2B-containing NMDA receptors as possible targets for the neuroprotective and antidepressant effects of fluoxetine. Neurochem Int 60 (2):170-176

73. Stewart SE, Yu D, Scharf JM, Neale BM, Fagerness JA, Mathews CA, Arnold PD, Evans PD, Gamazon ER, Davis LK, Osiecki L, McGrath L, Haddad S, Crane J, Hezel D, Illman C, Mayerfeld C, Konkashbaev A, Liu C, Pluzhnikov A, Tikhomirov A, Edlund CK, Rauch SL, Moessner R, Falkai P, Maier W, Ruhrmann S, Grabe HJ, Lennertz L, Wagner M, Bellodi L, Cavallini MC, Richter MA, Cook EH, Jr., Kennedy JL, Rosenberg D, Stein DJ, Hemmings SM, Lochner C, Azzam A, Chavira DA, Fournier E, Garrido H, Sheppard B, Umana P, Murphy DL, Wendland JR, Veenstra-VanderWeele J, Denys D, Blom R, Deforce D, Van Nieuwerburgh F, Westenberg HG, Walitza S, Egberts K, Renner T, Miguel EC, Cappi C, Hounie AG, Conceicao do Rosario M, Sampaio AS, Vallada H, Nicolini H, Lanzagorta N, Camarena B, Delorme R, Leboyer M, Pato CN, Pato MT, Voyiaziakis E, Heutink P, Cath DC, Posthuma D, Smit JH, Samuels J, Bienvenu OJ, Cullen B, Fyer AJ, Grados MA, Greenberg BD, McCracken JT, Riddle MA, Wang Y, Coric V, Leckman JF, Bloch M, Pittenger C, Eapen V, Black DW, Ophoff RA, Strengman E, Cusi D, Turiel M, Frau F, Macciardi F, Gibbs JR, Cookson MR, Singleton A, Hardy J, Crenshaw AT, Parkin

MA, Mirel DB, Conti DV, Purcell S, Nestadt G, Hanna GL, Jenike MA, Knowles JA, Cox N, Pauls DL (2013) Genome-wide association study of obsessive-compulsive disorder. Mol Psychiatry 18 (7):788-798

74. Tye KM, Deisseroth K (2012) Optogenetic investigation of neural circuits underlying brain disease in animal models. Nat Rev Neurosci 13 (4):251-266

75. Ahrens S, Jaramillo S, Yu K, Ghosh S, Hwang GR, Paik R, Lai C, He M, Huang ZJ, Li B (2015) ErbB4 regulation of a thalamic reticular nucleus circuit for sensory selection. Nat Neurosci 18 (1):104-111

76. Anderson MP, Mochizuki T, Xie J, Fischler W, Manger JP, Talley EM, Scammell TE, Tonegawa S (2005) Thalamic Cav3.1 T-type Ca2+ channel plays a crucial role in stabilizing sleep. Proc Natl Acad Sci U S A 102 (5):1743-1748

77. Salim S (2014) Oxidative stress and psychological disorders. Curr Neuropharmacol 12 (2):140-147

78. Selek S, Herken H, Bulut M, Ceylan MF, Celik H, Savas HA, Erel O (2008) Oxidative imbalance in obsessive compulsive disorder patients: a total evaluation of oxidant-antioxidant status. Prog Neuropsychopharmacol Biol Psychiatry 32 (2):487-491

79. Kandemir H, Abuhandan M, Aksoy N, Savik E, Kaya C (2013) Oxidative imbalance in child and adolescent patients with obsessive compulsive disorder. J Psychiatr Res 47 (11):1831-1834

80. Bavarsad Shahripour R, Harrigan MR, Alexandrov AV (2014) N-

acetylcysteine (NAC) in neurological disorders: mechanisms of action and therapeutic opportunities. Brain Behav 4 (2):108-122

81. Oliver G, Dean O, Camfield D, Blair-West S, Ng C, Berk M, Sarris J (2015) N-acetyl cysteine in the treatment of obsessive compulsive and related disorders: a systematic review. Clin Psychopharmacol Neurosci 13 (1):12-24

82. Winner B, Winkler J (2015) Adult neurogenesis in neurodegenerative diseases. Cold Spring Harb Perspect Biol 7 (4):a021287

83. Zheng W, ZhuGe Q, Zhong M, Chen G, Shao B, Wang H, Mao X, Xie L, Jin K (2013) Neurogenesis in adult human brain after traumatic brain injury. J Neurotrauma 30 (22):1872-1880

84. Marlier Q, Verteneuil S, Vandenbosch R, Malgrange B (2015) Mechanisms and Functional Significance of Stroke-Induced Neurogenesis. Front Neurosci 9:458

85. Kernie SG, Parent JM (2010) Forebrain neurogenesis after focal Ischemic and traumatic brain injury. Neurobiol Dis 37 (2):267-274

ABSTRACT IN KOREAN (국문초록)

Ninjurin1 결손 마우스에서 강박 장애 유사증상 발현에 관한 연구

강박증(Obsessive-compulsive disorder, OCD)은 강박관념(obsession)과 불안에 근거한 반복적인 행동 (compulsion)을 주된 특징으로 하는 정신질환으로 세계 인구의 약 2 % 가량이 이 질환을 앓고 있다고 알려져있다. 분자 신경생물학의 발전으로 생쥐에서 인간의 강박증과 유사한 증세를 일으키는 유전자들이 일부 발견되었지만, 정신신경계 질환의 복잡성으로 인하여 몇 가지 유전자가 아닌, 다양한 유전자 및 인자들이 관여하는 것으로 보이며, 발병 원인 및 진행 과정을 이해하기 위하여 관련 유전자 발굴 및 그 분자 기전에 대한 집중적인 연구가 필요한 상황이다.

본 논문은 신경재생과 염증반응에 관련되어 있다고 알려져 있는 세포 부착 단백질인 Ninjurin1 (Ninj1) 과 강박증의

연관성을 연구하였다. *Ninj1* 결손 생쥐는 대표적인 강박증 증상인 반복 행동 및 불안 행동과 함께, compulsive grooming에 의한 hair loss를 보였으며, 이들에게서 자해로 인한 상처 (self-made lesion)를 관찰할 수 있었다. Ninj1은 조직학적으로 뇌의 cortico-thalamic circuits에 주로 발현되었으며, global *Ninj1* K/O뿐 아니라, 신경조직에 Ninj1을 선택적으로 K/O시킨 생쥐에서도 유사한 이상 행동을 보였다. 특히, *Ninj1* K/O 생쥐의 뇌를 관찰한 결과, 시냅스의 수와 뉴런의 branching이 현저히 감소해 있었으며, thalamic neuron의 신경 시냅스 전달 (synaptic transmission)에 이상을 나타내었다. 또한 *Ninj1* K/O 생쥐는 글루타메이트 레벨 감소 및 이온성 글루타메이트 수용체 증가와 같은 glutamatergic 증세가 발현되었다. 이러한 이상 행동이 면역/염증 반응 이상에 의한 결과가 아니라 신경정신장애 행동임을 검증하기 위하여, *Ninj1* K/O 생쥐에 강박장애 행동을 완화시키는 약물인 fluoxetine을 투여한 결과, compulsive grooming과 불안 장애 행동이 완화되고, hair loss의 진행이 멈춤을 확인하였다. 즉, *Ninj1* K/O 생쥐에서 관찰한

이상 행동이 강박 장애와 유사함을 규명하였다.

따라서, 본 연구는 Ninj1 이 생쥐 뇌신경의 정상적인 분화 및 기능에 관여하며, *Ninj1* K/O 생쥐에서 반복 및 불안 증상을 나타냄을 규명하여, 강박증의 발병 및 진행에 Ninj1이 관련될 가능성을 제시하였다. 이러한 결과는 신경정신장애 질환의 기전 이해 및 치료제 개발에 기여할 수 있을 것이라 기대된다.

Keywords : **Ninjurin1; obsessive-compulsive disorder; OCD-like behaviors; anxiety-like behaviors; fluoxetine; glutamate signaling**

Student number : **2010-22880**